

**TOPICS IN FLOW IN FRACTURED MEDIA**

**Andrew Milne, BSc. MSc.**

**Thesis submitted to the University of Nottingham for the degree of  
Doctor of Philosophy**

**April 2011**

# ABSTRACT

Many geological formations consist of crystalline rocks that have very low matrix permeability but allow flow through an interconnected network of fractures.

Understanding the flow of groundwater through such rocks is important in considering disposal of radioactive waste in underground repositories. A specific area of interest is the conditioning of fracture transmissivities on measured values of pressure in these formations. This is the process where the values of fracture transmissivities in a model are adjusted to obtain a good fit of the calculated pressures to measured pressure values.

While there are existing methods to condition transmissivity fields on transmissivity, pressure and flow measurements for a continuous porous medium there is little literature on conditioning fracture networks. Conditioning fracture transmissivities on pressure or flow values is a complex problem because the measured pressures are dependent on all the fracture transmissivities in the network.

This thesis presents two new methods for conditioning fracture transmissivities in a discrete fracture network on measured pressure values. The first approach adopts a linear approximation when fracture transmissivities are mildly heterogeneous; this approach is then generalised to the minimisation of an objective function when fracture transmissivities are highly heterogeneous. This method is based on a generalisation of previous work on conditioning transmissivity values in a continuous porous medium.

The second method developed is a Bayesian conditioning method. Bayes' theorem is used to give an expression of proportionality for the posterior

distribution of fracture log transmissivities in terms of the prior distribution and the data available through pressure measurements. The fracture transmissivities are assumed to be log normally distributed with a given mean and covariance, and the measured pressures are assumed to be normally distributed values each with a given error. From the expression of proportionality for the posterior distribution of fracture transmissivities the modes of the posterior distribution (the points of highest likelihood for the fracture transmissivities given the measured pressures) are numerically computed.

Both algorithms are implemented in the existing finite element code NAPSAC developed and marketed by Serco Technical Services, which models groundwater flow in a fracture network.

## **ACKNOWLEDGEMENTS**

I would like to thank Serco Assurance for their funding and access to their computer codes. Most importantly, I would like to thank my supervisors Andrew Cliffe and Paul Houston for their help and guidance throughout my PhD which has been invaluable.

# PUBLICATIONS

The following paper has been accepted for publication based on research presented in this thesis:

A. Milne, K. A. Cliffe, D. Holton, P. Houston, C. P. Jackson, S. Joyce.

“Conditioning Discrete Fracture Networks of Groundwater Flow”. *International Journal of Numerical Analysis and Modeling*.

# CONTENTS

<b>ABSTRACT.....</b>	<b>II</b>
<b>ACKNOWLEDGEMENTS .....</b>	<b>IV</b>
<b>PUBLICATIONS.....</b>	<b>V</b>
<b>CONTENTS.....</b>	<b>VI</b>
<b>1 – INTRODUCTION AND LITERATURE REVIEW.....</b>	<b>1</b>
<b>1.1 – INTRODUCTION TO FLOW IN A POROUS MEDIUM .....</b>	<b>4</b>
1.1.1 - THE CONSTITUTIVE RELATIONSHIP AND GOVERNING EQUATION FOR GROUNDWATER FLOW .....	7
1.1.3 - THE GROUNDWATER FLOW EQUATION.....	10
<b>1.2 - REPRESENTATION OF THE GEOLOGICAL AREA SURROUNDING     UNDERGROUND NUCLEAR WASTE REPOSITORIES .....</b>	<b>12</b>
<b>1.3 – GENERATION OF A DISCRETE FRACTURE NETWORK MODEL AND ITS     FLOW PROPERTIES .....</b>	<b>16</b>
1.3.1 - FLOW IN A SINGLE FRACTURE .....	16
1.3.2 - PROPERTIES OF DISCRETE FRACTURE NETWORKS .....	19
<b>1.4 - NUMERICAL MODELLING OF GROUNDWATER FLOW IN A FRACTURE     NETWORK.....</b>	<b>21</b>
<b>1.5 - CONDITIONING A GROUNDWATER FLOW MODEL .....</b>	<b>23</b>
1.5.1 – CONDITIONING POROUS MEDIUM MODELS AND INVERSE PROBLEMS .....	25
1.5.3 – GENERAL STRUCTURE OF INVERSE METHODS.....	29
1.5.4 - SUMMARY OF INTERPRETATIONS OF PROBABILITY .....	32
1.5.5 – CONDITIONING TRANSIENT GROUNDWATER FLOW .....	33
1.5.6 – CONDITIONING MULTIPLE REALISATIONS .....	34
<b>1.6 - THESIS CONTRIBUTIONS.....</b>	<b>35</b>
<b>2 - FINITE ELEMENT FORMULATION FOR GROUNDWATER FLOW IN DISCRETE FRACTURE NETWORKS.....</b>	<b>37</b>

<b>2.1 – CALCULATING THE PRESSURE OVER TWO INTERSECTING FRACTURES.....</b>	<b>38</b>
2.1.1 – ALGORITHM TO CALCULATE THE PRESSURE FIELD OVER TWO INTERSECTING FRACTURES USING THE FINITE ELEMENT APPROACH...46	
2.1.2 – ONE DIMENSIONAL EXAMPLE .....	48
<b>2.2 – CALCULATING THE PRESSURE AT FRACTURE INTERSECTIONS IN A DISCRETE FRACTURE NETWORK .....</b>	<b>56</b>
<b>2.3 – NUMERICAL MODEL OF A PUMPING BOREHOLE .....</b>	<b>59</b>
<b>2.4 –ALGORITHM TO CALCULATE THE PRESSURE AT FRACTURE INTERSECTIONS IN A DISCRETE FRACTURE NETWORK USING THE FINITE ELEMENT APPROACH.....</b>	<b>65</b>
<b>2.5 – COMPARISON OF THE BASIS FUNCTION APPROACH TO A STANDARD FINITE ELEMENT APPROACH .....</b>	<b>66</b>
<b>3 - DEVELOPMENT OF THE BASIS VECTOR CONDITIONING METHOD.....</b>	<b>70</b>
3.1 – SUMMARY OF CLIFFE AND JACKSON’S CONDITIONING METHOD.....	70
3.2 – OUTLINE OF THE BASIS VECTOR CONDITIONING METHOD .....	73
3.3 – CONDITIONING ON FRACTURE LOG TRANSMISSIVITIES .....	77
3.4 CONDITIONING ON LINEAR CONSTRAINTS .....	85
3.5 – INTRODUCTION TO THE ADJOINT METHOD .....	90
3.7 – CONDITIONING ON PRESSURES WHEN VARIABILITY IS LARGE.....	96
<b>4 – RESULTS OF THE BASIS VECTOR CONDITIONING METHOD .....</b>	<b>101</b>
4.1 – SIMPLE TEST CASES.....	102
4.1.1 - TEST CASE 1.....	103
4.1.2 - TEST CASE 2.....	107
4.1.3 - TEST CASE 3.....	109
4.1.4 - TEST CASE 4.....	112
4.1.3.1 - MULTIPLE SOLUTIONS IN TEST CASE 4.....	115

<b>4.2 OLKILUOTO TEST CASE 1.....</b>	<b>119</b>
4.2.1 - SENSITIVITY ANALYSIS .....	134
4.2.2 – CONDITIONED FRACTURE TRANSMISSIVITIES .....	139
4.2.3 - CONDITIONING ON DIFFERENT SETS OF FRACTURE TRANSMISSIVITIES .....	147
<b>4.3 - CHAPTER SUMMARY AND CONCLUSIONS .....</b>	<b>151</b>
<b>5 – BAYESIAN CONDITIONING METHOD .....</b>	<b>156</b>
<b>5.1 - MATHEMATICAL FORMULATION OF THE BAYESIAN CONDITIONING METHOD.....</b>	<b>156</b>
<b>5.2 – BAYESIAN CONDITIONING USING OLKILUOTO TEST CASE 1.....</b>	<b>163</b>
5.2.1 – DEVELOPMENT OF A NUMERICAL ALGORITHM TO IMPROVE RESULTS FROM THE BAYESIAN CONDITIONING METHOD .....	167
5.2.2 - CONDITIONED FRACTURE SETS.....	175
<b>5.3 – OLKILUOTO TEST CASE 2.....</b>	<b>183</b>
5.3.1 OLKILUOTO TEST CASE 2a .....	185
5.3.2 – OLKILUOTO TEST CASE 2b.....	192
<b>5.4 - CHAPTER SUMMARY AND CONCLUSIONS .....</b>	<b>196</b>
<b>6 – SUMMARY AND CONCLUSIONS.....</b>	<b>199</b>
<b>APPENDIX A: MODIFICATION OF THE SENSITIVITIES TO HANDLE MULTIPLE BOREHOLE INTERSECTIONS .....</b>	<b>207</b>
<b>REFERENCES .....</b>	<b>214</b>

# 1 – INTRODUCTION AND LITERATURE REVIEW

Many geological formations consist of crystalline rocks that have very low permeability but allow flow through an interconnected network of fractures.

Understanding the flow of groundwater through such formations is important to a number of industries worldwide, including the nuclear and hydrocarbon industries. This thesis focuses on developing methods for assigning transmissivities to the fractures in a fracture network model so as to obtain a good match to quantities (such as pressure) that can be measured at boreholes. Here we shall concentrate on applications to the nuclear industry, though our conditioning methods can be exploited in other areas of application.

In many countries the civil nuclear industry is investigating the feasibility of long term disposal of radioactive waste in repositories located deep in geological formations consisting of mostly crystalline rock. The main transport route to the surface environment, if waste were to leak from its container, would be through groundwater flow. Crystalline rock has a very low permeability and is frequently fractured. In this setting, groundwater flow occurs through the network of fractures. When there is no interaction between the flow in the fractures and the surrounding rock matrix, this is known as a discrete fracture network (DFN).

In order to develop a DFN model we borrow terminology and ideas that describe flow in a continuous porous medium (CPM). Indeed, CPM models can be used as

an alternative to DFN models when modelling the area surrounding a nuclear waste repository. Thus, this chapter explains the basics of flow in a CPM and also discusses the merits of DFN and CPM approaches to modelling groundwater flow in geological rocks.

A DFN approach is most suitable for modelling flow in crystalline rock in the area close to a nuclear waste repository because at this scale flow will primarily occur through fractures in the rock (whose location may also be known). The basic theory and modelling assumptions of flow in a single fracture and in a DFN are described. The generation of a DFN and its connectivity is then discussed in this chapter. With a DFN in place one must consider how to solve for the pressure within this complicated geometry. Both finite difference and finite element methods can be exploited, though in this thesis we focus on a finite element formulation of the problem which solves for a pressure distribution across the DFN. It is these pressures that should agree with available pressure measurements for the model to be considered as an accurate representation of the physical process. The flow in the network can be obtained by applying Darcy's law to the pressure values in the DFN. Though not part of this thesis, when flow has been solved for in the DFN particle transport calculations can also be made.

When a DFN model has been generated, the model parameters (fracture transmissivities) should be calibrated so that the calculated pressures at measurement points agree with measured pressure values. This conditioning procedure is similar to existing inverse methods. These inverse methods condition transmissivity fields on measured transmissivities, pressures or flows in CPMs. However, there are no existing methods for conditioning fracture transmissivities

in a DFN and this is the purpose of the newly proposed conditioning methods presented in this thesis.

Our problem can be summarised in a continuous setting (before discretisation of the domain) as follows

Determine a field  $\mathbf{T}$  such that we find,

$$\min \left\| \mathbf{P}(\mathbf{x}_M) - \mathbf{P}_M \right\| ,$$

under the constraint,

$$\nabla \cdot (\mathbf{T} \nabla \mathbf{P}) = \mathbf{0}, \quad \text{in } \Omega,$$

subject to appropriate boundary conditions,

(1.1)

where  $\mathbf{T}$  is a vector of fracture transmissivities (containing hundreds or even thousands of fracture transmissivities),  $\mathbf{P}_M$  is a vector of measured pressures which are to be matched,  $\mathbf{P}$  is a vector of calculated pressures,  $\mathbf{x}_M$  denotes the measurement points,  $\Omega$  is the domain of the fracture network and  $\|\cdot\|$  denotes the Euclidean norm. Generally, there are far fewer pressure measurements than fracture transmissivities. Boundary conditions are imposed on the boundaries of the problem domain  $\Omega$  and on fracture intersections and are fully explained in chapter 2. The constraint in (1.1) is the steady state groundwater flow equation and is formally introduced in the next section.

Section 1.1 of this chapter describes the basics of flow in a CPM and introduces the necessary terminology and equations. Section 1.2 discusses the different approaches that can be used to model the area surrounding a nuclear waste repository. The merits of these approaches and the scales on which they are most relevant are discussed and it is explained why we take a DFN approach. Thus, section 1.3 focuses on a DFN approach and describes how one can be generated

with given flow properties. The numerical methods that can be utilised to solve for pressure distributions and flow in a DFN are discussed in section 1.4. Finally, section 1.5 discusses how groundwater flow models are conditioned and introduces inverse methods for CPMs from which we borrow many ideas for our new conditioning methods for conditioning fracture transmissivities in a DFN.

## 1.1 – INTRODUCTION TO FLOW IN A POROUS MEDIUM

This section provides an introduction to the basic concepts of flow in a continuous porous medium relevant to the work in this thesis. A more detailed description can be found in either Bear (1972) or Delleur (1999). A porous medium is a medium that is a solid material containing pores (or void spaces) through which fluid can flow, provided the pore space is interconnected. The porosity  $n$ , of a material is defined as the volume of the pore space in the material  $V_p$ , divided by the total volume  $V_t$ , of both pores and solid material, i.e. ,

$$n = \frac{V_p}{V_t}. \quad (1.2)$$

We now consider the flow of groundwater through a porous medium. A measure of the compressibility of a fluid is given by its isothermal compressibility  $\beta$ . At a constant mass and at constant room temperature, the isothermal compressibility of water  $\beta_w$  (Domenico and Schwartz 1990) has a very low value and thus it is common in groundwater flow calculations to assume that water is incompressible.

Hydraulic head  $h$ , is a common measurement used in hydrogeology and is often used instead of pressure measurements. It is defined at a point as

$$h = Z + \frac{P_G}{\rho g}, \quad (1.3)$$

where  $Z$  is the elevation head, which is the vertical distance of the reference point at which  $h$  is measured above a datum point,  $\rho$  is the density of water,  $P_G$  is the groundwater pressure and  $g$  is gravitational acceleration. The term  $\rho g$  represents the specific weight of water. Equation (1.3) is more commonly stated as

$$h = Z + \Psi, \quad (1.4)$$

where  $\Psi$  is called the pressure head. Hydraulic head has the dimension of length. Details of this relationship are explained in Bear (1972). It is also common in groundwater calculations to use the residual pressure  $P$  defined as

$$P = P_G + \rho g Z. \quad (1.5)$$

The dynamic viscosity  $\mu$  of a fluid gives a measure of the resistance of the fluid to flow. For scalar values, it is equal to the ratio of shearing stress  $\tau$  to the velocity gradient in the fluid. For a fluid flowing past a solid boundary, the shearing stress is defined as the stress applied to the fluid which acts in a parallel

direction to the boundary. The velocity gradient is denoted  $\frac{dV_x}{dz}$ , where  $x$  is the direction of the fluid flow and  $z$  is the axis normal to the boundary. Thus, the dynamic viscosity  $\mu$  is defined as

$$\mu = \tau / \left( \frac{dV_x}{dz} \right). \quad (1.6)$$

It should be noted that this explanation assumes scalar values. For three-dimensional flow, the shearing stress tensor  $\tau_{ij}$ ,  $i, j = 1, \dots, 3$ , is related to the components of the velocity gradient by

$$\tau_{ij} = \mu \left( \frac{dV_i}{dx_j} \right), \quad i, j = 1, \dots, 3. \quad (1.7)$$

The dynamic viscosity  $\mu$  is related to the kinematic viscosity  $\nu$ , by the relationship

$$\mu = \rho \nu. \quad (1.8)$$

### 1.1.1 - THE CONSTITUTIVE RELATIONSHIP AND GOVERNING EQUATION FOR GROUNDWATER FLOW

We start this section by defining some properties of a CPM with respect to its hydraulic conductivity. A CPM is said to be homogeneous with respect to its hydraulic conductivity if the hydraulic conductivity is independent of position in the CPM. Otherwise the CPM is heterogeneous with respect to the hydraulic conductivity. A CPM is said to be isotropic with respect to its hydraulic conductivity if the hydraulic conductivity is independent of direction within the medium. If the hydraulic conductivity varies with direction at any point within the CPM then the CPM is said to be anisotropic.

One of the most important equations in the study of groundwater flow is Darcy's law. This provides a constitutive relationship of the volumetric flow rate, and the head gradient; written in 3D form, we have

$$\mathbf{q} = -\mathbf{K}\nabla h . \quad (1.9)$$

where  $\nabla$  is the three dimensional gradient operator,  $\mathbf{q}$  represents the three dimensional volumetric flow rate per unit area,  $\mathbf{K}$  is a  $3 \times 3$  matrix, which we assume is written as  $\mathbf{K} = K\mathbf{I}$ , where  $K$  is a coefficient of proportionality, called the hydraulic conductivity, with units of length divided by time, and  $\mathbf{I}$  is the  $3 \times 3$  identity matrix. Thus, equation (1.9) represents an isotropic, homogeneous medium. For the case of a heterogeneous, anisotropic CPM,  $\mathbf{K}$  would be a full matrix. Darcy (1856) performed experiments on the filtration of water through

sand columns and discovered that the rate of flow through a sand column was proportional to the loss of head and empirically stated Darcy's law. It is possible to derive Darcy's Law from the Navier-Stokes equations (Neuman 1977).

Furthermore, Bear (1972) gives derivations of Darcy's law for flow in capillary tube models, pipes and open channels. A generalisation of Darcy's law describing the flow of a fluid in a porous medium when the fluid has a variable density (and viscosity) can be found in Bear (1972) or Delleur (1999).

Darcy's law (1.9) defines the hydraulic conductivity  $K$  as the volumetric flow rate per unit head gradient. Hydraulic conductivity describes the properties of both the medium and the fluid flowing through it and is expressed as

$$K = \frac{k\rho g}{\mu}, \quad (1.10)$$

where  $k$  is the intrinsic permeability which is the fundamental property describing the ease with which a porous medium will transmit a fluid and has units of length squared. Different empirical approximations have been suggested such as

$$k = Cd^2, \quad (1.11)$$

by Krumbein and Monk (1943), where  $d$  is the average pore diameter and  $C$  is an empirical constant dependent upon packing and sorting of the pores. Other empirical approximations have been suggested, for example, by Archie (1942). The intrinsic permeability is dependent on the geometry of the porous medium.

When considering layers of porous media, it is more common to use the term transmissivity  $T$  which describes the ease with which a fluid moves through a large porous medium body, such as a horizontal or layered aquifer where the thickness of the aquifer is small compared to its lateral extent. If the  $z$ -axis is taken to be perpendicular to the direction of flow, the transmissivity  $T$  is defined as the product of the average (over a vertical line parallel to the  $z$  axis) hydraulic conductivity  $\bar{K}$  and aquifer thickness  $b$ . Accordingly,

$$T = \bar{K}b, \quad (1.12)$$

where

$$\bar{K} = \int_0^b K(z) dz. \quad (1.13)$$

In a homogeneous, isotropic aquifer (1.12) simplifies to

$$T = Kb. \quad (1.14)$$

Transmissivity has units of length squared divided by time. It is useful to use transmissivity when describing fracture properties because  $b$  is taken to be the fracture aperture (distance between the walls of the fracture).

We point out that there there is a range of validity of Darcy's law. The limit of validity of Darcy's law can be stated in terms of the Reynolds number  $Re$

$$Re = \frac{VD}{\nu}, \quad (1.15)$$

where  $V$  is the groundwater velocity,  $\nu$  is the kinematic viscosity of the groundwater and  $D$  is a representative length (often taken to be equal to the average grain diameter of the CPM (Bear and Verruijt 1987)). The Reynolds number is a dimensionless number that expresses the ratio of inertial to viscous forces acting on a fluid. It can be used as a criterion to distinguish between laminar flow occurring at low velocities and turbulent flow at higher velocities. Deviations from Darcy's law occur when inertial forces become effective and when turbulent flow occurs. The Reynolds number at which Darcy's law fails is dependent on the geometry of the porous medium (Lindquist 1933; Bakhmeteff and Feodoroff 1937; Schneebeli 1955). It is generally accepted that Darcy's law is valid as long as the Reynolds number based on average grain diameter does not exceed some value between 1 and 10. Due to the low velocities of groundwater in crystalline rock fractures, the Reynolds number will be less than one and it is safe to assume that Darcy's law holds as long as there are no large flow sources or sinks present.

### 1.1.3 - THE GROUNDWATER FLOW EQUATION

The main equation used to describe the flow of groundwater through a CPM is the groundwater flow equation. It is derived by combining the continuity equation with Darcy's law (1.9). We consider an incompressible fluid (groundwater) in steady state conditions. The continuity equation is given as

$$\nabla \cdot \mathbf{q} = 0, \quad (1.16)$$

where  $\cdot$  denotes the dot product. Then inserting Darcy's law (1.9) into the continuity equation (1.16) we obtain the steady state groundwater flow equation, namely,

$$\nabla \cdot (\mathbf{K}(\nabla h)) = \mathbf{0}. \quad (1.17)$$

In a fracture with a constant aperture  $b$  (1.17) can be written in terms of the residual pressure  $P$  as

$$\nabla \cdot \left( \frac{1}{\rho g} \mathbf{T}(\nabla P) \right) = \mathbf{0}. \quad (1.18)$$

For an alternative version of the groundwater flow equation derived for the transient case with a compressible fluid, see Bear and Verruijt (1987) or Delleur (1999).

The continuum approach to solving groundwater flow problems breaks down at the microscopic level. That is, when looking at a small enough volume, the concept of a porous medium is no longer valid. At the microscopic level, a point is either located in a pore or is part of the solid material and the porosity (1.2) becomes either 1 or 0. Similarly, all the subsequent equations in this section break down. This ambiguity is avoided by considering only macroscopic properties, where the average behaviour is described. In this setting, it does not matter whether a point belongs to the solid space or the pore space. This approach was addressed by Bear (1972) who developed the concept of a representative elementary volume (REV). The size of the REV is not determined but is assumed

that it is much larger than the pore scale and much smaller than the scale of the porous medium. Macroscopic variables, such as  $K$ , are defined as average values over the REV.

## **1.2 - REPRESENTATION OF THE GEOLOGICAL AREA SURROUNDING UNDERGROUND NUCLEAR WASTE REPOSITORIES**

When considering nuclear waste disposal in underground repositories the main transport route to the surface environment, if waste were to leak from its container, would be through groundwater flow. The simplest possible approach is to model the surrounding rock as a CPM with homogeneous hydraulic conductivity. In this case the steady state groundwater flow equation (1.17) would be solved for the pressure at each point in the medium along with appropriate boundary conditions (such as constant pressure at boundaries or prescribed inflow to a boundary) and possibly flow source/sink terms in the domain. The approach of approximating the surrounding geological area as a single continuum with a homogenous hydraulic conductivity field is not sufficiently accurate as the surrounding area will consist of different media, each with separate hydraulic conductivity values and separate properties such as fracturing.

Alternatively, models have been developed where different porous media can be modelled by assuming that the hydraulic conductivity field is heterogeneous and using the appropriate version of the groundwater flow equation (1.17) to solve for

the flow (Bear and Verruijt 1987). This approach assumes that there is a known analytic value for each term of the transmissivity tensor. The drawback of this CPM approach is that it cannot model small individual fractures in the domain, which despite being small can provide a key route for groundwater flow and dispersion of waste particles.

The choice of a CPM or DFN model is dependent on the scale of the problem and the geometry of the fracture system. CPM models should be used for rock masses with no fractures or with many fractures. The behaviour for a rock mass with many fractures is established through equivalent properties (Marsily 1997; Adler and Thovert 1999; Bogdanov, Mourzenko et al. 2003); that is, properties that are averaged over a given volume or area. CPM models fail to account for large scale fractures in a rock mass which will provide major flow routes through the rock. The DFN approach is most suitable for moderately fractured rock masses. DFN models have the advantage that they correctly describe the physical nature of flow in a fractured rock. However, they are limited by the fact that the true fracture geometry and hydraulic properties are largely unknown. A DFN model can be combined with a CPM model where flow and solute transfer occurs between the boundaries of the CPM and the DFN (Grisak and Pickens 1980; Huyakorn, Lester et al. 1983). This approach is best used when there are a small number of large scale fractures in the domain.

The scale at which a site is modelled will determine the amount of fracturing that is included in the numerical model. Fractures exist on a wide range of scales from  $10^{-6}$  m to  $10^4$  m. Throughout this scale range the fractures have a significant effect on flow properties.

Bear (1993) defined four scales in a fractured medium where different approaches can be applied. They are the very-near field scale, the near field scale, the far field scale and the very-far field scale. The very-near field scale is where flow and solute transport is dominated by a single fracture. At the near field scale, flow and transport are dominated by a few well defined fractures. The interaction between the fractures and the rock matrix may play a role. In the near field scale, major fractures are usually defined deterministically and minor fractures are determined stochastically. At the far-field scale, multiple continua are used to represent the rock matrix, the major fractures and the minor fractures. At the very-far-field scale, a single continuum is used to represent the fractured medium with equivalent physical properties representing the average value over the medium. The modelling of fractured crystalline rock as a DFN as investigated in this thesis is at the near field scale. When using a near field approach it is common practice for large scale fractures to be inserted into a model deterministically, but the majority of fractures will be treated stochastically (Hartley, Holton et al. 2008). Selroos et al. (2001) suggested that at a large regional scale, flow should be modelled by a stochastic continuum approach, originally proposed by Neuman (1987), whilst at a smaller site scale a DFN model should be used. These two approaches can then be combined into one model.

The stochastic field approach is based on the fact that detailed field measurements in fractured rocks represent volumes which are often intersected by few fractures. It is argued that it is not feasible to interpret these measurements using DFN models. Instead, the tests are interpreted by treating the rock as a locally uniform continuum. This results in bulk transmissivities that vary erratically from one test

interval to another. Thus, it is best if measurements can be taken at regular intervals.

Potential sites for underground nuclear waste repositories have different rock types such as clay (which is not fractured), granitic or crystalline rock (Witherspoon 1991; Witherspoon 1996; Witherspoon and Bodvarsson 2001; Witherspoon and Bodvarsson 2006). This thesis focuses on crystalline rock where data is available to us from such sites.

The exchange of solute mass (through molecular diffusion) between fluid in the fractures and fluid in the rock matrix is called matrix diffusion. If fractures were to interact with the rock matrix it is through matrix diffusion. In radioactive waste disposal, the study of matrix diffusion involves the exchange of radionuclides from the fractures to the rock matrix. Grisak and Pickens (1980) concluded that matrix diffusion is negligible in solute transport studies in fractured media if the rock matrix has a very low porosity and, consequently, there is very little storage space.

Crystalline rock is a very impermeable material and is frequently fractured. While there will be an interaction between flow in fractures and the surrounding rock matrix in other rock types, a good modelling assumption for crystalline rock is that groundwater flow occurs only through the interconnected fracture network. This assumption is based on the fact that dense crystalline rock has a small porosity value (Freeze and Cherry 1979) and from this we conclude that matrix diffusion does not play an important role. Therefore, crystalline rock can be modelled as a DFN where the rock matrix is assumed to be impermeable and the fractures do not interact with it in any way.

Generally, it is assumed that the fractures have a higher transmissivity than the rock matrix and provide the main transport route for groundwater. Fracture networks are also of interest when fracture transmissivities are lower than that of the surrounding rock matrix. They then act as potential barriers to groundwater flow. This area has been studied by Neuman and Simpson (1985) and Neuman and Neretnieks (1990).

### **1.3 – GENERATION OF A DISCRETE FRACTURE NETWORK MODEL AND ITS FLOW PROPERTIES**

In this section we focus on the DFN approach to modelling crystalline rock around a nuclear waste repository. Firstly, flow in a single fracture is considered after which the generation of fractures networks and their flow properties are discussed.

#### **1.3.1 - FLOW IN A SINGLE FRACTURE**

Before considering a fracture network it is important to consider the flow in a single fracture. The classical view of a rock fracture is that it comprises of a pair of smooth, parallel plates. In reality the roughness of rock fracture surfaces is usually irregular. We first consider the parallel plate model of a fracture where the fracture walls are represented as two smooth parallel plates. Groundwater is assumed to be a viscous incompressible fluid and is flowing in a channel between

the two parallel plates. Thus, the groundwater motion can be described by the Navier-Stokes equations. An important relationship known as the cubic law can then be derived (Bear 1972) from the Navier-Stokes equations. Indeed, this states that the transmissivity  $T$  of a fracture is proportional to the cube of the fracture aperture  $b$  (the distance between the walls of the fracture), i.e. ,

$$T = \frac{\rho g b^3}{12\mu}, \quad (1.19)$$

where  $\rho$  is the density of groundwater,  $g$  is gravitational acceleration and  $\mu$  is the dynamic viscosity of water. This transmissivity value is then used to in the groundwater flow equation (1.18).

The critical assumption of the cubic law is that the aperture is constant across a fracture. Zimmerman and Bodvarsson (1996) give an analytic analysis to the problem of fluid flow through rock fractures. They show that if the aperture varies as a continuous function across a fracture surface, then the Reynolds lubrication model can be used to solve for the pressure across that fracture. Under the assumption that viscous forces dominate inertial forces and changes in aperture across the fracture occur gradually, the Navier-Stokes equations reduces to Reynolds lubrication equation. Thus, if we consider a fracture where the aperture varies in the  $z$ -plane the lubrication model is

$$\nabla \cdot [b^3(x, y)\nabla P(x, y)] = 0, \quad (1.20)$$

where  $b^3(x, y)$  denotes the cube of the fracture aperture as a function of its position in the  $x - y$  plane.

This approach is limited in that we assume there is a gradual change in the fracture aperture. Alternatively, wall roughness can be represented by splitting a fracture into grid blocks. Each block is assigned a different aperture value and it is assumed that the cubic law holds locally in each grid.

Nordqvist, Tsang et al. (1992) developed a variable aperture fracture network model using a fracture network of circular discs randomly and independently distributed in space. Each individual fracture was divided into grid blocks with different aperture values. The cubic law was assumed to hold on each individual block and the pressure difference between two adjacent nodes could be calculated due to this assumption. Additionally, the model assumed there was conservation of mass between adjacent blocks. Particles were inserted at one face of the cubic domain where they were transported due to flow across the fracture network. Breakthrough curves were plotted for the particles and showed dispersion on two levels. There was a small scale level of dispersion as a result of the variable aperture nature of the fractures and a larger scale level of dispersion as a result of the number of different transport routes through the network.

Tsang and Tsang (1987) noted that experimental evidence of channelling in fractures suggested the cubic law to be invalid and proposed a channel model of flow through fractures. They characterised channels by an aperture density distribution and a spatial correlation length. The pressure profile and tracer breakthrough curves were obtained for a single fracture.

Moreno, Tsang et al. (1988) modelled flow and solute transport through a single fracture discretised into a square mesh to which variable apertures were assigned.

Their calculations showed that flow occurred in preferred paths or channels. The solute transport was calculated using a particle tracking method. The spatial and time variations of tracer breakthrough were shown; these results were found to be dependent on the aperture density function.

Problems arise with how fracture apertures are measured in a variable aperture fracture due to the geometries of the fracture surfaces (Ge 1997). However, this problem does not occur when using a parallel plate model of a fracture.

In our case we do not have nearly enough information about the geometry of individual fracture surfaces. We are dealing with hundreds or even thousands of fractures with a limited number of measurement values, so it is impossible to have a detailed enough picture of the individual fractures to take advantage of variable aperture models. Instead, when dealing with a large fracture network where information on the fractures is scarce, it is desirable to use simple models of the individual fractures, one of which is the parallel plate model.

### 1.3.2 - PROPERTIES OF DISCRETE FRACTURE NETWORKS

Fracture networks can be characterised geometrically by their length, orientation, location, density and aperture value. These geometric properties are obtained from statistical distributions. Recent studies show that power law distributions describe many fracture properties and spatial distributions (Bonnet et al. 2001), including fracture length (Dreuzy et al. 2001), density and aperture.

A power law distribution  $n(w)$ , where  $w$  refers to the fracture property of interest (length, orientation etc.) is of the form

$$n(w) = Aw^{-a}, \quad (1.21)$$

where both  $A$  and  $a$  are positive constants. Other distributions such as lognormal, exponential and gamma distributions can also be used to adequately describe fracture properties. The distributions that are used and their parameters are site specific. That is they are dependent on the geology of the site. For example, the rock type and the stresses exerted on the rock will determine the value of the distribution parameters. The length scale over which power laws adequately describe fracture properties varies depending on the parameters used. Bonnet, Bour et al. (2001) show parameter values used for power laws in previous publications for different length scales and sites; these values vary widely. A discussion of fractal characterizations of fracture networks is given in Bonnet, Bour et al. (2001).

We are mostly interested in the distributions of fracture transmissivities. These are related to the fracture aperture by the cubic law (1.19). Bonnet, Bour et al. (2001) noted that fracture aperture distributions can be described as both log-normal (Snow 1970) and power law (Marrett 1996). The distribution that best describes the mean value and spread of aperture values will be dependent on the site being studied.

The connectivity is a critical property of a fracture network. Percolation theory can be used to characterise the connectivity of a fracture network (Berkowitz and Ewing 1998). The percolation threshold is defined as the density of fractures

above which the connectivity of fractures is sufficient to permit flow through a portion of the network from one side of the network domain to the other.

Experiments have shown that there is strong evidence of channelling and highly preferential flow paths in individual fractures (as previously discussed) and in fracture networks (Nordqvist, Tsang et al. 1992). Cacas, LeDoux et al. (1990), (1990) suggested that the channelling found in fracture networks is due to a broad distribution of fracture transmissivities.

Sometimes DFNs are generated by placing all the fractures into the model deterministically with no stochastic treatment. Fractures can be placed in the model to correspond to known observations at a test site. For example, Kurtzman, Nativ et al. (2007) used deterministic fractures in a DFN model, the location of which were based on the observation that flow mainly occurred at a given fracture outcrop.

## **1.4 - NUMERICAL MODELLING OF GROUNDWATER FLOW IN A FRACTURE NETWORK**

The groundwater flow equation (1.17) can be solved analytically for simple domains and boundary conditions (Tolikas, Sidiropoulos et al. 1984). For any physically realistic cases it must be solved computationally. An extensive description of numerical methods that can be used to model fractured rock is given by Jing (2003).

Finite Difference Methods (FDM) can be used to numerically model CPMs (McDonald and Harbaugh 1988). Due to the regular grid systems used in regular FDMs it is difficult to model fracture systems with complex geometries using a regular FDM. Finite volume methods have also been developed to model DFNs (Jing 2003). However, we shall focus on the FE approach to modelling a DFN as the existing code available to us takes this approach.

The FEM is the most well known discretisation technique used in DFN flow models (Jing 2003). The basic concept is that individual fractures are represented as planar shapes such as circular discs (Cacas, Ledoux et al. 1990; Cacas, Ledoux et al. 1990; Nordqvist, Tsang et al. 1992) or rectangles (Hartley, Holton et al. 2008) in a domain. A FEM mesh is imposed over individual fractures and the flow or pressure equations are solved. The transmissivity field within an individual fracture can be constant or can be spatially distributed. Fracture intersections are discretised and boundary conditions are imposed on the nodes representing the fracture intersections. The FE discretisation used in this thesis is described fully in chapter 2.

Huyakorn et al. (1983) provided early FE techniques used for modelling groundwater flow in fractured aquifers. They considered four different small scale conceptual models to investigate flow interaction between fractures and a rock matrix. An extended version of the transient groundwater flow equation which included a term representing the interaction between a porous rock matrix and fractures was used. Their FEM was based on a Galerkin discretisation of the flow in the fractures. Analytic solutions were available for the four models and it was found that the numerical models gave a close match to them using relatively coarse discretisations.

Grisak and Pickens (1980) considered matrix diffusion by modelling a single two dimensional fracture at the centre of matrix blocks. They modelled uni-directional flow in the fracture of a porous medium. The effect of matrix diffusion was approximated using the one dimensional version of Fick's second law of diffusion. The flow equations including a matrix diffusion term were solved using a FE approach. The computed FE solutions gave a good agreement to available analytic solutions.

In our work we employ the FE approach and use the FE code NAPSAC (Hartley, Holton et al. 2008). NAPSAC is a software package that models flow and transport through fractured rock. The models are based on a direct representation of the discrete fractures making up the flow-conducting network. NAPSAC uses a stochastic approach to generate networks of planes that have the same statistical properties as those that are measured for fractures in field experiments. The software allows for the flow through many thousands of fractures to be calculated accurately and for deterministic fractures to be included in a model domain.

## **1.5 - CONDITIONING A GROUNDWATER FLOW MODEL**

Calibration is the process of modifying or tuning the input parameters to a model until the output from the model matches observed data. We need to calibrate our computational model of a fracture network to ensure that the output matches measured values. This is done by conditioning fracture log transmissivities in the model based on the available measurements, ensuring that if a quantity corresponding to a measurement is computed in the model, it agrees with the

observed value (or matches the observed value as closely as possible). The log of fracture transmissivities are used because it ensures that conditioned fracture transmissivities have a positive value and are physically admissible.

A transmissivity field can be conditioned on measured transmissivity values using a linear interpolation method known as kriging. However, conditioning fracture transmissivities on pressure or flow values is a more complex problem because the measurements are not linearly related to the fracture transmissivities and they are dependent on all the fracture transmissivities in the network.

Conditioning is closely related to the inverse problem. This is where model parameters are obtained from observed data. The inverse method approach is exploited in many fields, here we are interested in using it in a hydrogeological setting. Indeed, our new conditioning methods use ideas from existing hydrogeological inverse methods in a CPM setting and develop them for a DFN setting. It should be noted that one approach is to approximate a fracture network as a CPM and then condition the transmissivities in the CPM setting (Yager 1997; Tiedeman, Goode et al. 1998). However, we consider conditioning fracture transmissivities in a DFN.

In this section we briefly introduce kriging and then go on to describe the ideas behind inverse methods in hydrogeology and how they relate to our new conditioning methods.

### 1.5.1 – CONDITIONING POROUS MEDIUM MODELS AND INVERSE PROBLEMS

A transmissivity field can be conditioned on measured transmissivity values by an interpolation technique known as kriging ( Journel and Huijbregts (1978); Isaaks and Srivastava (1989) ). Kriging is a regression technique used in geostatistics to approximate or interpolate data. Experimental data to be used may consist of a set of  $n$  discrete log transmissivity values  $X_i$ ,  $i = 1, \dots, n$ , (Delhomme 1978).

Kriging produces a linear interpolant between the  $n$  measured values. The kriging interpolant  $X^*$  at a point  $p^*$  obtained from the set of values  $X_i$  at points  $p_i$  is given by the linear combination

$$X^* = \sum_{i=1}^n \lambda_i X_i, \quad (1.22)$$

where  $\lambda_i$ ,  $1 \leq i \leq n$ , are a set of weights obtained by minimising an estimation

variance subject to the condition that  $\sum_{i=1}^n \lambda_i = 1$ .

Pressure values at measurement points are not linearly related to fracture transmissivities and an interpolation method such as kriging cannot be used when conditioning transmissivities on pressure measurements; instead inverse methods are employed. Inverse methods have also been developed in many fields but we shall focus on their development in the context of groundwater flow. For a concise description of the inverse method in this setting see for example, Sun

(1999). Alternatively, Chavent (2009) gives a good description of the mathematical foundations of the inverse method.

We consider a groundwater system governed by a PDE with parameters embedded in the equation which are spatially dependent. The inverse problem of parameter identification concerns the optimal determination of the parameters by observing the output of the dependent variable in the spatial and time domains (Yeh 1986).

As an example, consider a heterogeneous aquifer where the transmissivity field contains the parameters we seek. The spatial domain is continuous and the dimension of the parameter is theoretically infinite. However, we need to use a finite number of parameters. Parameterisation is the reduction of the number of parameters from the infinite dimension to a finite dimensional form. Our work is based in a DFN setting and the model parameters are the fracture transmissivities. They are constant on each fracture and the number of parameters is finite and equal to the number of fractures in the DFN model.

After parameterisation the model parameters are constant and deterministic.

However, this deterministic approach does not capture the variability of a distributed parameter. To remedy this, the model parameter can be represented as a random function with given properties such as a mean and variance. In our work random functions are characterised by the stochastic law where they are solely defined by their mean and covariance values. The inverse method is then used to identify these properties. In groundwater modelling, the parameter of interest is often the log transmissivity field. A prior estimation of the log transmissivity field can be used in a least squares minimisation problem of fitting pressure observations (Neuman and Yakowitz 1979). Stochastic inverse methods have

been used in two-dimensional steady flow problems (Hoeksema and Kitanidis 1984) and transient groundwater flow problems (Sun and Yeh 1985). The distribution of the initial fracture transmissivities is dependent on the site being modelled and the data available.

The inverse problem is often ill-posed by definition of Hadamard (1902). For our problem of interest, a set of fracture transmissivities that yield the measured pressures need not be a unique solution. In other words, there may be many sets of fracture transmissivities that produce the same set of measured pressure values. Additionally, the model parameters can be unstable. That is, small errors in pressure measurements will greatly alter the values of the identified transmissivities (Chavent 1974).

Inverse methods can be classified under one of two error criteria (Neuman 1973) used in the formulation of the inverse problem; the direct method (also termed the equation error criterion) or the indirect method (also termed output error criterion).

The available literature of inverse methods for groundwater flow systems use a CPM model or they use a CPM to approximate a fractured medium (Yager 1997; Tiedeman, Goode et al. 1998). An exception is recent work by Frampton and Cvetkovic (2010) who condition the parameters of a fracture transmissivity distribution in a DFN setting, but they do not condition fracture transmissivities directly. The principles of the inverse method are the same in a CPM and DFN setting and the discussion in this section applies to both settings. From hereon we assume that the model parameters are the fracture log transmissivities, contained in the vector  $\mathbf{X}$  and the measurements are pressures contained in the vector  $\mathbf{P}$ .

In the direct method the pressure measurements  $\mathbf{P}_M$  are interpolated across the model domain creating “observations” throughout the system. The governing equation (the groundwater flow equation) is then used to calculate corresponding log transmissivities  $\mathbf{X}$  for all “observations” of  $\mathbf{P}$ . However, the direct method is known to be unstable in the presence of common measurement errors (Yeh 1986). Most recent inverse methods use the indirect method. It acknowledges that measurements contain errors and finds the hydraulic properties that minimise these errors. In this approach,  $\mathbf{X}$  is determined from a limited number of observations scattered in a spatial and possibly space-time domain so that the objective function

$$E = \|\mathbf{P} - \mathbf{P}_M\|^2, \quad (1.23)$$

is minimised, where  $\|\cdot\|$  denotes the Euclidean norm and  $\mathbf{P}_M$  are the measured pressures at the measurement points. When (1.23) is used as an objective function the problem often becomes ill posed. To overcome this an additional term can be added so that the objective function becomes

$$E = \|\mathbf{P} - \mathbf{P}_M\|^2 + \lambda \|\mathbf{X} - \mathbf{X}_0\|^2, \quad (1.24)$$

where  $\mathbf{X}_0$  is an initial guess for the log transmissivities and  $\lambda$  is an unknown positive parameter. For a detailed discussion of how to choose an optimal value of  $\lambda$  see Chavent (2009). The addition of the extra term in (1.24) was first considered in the context of groundwater flow models by Neuman (1973) and was based on the work of Tikhonov (1963). Indeed, the

term in (1.24) can be viewed as a Tikhonov regularisation term (Tikhonov and Arsenin 1977). Other regularisation methods exist and Chavent (2009) provides a summary of these methods.

The minimisation of (1.23) or (1.24) is usually performed using the Levenberg-Marquardt method (Cooley 1985; Hill and Tiedeman 2007). This method is generally accepted to be the most efficient method for non-linear optimisation (Press, Flannery et al. 1986) and is used in the first of our new conditioning methods for the minimisation procedure.

### 1.5.3 – GENERAL STRUCTURE OF INVERSE METHODS

A common approach (Carrera, Alcolea et al. 2005) used to condition  $\mathbf{X}$  on measured pressure values  $\mathbf{P}$  is known as non-linear least squares minimisation. Here,  $\mathbf{P}$  is updated using a linear expression whilst minimising an objective function  $E$ . This linearised expression will be dependent on a sensitivity matrix  $\mathbf{L}_{\mathbf{P}\mathbf{X}}$  (Jacobian matrix) containing the derivatives of  $\mathbf{P}$  with respect to  $\mathbf{X}$ . The objective function  $E$  is usually given by (1.23), and has a non-linear dependence on  $\mathbf{X}$ . It is noted (Carrera, Alcolea et al. 2005) that most conditioning codes for least squares minimisation follow an iterative procedure as outlined below:

1. Initialisation: Read input data, set iteration counter  $i = 0$ , initialise parameters  $\mathbf{X}^0$ .

2. Solve the simulation problem  $\mathbf{P}(\mathbf{X}^i)$ , compute the objective function  $E$ , its gradient  $g$  and the Jacobian matrix  $\mathbf{L}_{\mathbf{pX}}$ .
3. Compute an updating vector  $\mathbf{d}$ , possibly using information on previous iterations, as well as  $g$  and  $\mathbf{L}_{\mathbf{pX}}$ .
4. Update parameters,  $\mathbf{X}^{i+1} = \mathbf{X}^i + \mathbf{d}$ .
5. If convergence of  $E$  has been reached, then stop. Otherwise, set  $i = i + 1$  and return to 2.

The calculation of the sensitivity matrix  $\mathbf{L}_{\mathbf{pX}}$  is vitally important as it is needed to calculate the update to  $\mathbf{P}$  and to calculate  $g$ . There are two main methods that can be used to compute  $\mathbf{L}_{\mathbf{pX}}$  and they are now discussed. Suppose, in a given DFN model, there are  $n$  fracture transmissivities,  $N$  nodes where the pressure is calculated and  $m$  pressure measurements. One approach is to calculate each sensitivity term using a finite difference approximation. This requires  $\mathbf{P}$  to be calculated at each node  $N$  for perturbations in each of the  $n$  fracture transmissivities (i.e.  $n$  solves of the governing pressure equation). The order of matrix operations required is  $O(nN^3)$  (where it has been assumed that Gaussian elimination is used to solve the governing equation).

Alternatively, an adjoint method can be used to calculate the sensitivity terms. It is described fully in chapter 3 as it is used in both of our conditioning methods to calculate sensitivities. An adjoint equation is solved to calculate an adjoint matrix taking  $O(mN^3)$  matrix operations. This adjoint matrix is then used to calculate sensitivities by a matrix multiplication using  $O(mN^2)$  matrix operations.

Therefore, the adjoint method for calculating sensitivities requires  $O(mN^3)$  operations. Thus, the adjoint method is very efficient in large scale models where  $m \ll n$ . The adjoint method is commonly used in models of this nature (Sun and Yeh 1985) and is used in different subject areas such as aeronautics (Giles and Pierce 2000).

The first of our newly proposed methods is based on a method for conditioning hydraulic conductivity in a CPM based on measured hydraulic head (Cliffe and Jackson 2000). This method has been modified for the case of a DFN and is described in detail in chapter 3.

The second conditioning method developed in this thesis takes a Bayesian approach to the conditioning and is described in chapter 5. After applying Bayes's theorem, a mode of the posterior distribution of the fracture log transmissivities is computed. This mode corresponds to the most likely set of fracture log transmissivities that will produce the measured pressures. This is similar to a maximum a posteriori probability approach (Kitanidis 1996) and maximum likelihood approach (Carrera and Neuman 1986). The mathematical setting of a Bayesian approach to the inverse problem for partial differential equations has been thoroughly reviewed by Stuart (2010). This Bayesian conditioning method takes a Bayesian interpretation of probability. As such, the next section briefly summarises some of the main interpretations of probability.

#### 1.5.4 - SUMMARY OF INTERPRETATIONS OF PROBABILITY

The classical view of probability is that an experiment can result in  $N$  mutually exclusive, equally likely outcomes. If  $N_A$  of these outcomes result in the occurrence of the an event  $A$  then the probability of  $A$  is defined as

$$P(A) = \frac{N_A}{N}. \text{ The major problem with the classical view of probability is}$$

that it assumes that there are a finite number of outcomes  $N$  that can be counted, which in many situations is not the case.

The frequentist view of probability is that the probability of an event is the events relative frequency over time. If  $n_A$  denotes the number of observations of an event  $A$  from  $n$  trials then the probability of  $A$  is given

$$\text{by } P(A) = \lim_{n \rightarrow \infty} \frac{n_A}{n}. \text{ The obvious breakdown of the frequentist view is that it}$$

requires an infinite number of trials  $n$  to define a probability, which is impossible.

The Bayesian approach (also known as the subjective view) requires the specification of some prior probability which is updated in light of new data.

The Bayesian view of probability regards probability as the “degree of belief” of the individual assessing the uncertainty of a given situation (Ramsey 1926). For example, in Chapter 5 the “degree of belief” is represented by our initial guess of fracture log transmissivities in our model and these are updated in light of measured pressure data.

For a full discussion on the different interpretations of probability see for example Fine (1973) or Hajek (2010).

### 1.5.5 – CONDITIONING TRANSIENT GROUNDWATER FLOW

The conditioning methods developed in this thesis condition fracture transmissivities on steady state pressure measurements. A possible extension of these conditioning methods is to modify them to condition on transient groundwater flow (this has not actually been done in this thesis, but is mentioned as a natural extension to the existing work). The reason that it would be useful to condition on transient groundwater flow is that in pumping well tests the pressure at a well will vary with time. To model the flow of groundwater with time it is necessary to model groundwater as a compressible fluid. Thus, the aim of conditioning in the transient case is to match a pressure profile over time at a measurement well. The transient groundwater flow equation for pressure  $P$  in a fracture with constant transmissivity  $T$  is

$$\frac{S}{\rho g} \frac{\partial P}{\partial t} = \frac{T}{\rho g} \nabla^2 P, \quad (1.25)$$

where  $S$  is a dimensionless constant known as the fracture storativity. It is defined as the volume of water released from (or added to) storage in the fracture per unit area of fracture and per unit change of the average pressure in the fracture. For the case of a compressible fluid its density will not be constant and is a function of pressure  $\rho = \rho(P)$ .

A DFN would be discretised in the same way as the steady state case and a forward difference could be used to approximate the time derivative in (1.25).

Sensitivities would ideally be calculated at each time step (this may result in long computational times, in which case they may have to be re-calculated after a given number of time steps) from the transient groundwater flow equation (1.25) instead of the steady state version (1.18).

In our steady state conditioning approach we condition the fracture transmissivities on steady state pressure measurements. Thus, it is possible to use these conditioned transmissivities as input to the transient groundwater flow equation (1.25).

#### 1.5.6 – CONDITIONING MULTIPLE REALISATIONS

Locations and properties of fractures at a site are generally unknown. In the case where fracture properties are known they can be inserted into a given model of the site, and the model is called a deterministic model. In the case where fracture properties are unknown it is common for the statistics of the fracture properties to be known (the distribution of fracture orientation or length for example). In what is known as a stochastic model, realisations of the fracture network geometry that exhibit the same statistics as the physical system are generated and used for simulation. Therefore, mean values and variances of fracture properties are analysed using multiple realisations of the fracture network.

There are two approaches that can be taken when conditioning multiple realisations. Firstly, the parameters of the distributions from which fracture transmissivities are generated, are conditioned on available measurements. Secondly, each individual realisation is conditioned. Our conditioning methods are designed for the second approach. Both conditioning methods developed take a DFN with a fixed geometry as their input. This DFN could be a deterministic model or it could be a single realisation from a stochastic model where the geometry is fixed for each realisation.

A high area of uncertainty comes from the geometry of the fractures. When using our conditioning methods in a stochastic model each realisation will have a different geometry. Thus, uncertainty in fracture geometry is dealt with by generating multiple realisations with different geometry, each of which has its fracture transmissivities conditioned on measured pressures.

## **1.6 - THESIS CONTRIBUTIONS**

This thesis develops two numerical conditioning methods that condition fracture transmissivities on pressure measurements in a DFN. The geometry of the DFN is not changed throughout the conditioning procedure. The pressure measurements are steady state pressures and as such steady state flow is assumed in the DFN. Groundwater is assumed to be incompressible due to the low value of the compressibility of water. However, when modelling pumping wells the groundwater needs to be modelled as a compressible fluid for flow to occur. Thus, if considering conditioning on transient pumping well data, this modification would need to be made to the conditioning methods. The conditioning methods

introduced in this thesis are the first to be developed for use in a large scale DFN setting.

The pressure in a DFN was calculated using a finite element code called NAPSAC, made available to us by Serco Assurance. In Chapter 2 we outline the finite element formulation used by NAPSAC to solve the steady state groundwater flow equation in a DFN. This chapter does not contain any original work, however there is no rigorous formulation available of the methods used, and as such this chapter provides a valuable insight into the details of the finite element formulation used by NAPSAC.

Chapter 3 introduces the first conditioning method developed, which we named the basis vector conditioning method. It is based on a previous conditioning method proposed by Cliffe and Jackson (1995; 2000) in a CPM setting. The source code for the basis vector conditioning method was written as a new subroutine in NAPSAC.

Chapter 4 provides results obtained using the basis vector conditioning method on four simple test cases and on a large scale test case which models the site for a potential nuclear waste repository in Finland.

Chapter 5 introduces the second conditioning method that was developed. The source code for this method was also written as a new subroutine in NAPSAC. The method is based on the use of Bayes theorem to calculate the mode of the posterior distribution of fracture transmissivities. This Bayesian conditioning method was used on the same large scale test case as the basis vector conditioning method, as well as two additional large scale test cases.

## **2 - FINITE ELEMENT FORMULATION FOR GROUNDWATER FLOW IN DISCRETE FRACTURE NETWORKS**

In this chapter we outline the finite element (FE) formulation employed within NAPSAC for calculating the pressure in a DFN. Here, individual fractures are discretised into what we call ‘local nodes’ while fracture intersections are subsequently discretised into what are referred to as “global nodes”. Within this formulation, local and global basis functions are assigned to each local and global node, respectively. The construction of the global basis functions differs from that of the local basis functions. At fracture intersections, the pressure is calculated by enforcing conservation of flow at each intersection; the pressure across the network is then approximated as a linear combination of the global basis functions and the pressures on fracture intersections. We refer to this method as the global basis function FE approach. These ideas are formally introduced in section 2.1 which considers the case of calculating the pressure field over two intersecting fractures. The global basis function FE approach to this problem is described and a numerical algorithm for determining the pressure over two intersecting fractures using this FE formulation is given. A simple one dimensional example is used to clarify the techniques employed. The ideas developed in section 2.1 are then extended in section 2.2 to the case of calculating the pressure at fracture intersections in a DFN. Section 2.3 addresses the problem that the analytical solution of a pumping borehole calculates pressure values that vary

logarithmically with the radius from the borehole. When a DFN is discretised into a FE mesh, the FE method will struggle to match the analytic solution close to a pumping borehole due to the asymptotic nature of the logarithm function. Indeed, given the typical mesh size used in the FE discretisation, this scheme can give inaccurate results in the area surrounding a pumping borehole. To remedy this, the analytical and FE solutions can be combined to produce a more accurate numerical model.

The numerical algorithm to calculate the pressure at fracture intersections in a large scale DFN is given in section 2.4. Section 2.5 compares the global basis function FE approach to a standard FE approach where all basis functions have a similar structure and the system is solved as one with flow boundary conditions enforced on fracture intersections (Quarteroni and Valli 1999). Section 2.5 goes on to show that when there is a local node corresponding to every global node in the global basis function FE approach, it is equivalent to a standard FE approach. The benefit of using the global basis function FE approach is that it allows for fracture intersections be discretised using a small number of global nodes which reduces the computational time required to solve for pressure in a DFN. This is vitally important when dealing with large scale DFNs such as ones we use as test cases.

## **2.1 –CALCULATING THE PRESSURE OVER TWO INTERSECTING FRACTURES**

The problem domain  $\Omega$  is partitioned into two non-overlapping sub-domains (that represent two fractures)  $f_1$  and  $f_2$  with boundaries  $\partial f_1$  and

$\partial f_2$ , respectively. The fracture intersection is defined as  $\Gamma := f_1 \cap f_2$ . The residual pressure

$$P = P_G + \rho g (z - z_0), \quad (2.1)$$

is to be calculated across  $f_1$  and  $f_2$ , where  $P_G$  is the groundwater pressure,  $\rho$  is the groundwater density,  $g$  is gravitational acceleration,  $z$  is the

elevation and  $z_0$  is a reference elevation. Defining  $\tilde{T}_f := \frac{T_f}{\rho g}$ , the steady

state groundwater flow equation

$$\nabla \cdot (\tilde{T}_f \nabla P) = 0 \quad (2.2)$$

is solved on each fracture  $f_1$  and  $f_2$  with constant transmissivities  $T_{f_1}$  and  $T_{f_2}$ , respectively, (therefore  $\tilde{T}_f$  is a constant scalar on a fracture  $f$ ) where

$\nabla$  is the two dimensional gradient operator. It is assumed that there are

Dirichlet boundary conditions on the boundaries  $\partial f_1$  and  $\partial f_2$ . At the fracture

intersection the following conditions hold:

1 – The groundwater pressure is continuous between intersecting fractures.

That is  $P|_{f_1 \cap \Gamma} = P|_{f_2 \cap \Gamma}$ .

2 – Groundwater is conserved at an intersection, so that groundwater which flows out of one fracture flows into the other and there is no build up of

groundwater at the intersection. In the continuous setting this is written as

$Q_{f_1} = \tilde{T}_{f_1} \nabla P_{f_1} = Q_{f_2} = \tilde{T}_{f_2} \nabla P_{f_2}$ , where  $Q_{f_1}$  and  $Q_{f_2}$  are the flows coming from  $f_1$  and  $f_2$ , respectively, and  $P_{f_1}$  and  $P_{f_2}$  are the pressures on  $f_1$  and  $f_2$ , respectively.

The FE approach to solving (2.2) on each fracture along with the intersection conditions is now set out. A mesh  $\tau_{f_1} \{ \kappa_{f_1} \}$  is created over  $f_1$  consisting of triangular elements  $\kappa_{f_1}$ . Also,  $N_{f_1}$  is defined to be the set of  $n_{f_1}$  local nodes contained in  $\tau_{f_1}$ . Similarly, a mesh  $\tau_{f_2} \{ \kappa_{f_2} \}$  is created over  $f_2$  consisting of triangular elements  $\kappa_{f_2}$ . The set of local nodes contained in  $\tau_{f_2}$  is denoted by  $N_{f_2}$  and we set  $n_{f_2} = \text{card} \{ N_{f_2} \}$ , where  $\text{card} \{ \cdot \}$  denotes the cardinality.

The fracture intersection  $\Gamma$  is discretised into a set of  $n_\Gamma$  global nodes, denoted by  $N_\Gamma$ . For simplicity, we assume that each global node on the fracture intersection  $\Gamma$  corresponds to a local node on  $f_1$  and  $f_2$ . That is, we define the set of global nodes as  $N_\Gamma := N_{f_1} \cap N_{f_2}$ . This requires  $\tau_{f_1}$  and  $\tau_{f_2}$  to match on  $\Gamma$ . To formalise this statement, let  $\varepsilon_{f_i}$ ,  $i = 1, 2$  denote the set of edges in  $\tau_{f_i}$ . Then it is necessary that  $\Gamma \subset \varepsilon_{f_1}$  and  $\Gamma \subset \varepsilon_{f_2}$ . Furthermore,

$\exists \varepsilon_{\Gamma_{f_1}} \in \varepsilon_{f_1}$  such that  $\cup \varepsilon_{\Gamma_{f_1}} = \Gamma$  and  $\varepsilon_{\Gamma_{f_2}} \in \varepsilon_{f_2}$  such that  $\cup \varepsilon_{\Gamma_{f_2}} = \Gamma$  and

assume  $\varepsilon_{\Gamma_{f_1}} = \varepsilon_{\Gamma_{f_2}}$ . This implies that the set of local nodes from  $f_1$  and  $f_2$

are identical on the intersection  $\Gamma$ .

The local piecewise linear basis function  $\phi_i^{f_1}$  corresponding to a node

$i \in N_{f_1}$  is defined at all nodes in  $N_{f_1}$  as

$$\phi_{i,j}^{f_1} = \delta_{ij}, \quad j \in N_{f_1}, \quad j = 1, \dots, n_{f_1}, \quad (2.3)$$

where  $\delta_{ij}$  is the Kronecker delta function and  $\phi_{i,j}^{f_1}$  denotes the value of  $\phi_i^{f_1}$  at local node  $j$ . Thus,  $\phi_i^{f_1}$  takes the value 1 at local node  $i$  and 0 at all other local nodes on  $f_1$ . Similarly, the local piecewise linear basis function for a node  $i \in N_{f_2}$  is defined at all nodes in  $N_{f_2}$  as

$$\phi_{i,j}^{f_2} = \delta_{ij}, \quad j \in N_{f_2}, \quad j = 1, \dots, n_{f_2}. \quad (2.4)$$

Now, the FE spaces of the local basis functions are defined as

$$\begin{aligned} V_{f_1} &= \text{Finite element space of piecewise linear functions defined on } \tau_{f_1} = \text{span} \left\{ \phi_i^{f_1} \right\}_{1 \leq i \leq n_{f_1}}, \\ V_{f_2} &= \text{Finite element space of piecewise linear functions defined on } \tau_{f_2} = \text{span} \left\{ \phi_i^{f_2} \right\}_{1 \leq i \leq n_{f_2}}. \end{aligned} \quad (2.5)$$

A Sobolov space  $H^1(\Omega)$  for the set of all functions  $u \in L_2$  over a domain

$\Omega$  is defined as

$$H^1(\Omega) := \left\{ u : \Omega \rightarrow \mathbb{R} \left| u, \frac{du}{dx}, \frac{du}{dy} \in L_2(\Omega) \right. \right\}, \quad (2.6)$$

where  $L_2(\Omega)$  denotes the space of functions that are square integrable in the sense of Lebesgue, i.e.

$$L_2(\Omega) := \left\{ u : \Omega \rightarrow \mathbb{R} \left| \int_{\Omega} u^2 < \infty \right. \right\}. \quad (2.7)$$

Then the finite element function spaces are defined as

$$\begin{aligned} V_{f_1} &:= \left\{ \phi \in H^1(f_1) \mid \phi = 0 \text{ on } \partial f_{1D} \right\}, \\ V_{f_2} &:= \left\{ \phi \in H^1(f_2) \mid \phi = 0 \text{ on } \partial f_{2D} \right\}, \end{aligned} \quad (2.8)$$

where  $\partial f_{iD}$ ,  $i = 1, \dots, 2$  is the boundary on  $f_i$ ,  $i = 1, \dots, 2$  with Dirichlet boundary conditions.

For each global node  $I = 1, \dots, n_T$ , a corresponding global basis function  $\Psi_I$  is calculated over the problem domain  $\Omega$ . We denote  $\Psi_I^{f_1}$  to be the restriction of  $\Psi_I$  over  $f_1$  and  $\Psi_I^{f_2}$  to be the restriction of  $\Psi_I$  over  $f_2$ . Therefore,  $\Psi_I = \Psi_I^{f_1} + \Psi_I^{f_2}$ . Now, the global basis function  $\Psi_I^{f_1}$  is calculated at all local nodes  $i \in N_{f_1}$  and is given by the linear combination of the local basis functions  $\phi_i^{f_1}$ ,  $\forall i \in N_{f_1}$ . That is

$$\Psi_I^{f_1} = \sum_{j=1}^{n_{f_1}} \phi_j^{f_1} \Psi_{I,j}^{f_1}, \quad (2.9)$$

where  $\Psi_{I,j}^{f_1}$  represents the value of  $\Psi_I^{f_1}$  at local node  $j$ . Similarly, on  $f_2$  we have

$$\Psi_I^{f_2} = \sum_{j=1}^{n_{f_2}} \phi_j^{f_2} \Psi_{I,j}^{f_2}. \quad (2.10)$$

On each fracture,  $\Psi_I$  is calculated as the FE solution to the steady state groundwater flow equation (2.2) with  $P$  replaced by  $\Psi_I$  and boundary conditions of  $\Psi_I = 1$  at global node  $I$  and  $\Psi_I = 0 \forall N_\Gamma \neq I$ . Therefore, the contributions  $\Psi_I^{f_1}$  and  $\Psi_I^{f_2}$  to the basis function  $\Psi_I$  corresponding to the global node  $I$  are calculated by solving the PDE systems

$$\begin{aligned} \tilde{T}_{f_1} \sum_{j=1}^{n_{f_1}} \Psi_{I,j}^{f_1} \int_{f_1} \nabla \phi_i^{f_1} \cdot \nabla \phi_j^{f_1} = 0, \quad i=1, \dots, n_{f_1}, \quad \forall \phi^{f_1} \in V_{f_1}, \\ \text{with } \Psi_I^{f_1} = \begin{cases} 1, & \text{at global node } I, \\ 0, & \forall N_\Gamma \neq I \\ 0, & \text{on } \partial f_1. \end{cases} \end{aligned} \quad (2.11)$$

and

$$\begin{aligned} \tilde{T}_{f_2} \sum_{j=1}^{n_{f_2}} \Psi_{I,j}^{f_2} \int_{f_2} \nabla \phi_i^{f_2} \cdot \nabla \phi_j^{f_2} = 0, \quad i=1, \dots, n_{f_2}, \quad \forall \phi^{f_2} \in V_{f_2}, \\ \text{with } \Psi_I^{f_2} = \begin{cases} 1, & \text{at global node } I, \\ 0, & \forall N_\Gamma \neq I \\ 0, & \text{on } \partial f_2. \end{cases} \end{aligned} \quad (2.12)$$

The weak form of the groundwater flow equation is obtained by multiplying (2.2) by local basis functions  $\phi$  and integrating over the fracture. Gauss's divergence theorem is then used to obtain the form seen in (2.11) and (2.12).

The FE space of the global basis functions is defined as

$$V_\Gamma = \text{span}_{I \in N_\Gamma} \{\Psi_I\}. \quad (2.13)$$

It is necessary to calculate a contribution  $\Psi_{ID}$  to the global basis function that takes the Dirichlet boundary conditions into account. The contributions  $\Psi_{ID}^{f_1}$  on  $f_1$  and  $\Psi_{ID}^{f_2}$  on  $f_2$  to  $\Psi_{ID}$  are calculated by solving the PDE systems

$$\begin{aligned} \tilde{T}_{f_1} \sum_{j=1}^{n_{f_1}} \Psi_{(ID),j}^{f_1} \int_{f_1} \nabla \phi_i^{f_1} \cdot \nabla \phi_j^{f_1} = 0, \quad i=1, \dots, n_{f_1}, \quad \forall \phi^{f_1} \in V_{f_1}, \\ \text{with } \Psi_{(ID),j}^{f_1} = \begin{cases} 0, & \forall N_\Gamma, \\ P_D, & \text{on } \partial f_1, \end{cases} \end{aligned} \quad (2.14)$$

and

$$\begin{aligned} \tilde{T}_{f_2} \sum_{j=1}^{n_{f_2}} \Psi_{(ID),j}^{f_2} \int_{f_2} \nabla \phi_i^{f_2} \cdot \nabla \phi_j^{f_2} = 0, \quad i=1, \dots, n_2, \quad \forall \phi^{f_2} \in V_{f_2}, \\ \text{with } \Psi_{(ID),j}^{f_2} = \begin{cases} 0, & \forall N_\Gamma, \\ P_D, & \text{on } \partial f_2. \end{cases} \end{aligned} \quad (2.15)$$

Here,  $\Psi_{(ID),j}^{f_1}$  and  $\Psi_{(ID),j}^{f_2}$  denote the value of  $\Psi_{ID}^{f_1}$  and  $\Psi_{ID}^{f_2}$ , respectively, at local node  $j$ , and  $P_D$  are Dirichlet pressure values. The flow  $Q_I$  at a global node  $I = 1, \dots, n_\Gamma$  from a fracture  $f = f_1, f_2$ , is calculated as

$$Q_I = \int_f \nabla \Psi_I \cdot (\tilde{T}_f \nabla \hat{P}) \quad \forall \Psi_I \in V_\Gamma, \quad (2.16)$$

where  $\hat{P}$  is defined as

$$\hat{P} = \sum_{J=1}^{n_\Gamma} (\Psi_{JD} + \Psi_J P_{\Gamma_J}), \quad J \in N_\Gamma, \quad (2.17)$$

where  $P_{\Gamma_J}$  is the pressure at global node  $J$ . The pressure  $P_\Gamma$  at the fracture intersection  $\Gamma$  can be calculated by enforcing the condition that flow is conserved at the fracture intersection, and using (2.16)

$$\int_{f_1} \nabla \Psi_I^{f_1} \cdot (\tilde{T}_{f_1} \nabla(\hat{P})) + \int_{f_2} \nabla \Psi_I^{f_2} \cdot (\tilde{T}_{f_2} \nabla(\hat{P})) = 0, \quad I = 1, \dots, n_\Gamma. \quad (2.18)$$

Then inserting (2.17) into (2.18) gives

$$\begin{aligned} & \sum_{J=1}^{n_\Gamma} \left( \tilde{T}_{f_1} \int_{f_1} (\nabla \Psi_I^{f_1} \cdot \nabla \Psi_{JD}^{f_1}) + \tilde{T}_{f_1} P_{\Gamma_J} \int_{f_1} (\nabla \Psi_I^{f_1} \cdot \nabla \Psi_J^{f_1}) \right) + \\ & \sum_{J=1}^{n_\Gamma} \left( \tilde{T}_{f_2} \int_{f_2} (\nabla \Psi_I^{f_2} \cdot \nabla \Psi_{JD}^{f_2}) + \tilde{T}_{f_2} P_{\Gamma_J} \int_{f_2} (\nabla \Psi_I^{f_2} \cdot \nabla \Psi_J^{f_2}) \right) = 0, \quad I = 1, \dots, n_\Gamma. \end{aligned} \quad (2.19)$$

Let  $\langle a, b \rangle_f := \int_f ab$ , then defining

$$A_{IJ} = \tilde{T}_{f_1} \langle \nabla \Psi_I^{f_1}, \nabla \Psi_J^{f_1} \rangle_{f_1} + \tilde{T}_{f_2} \langle \nabla \Psi_I^{f_2}, \nabla \Psi_J^{f_2} \rangle_{f_2}, \quad I, J = 1, \dots, n_\Gamma, \quad (2.20)$$

and

$$B_I = -\tilde{T}_{f_1} \sum_{J=1}^{n_\Gamma} \langle \nabla \Psi_I^{f_1}, \nabla \Psi_{JD}^{f_1} \rangle_{f_1} - \tilde{T}_{f_2} \sum_J \langle \nabla \Psi_I^{f_2}, \nabla \Psi_{JD}^{f_2} \rangle_{f_2}, \quad I = 1, \dots, n_\Gamma, \quad (2.21)$$

the matrix system corresponding to (2.18) can be written as

$$\begin{pmatrix} A_{11} & \dots & A_{n_\Gamma 1} \\ \dots & \dots & \dots \\ A_{n_\Gamma 1} & \dots & A_{n_\Gamma n_\Gamma} \end{pmatrix} \begin{pmatrix} P_{\Gamma_1} \\ \dots \\ P_{\Gamma_{n_\Gamma}} \end{pmatrix} = \begin{pmatrix} B_1 \\ \dots \\ B_{n_\Gamma} \end{pmatrix}. \quad (2.22)$$

The matrix system (2.22) is then solved for  $P_\Gamma$  and the pressure over  $f_1$  and  $f_2$  can be calculated using the approximation (2.17). To summarise this section, a numerical algorithm for solving the pressure over two intersecting fractures is now given.

### 2.1.1 – ALGORITHM TO CALCULATE THE PRESSURE FIELD OVER TWO INTERSECTING FRACTURES USING THE FINITE ELEMENT APPROACH

This section presents a numerical algorithm that calculates the pressure over two non-overlapping fractures  $f_1$  and  $f_2$  intersecting along a fracture intersection  $\Gamma$ . It is assumed that there are Dirichlet boundary conditions on the fracture boundaries  $\partial f_1$  and  $\partial f_2$ . The algorithm is as follows:

- Assign a mesh  $\tau_{f_1} \{ \kappa_{f_1} \}$  over  $f_1$  consisting of triangular elements  $\kappa_{f_1}$  and define a set  $N_{f_1}$  containing  $n_{f_1}$  local nodes. Calculate local basis functions  $\phi_i^{f_1}$  on  $f_1$  using (2.3).
- Assign a mesh  $\tau_{f_2} \{ \kappa_{f_2} \}$  over  $f_2$  consisting of triangular elements  $\kappa_{f_2}$  and define a set  $N_{f_2}$  containing  $n_{f_2}$  local nodes. Calculate local basis functions  $\phi_i^{f_2}$  on  $f_2$  using (2.4).
- Discretise the fracture intersection  $\Gamma$  into  $n_\Gamma$  global nodes belonging to a set  $N_\Gamma$  such that  $N_\Gamma = N_{f_1} \cap N_{f_2}$ .
- DO  $I = 1, \dots, n_\Gamma$  :
  - Calculate  $\Psi_I^{f_1}$  using (2.11) and  $\Psi_I^{f_2}$  using (2.12)
  - Calculate  $\Psi_{ID}^{f_1}$  using (2.14) and  $\Psi_{ID}^{f_2}$  using (2.15).
- END DO.
- Calculate  $A_{IJ}$  defined in (2.20) and  $B_J$  defined in (2.21),  
 $I, J = 1, \dots, n_\Gamma$ .

- Calculate  $P_{\Gamma_I}$ ,  $I = 1, \dots, n_{\Gamma}$  by solving the matrix system (2.22).
- Calculate the pressure across the fractures using the approximation

$$\hat{P} = \sum_{J=1}^{n_{\Gamma}} (\Psi_{JD} + \Psi_J P_{\Gamma J}).$$

### 2.1.2 – ONE DIMENSIONAL EXAMPLE

A deliberately simple one dimensional model has been designed to illustrate the FE techniques introduced in this chapter. The domain ( $0 \leq x \leq 4$ ) consists of fracture 1, denoted by  $f_1$  ( $0 \leq x \leq 2$ ) with a transmissivity of  $\tilde{T}_{f_1}$  and fracture 2 denoted by  $f_2$  ( $2 \leq x \leq 4$ ) with a transmissivity of  $\tilde{T}_{f_2}$  which intersect at an intersection point  $\Gamma$  at  $x = 2$ . There are pressure boundary conditions of  $P(x=0) = P_A \geq 0$  and  $P(x=4) = 0$ . Figure 1 shows the problem domain where  $f_1$  and  $f_2$  have each been discretised into two local nodes and there is one global node at the fracture intersection.

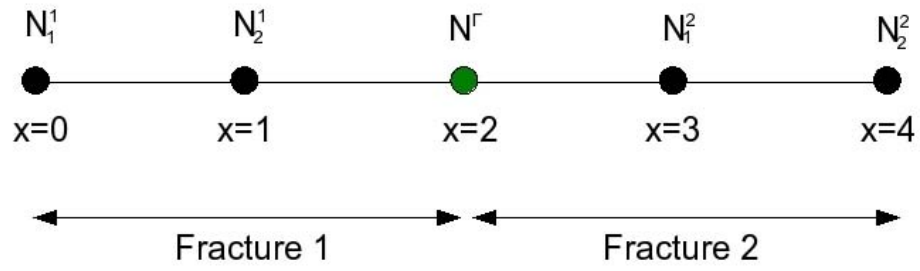


**Figure 1.** Discretisation of two intersecting fractures.

### 2.1.2.1- ANALYTICAL SOLUTION

The pressure  $P_{f_1}$  on  $f_1$ ,  $0 \leq x \leq 2$  can be written as

$$P_{f_1} = Ax + P_A, \quad (2.23)$$

where  $A$  is a constant. The pressure  $P_{f_2}$  on  $f_2$ ,  $2 \leq x \leq 4$ , can be written as

$$P_{f_2} = C(x-4), \quad (2.24)$$

where  $C$  is a constant. At the intersection  $\Gamma(x=2)$

$$P_{f_1} = P_{f_2} \Rightarrow C = -\left(A + \frac{1}{2}P_A\right). \quad (2.25)$$

Additionally, at  $\Gamma(x = 2)$

$$\begin{aligned}
 Q_{f_1} &= \tilde{T}_{f_1} \frac{dP_{f_1}}{dx} = Q_{f_2} = \tilde{T}_{f_2} \frac{dP_{f_2}}{dx}, \\
 \Rightarrow \tilde{T}_{f_1} A &= -\tilde{T}_{f_2} \left( A + \frac{1}{2} P_A \right), \\
 \Rightarrow A &= -\frac{P_A}{2 \left( \frac{\tilde{T}_{f_1}}{\tilde{T}_{f_2}} + 1 \right)}.
 \end{aligned} \tag{2.26}$$

Therefore,

$$\begin{cases}
 P_{f_1} = -\left( \frac{P_A}{2 \left( \frac{\tilde{T}_{f_1}}{\tilde{T}_{f_2}} + 1 \right)} \right) x + P_A, \\
 P_{f_2} = -\frac{1}{2} P_A \left( 1 - \frac{1}{\left( \frac{\tilde{T}_{f_1}}{\tilde{T}_{f_2}} + 1 \right)} \right) (x-4).
 \end{cases} \tag{2.27}$$

It follows that the pressure  $P_\Gamma$  at the intersection  $\Gamma$  is given by

$$P_\Gamma = P_A \left( 1 - \frac{1}{\left( \frac{\tilde{T}_{f_1}}{\tilde{T}_{f_2}} + 1 \right)} \right). \tag{2.28}$$

### 2.1.2.2 – GLOBAL BASIS FUNCTION APPROACH

The discretisation introduced in Figure 1 is used to apply the global basis function approach. The local basis functions  $\phi_i^{f_1}$  on  $f_1$  and their derivatives are defined as

$$\begin{aligned}\phi_1^{f_1} &= \begin{cases} -x, & 0 \leq x \leq 1 \\ 0, & \text{else} \end{cases} & \frac{d\phi_1^{f_1}}{dx} &= \begin{cases} -1, & 0 \leq x \leq 1 \\ 0, & \text{else} \end{cases} \\ \phi_2^{f_1} &= \begin{cases} x, & 0 \leq x \leq 1 \\ 2-x, & 1 \leq x \leq 2 \end{cases} & \frac{d\phi_2^{f_1}}{dx} &= \begin{cases} 1, & 0 \leq x \leq 1 \\ -1, & 1 \leq x \leq 2. \end{cases}\end{aligned}\tag{2.29}$$

The local basis functions  $\phi_i^{f_2}$  on  $f_2$  and their derivatives are defined as

$$\begin{aligned}\phi_1^{f_2} &= \begin{cases} x-2, & 2 \leq x \leq 3 \\ 4-x, & 3 \leq x \leq 4 \end{cases} & \frac{d\phi_1^{f_2}}{dx} &= \begin{cases} 1, & 2 \leq x \leq 3 \\ -1, & 3 \leq x \leq 4 \end{cases} \\ \frac{d\phi_2^{f_2}}{dx} &= \begin{cases} x-3, & 3 \leq x \leq 4 \\ 0, & \text{else} \end{cases} & \frac{d\phi_2^{f_2}}{dx} &= \begin{cases} 1, & 3 \leq x \leq 4 \\ 0, & \text{else.} \end{cases}\end{aligned}\tag{2.30}$$

For this 1D example there is only one global basis function  $\Psi = \Psi^{f_1} + \Psi^{f_2}$  corresponding to global node  $N_\Gamma$ . Thus, the FE spaces are given by

$$\begin{aligned}V_{f_1} &= \text{span}\{\phi_1^1, \phi_2^1\}, \\ V_{f_2} &= \text{span}\{\phi_1^2, \phi_2^2\}, \\ V_\Gamma &= \text{span}\{\Psi\}.\end{aligned}\tag{2.31}$$

The global basis function  $\Psi^f$  on a fracture  $f = f_1, f_2$  is calculated by solving

$$\tilde{T}_f \sum_{j=1}^2 \Psi_j^f \int_f \frac{d\phi_i^f}{dx} \frac{d\phi_j^f}{dx} = 0, \quad i = 1, 2, \quad (2.32)$$

with  $\Psi^f = \begin{cases} 1, & \text{at } N_\Gamma, \\ 0, & \text{otherwise.} \end{cases}$

The basis function  $\Psi^{f_1}$  over  $f_1$  is calculated using (2.32) as

$$\Psi^{f_1} = \frac{1}{2}x, \quad 0 \leq x \leq 2. \quad (2.33)$$

Therefore,

$$\frac{d\Psi^{f_1}}{dx} = \frac{1}{2}, \quad 0 \leq x \leq 2. \quad (2.34)$$

The basis vector  $\Psi^{f_2}$  over  $f_2$  is calculated using (2.32) as

$$\Psi^{f_2} = -\frac{1}{2}(x-4), \quad 2 \leq x \leq 4, \quad (2.35)$$

and it follows that

$$\frac{d\Psi^{f_2}}{dx} = -\frac{1}{2}, \quad 2 \leq x \leq 4. \quad (2.36)$$

The contribution of the Dirichlet boundary conditions to the global basis

function  $\Psi_D = \Psi_D^{f_1} + \Psi_D^{f_2}$  on a fracture  $f$  are calculated as

$$\begin{aligned} \tilde{T}_f \sum_{j=1}^2 \Psi_{D,j}^f \int_f \frac{d\phi_i}{dx} \frac{d\phi_j}{dx} = 0, \quad i=1,2, \\ \text{with } \Psi_{D,j}^f = \begin{cases} 0, & \text{at } N_\Gamma \text{ and } N_2^2, \\ P_A, & \text{at } N_1^{f_1}. \end{cases} \end{aligned} \quad (2.37)$$

This yields

$$\Psi_D^{f_1} = P_A \left( 1 - \frac{1}{2}x \right), \quad 0 \leq x \leq 2. \quad (2.38)$$

and

$$\Psi_D^{f_2} = 0, \quad 2 \leq x \leq 4. \quad (2.39)$$

Figure 2 shows the global basis functions (2.33), (2.35) and (2.38) calculated for this problem compared to the analytical pressure solution (2.28) for the values  $P_A = 5$ ,  $\tilde{T}_{f_1} = 1.0\text{E-}9$ ,  $\tilde{T}_{f_2} = 2.0\text{E-}9$ . For this 1D example the pressure is approximated as

$$\hat{P} = \Psi_D + \Psi P_\Gamma, \quad (2.40)$$

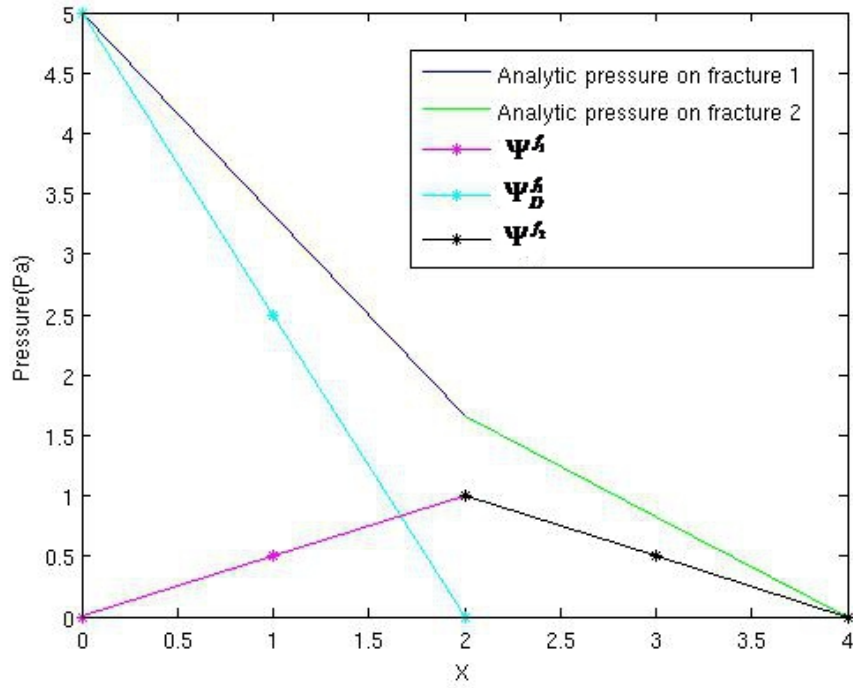


**Figure 2.** Plot of the analytical pressure over the two fractures compared to the global basis vectors  $\Psi^{f_1}$ ,  $\Psi_D^{f_1}$  and  $\Psi^{f_2}$ .

The flow contribution from  $f_1$  is given by

$$\begin{aligned}
 Q_{f_1} &= \tilde{T}_{f_1} \left( \int_{f_1} \frac{d\Psi^{f_1}}{dx} \frac{d\Psi_D^{f_1}}{dx} dx + P_\Gamma \int_{f_1} \frac{d\Psi^{f_1}}{dx} \frac{d\Psi_D^{f_1}}{dx} dx \right) \\
 &= \tilde{T}_{f_1} \left( \int_{x=0}^2 \left( -\frac{1}{4} P_A \right) dx + P_\Gamma \int_{x=0}^2 \left( \frac{1}{4} \right) dx \right) \\
 &= \frac{1}{2} \tilde{T}_{f_1} (P_\Gamma - P_A).
 \end{aligned} \tag{2.41}$$

Now, the flow contribution from  $f_2$  is given by

$$\begin{aligned}
Q_{f_2} &= \tilde{T}_{f_2} P_\Gamma \int_{f_2} \frac{d\Psi^{f_2}}{dx} \frac{d\Psi^{f_2}}{dx} dx \\
&= \tilde{T}_{f_2} P_\Gamma \int_{x=0}^2 \left( \left( -\frac{1}{2} \right)^2 \right) dx \\
&= \frac{1}{2} \tilde{T}_{f_2} P_\Gamma.
\end{aligned} \tag{2.42}$$

At the fracture intersection  $\Gamma$ , the sum of the flow  $Q_{f_1}$  from  $f_1$  and the flow  $Q_{f_2}$  from  $f_2$  is equal to zero

$$Q_{f_1} + Q_{f_2} = 0. \tag{2.43}$$

Inserting equations (2.41) and (2.42) into (2.43) yields

$$\frac{1}{2} \tilde{T}_{f_1} (P_\Gamma - P_A) + \frac{1}{2} \tilde{T}_{f_2} P_\Gamma = 0. \tag{2.44}$$

Thereby,

$$\begin{aligned}
P_\Gamma &= \frac{\tilde{T}_{f_1} P_A}{\left( \tilde{T}_{f_1} + \tilde{T}_{f_2} \right)} \\
&= \frac{\left( \frac{\tilde{T}_{f_1}}{\tilde{T}_{f_2}} P_A \right)}{\left( \frac{\tilde{T}_{f_1}}{\tilde{T}_{f_2}} + 1 \right)} \\
&= P_A \left( 1 - \frac{1}{\left( \frac{\tilde{T}_{f_1}}{\tilde{T}_{f_2}} + 1 \right)} \right).
\end{aligned} \tag{2.45}$$

The pressure  $P_\Gamma$  calculated at the intersection  $\Gamma$  using the basis function approach (2.45) is therefore identical to that given by the analytical solution (2.28).

## **2.2 – CALCULATING THE PRESSURE AT FRACTURE INTERSECTIONS IN A DISCRETE FRACTURE NETWORK**

In this section the global basis function FE formulation introduced for two intersecting fractures in section 2.1 is extended to the case of a DFN containing many fractures. The same approach is taken, however, when calculating the flow at a global node, the value is dependent not only on the pressures at that fracture intersection but also at separate fracture intersections on the intersecting fractures.

We consider a large scale DFN with a problem domain  $\Omega$  partitioned into  $r$  non-overlapping sub domains (representing the  $r$  fractures) some of which are in contact with the boundaries of  $\Omega$ . There are  $s$  fracture intersections

$\Gamma_I$ ,  $I = 1, \dots, s$ , each of which is discretised into  $n_{\Gamma_I}$ ,  $I = 1, \dots, s$ , global nodes contained in the set  $N_{\Gamma_I}$ . Thus, the total number of global nodes contained in the

DFN is  $n_\Gamma = \sum_{I=1}^s n_{\Gamma_I}$ . The continuity of pressure and groundwater flow (introduced

in section 2.1) are enforced at every fracture intersection. Each global basis function on an intersection will belong to the FE space defined as

$$V_{\Gamma_I} = \text{span}_{I \in N_{\Gamma_I}} \{ \Psi_I \}. \quad (2.46)$$

For the overall DFN all the  $n_\Gamma$  global nodes are divided into two sets:

$D$  - The global nodes at which there is a Dirichlet boundary condition for the pressure.

$E$  - The remaining global nodes, some of which have a specified inflow.

The flow contribution from a fracture  $f$  at a global node  $I = 1, \dots, n_\Gamma$  resulting from the global basis function FE treatment is given by (2.16). Dividing the global nodes as described yields

$$\begin{aligned} & \sum_{J \in E} \left( \sum_{f \text{ containing } I} \int \nabla \Psi_I \cdot \tilde{T}_f \nabla \Psi_J P_J \right) \\ & + \sum_{J \in D} \left( \sum_{f \text{ containing } I} \int \nabla \Psi_I \cdot \tilde{T}_f \nabla \Psi_J P_J \right) = -Q_I, \quad I \in E. \end{aligned} \quad (2.47)$$

and

$$P_I = P_{I_0}, \quad I \in D, \quad (2.48)$$

where  $I$  and  $J$  refer to the global nodes in the model,  $P_{I_0}$  is the value of the pressure at a Dirichlet boundary condition node  $I$  and  $Q_I$  represents the boundary

conditions used and may contain known flow values. Now, defining the terms in (2.47) and (2.48) in matrix notation as

$$\begin{aligned}\mathbf{A}_{EE} &= \sum_{J \in E} \left( \sum_{f \text{ containing } I_f} \int \nabla \Psi_I \cdot \tilde{T}_f \nabla \Psi_J \right), \quad I \in E, \\ \mathbf{A}_{ED} &= \sum_{J \in D} \left( \sum_{f \text{ containing } I_f} \int \nabla \Psi_I \cdot \tilde{T}_f \nabla \Psi_J \right), \quad I \in E,\end{aligned}\tag{2.49}$$

allows us to combine (2.47) and (2.48) and write the system as

$$\begin{pmatrix} \mathbf{A}_{EE} & \mathbf{A}_{ED} \\ \mathbf{0} & \mathbf{I} \end{pmatrix} \begin{pmatrix} \mathbf{P}_E \\ \mathbf{P}_D \end{pmatrix} = \begin{pmatrix} \mathbf{Q}_E \\ \mathbf{P}_{D0} \end{pmatrix},\tag{2.50}$$

where the pressure has been split into pressure values  $\mathbf{P}_E$  on global nodes in set  $E$  and pressure values  $\mathbf{P}_D$  on Dirichlet global nodes  $D$ , the values of which are contained in  $\mathbf{P}_{D0}$ . Furthermore, at Dirichlet boundary condition nodes where  $\mathbf{P}_D$  is known, the flow to that node  $\mathbf{Q}_D$  is computed. This is done by adding an extra set of equations to (2.50) giving

$$\begin{pmatrix} \mathbf{A}_{EE} & \mathbf{A}_{ED} & \mathbf{0} \\ \mathbf{A}_{DE} & \mathbf{A}_{DD} & -\mathbf{I} \\ \mathbf{0} & \mathbf{I} & \mathbf{0} \end{pmatrix} \begin{pmatrix} \mathbf{P}_E \\ \mathbf{P}_D \\ \mathbf{Q}_D \end{pmatrix} = \begin{pmatrix} \mathbf{Q}_E \\ \mathbf{0} \\ \mathbf{P}_{D0} \end{pmatrix},\tag{2.51}$$

where

$$\begin{aligned}\mathbf{A}_{DE} &= \sum_{J \in E} \left( \sum_{f \text{ containing } I_f} \int \nabla \Psi_I \cdot \tilde{T}_f \nabla \Psi_J \right), \quad I \in D, \\ \mathbf{A}_{DD} &= \sum_{J \in D} \left( \sum_{f \text{ containing } I_f} \int \nabla \Psi_I \cdot \tilde{T}_f \nabla \Psi_J \right), \quad I \in D.\end{aligned}\tag{2.52}$$

The matrix system (2.51) is then solved for the unknown pressure values on fracture intersections  $\mathbf{P}_e$  and the flow into Dirichlet nodes  $\mathbf{Q}_D$ .

### 2.3 – NUMERICAL MODEL OF A PUMPING BOREHOLE

This section considers how the FE method approximates flow at a pumping borehole intersected by a fracture. A borehole is a well of small radius that has been drilled into the rock. Boreholes can be pumped to create a flow or they can be non-pumping. Measurements are made at boreholes which generally intersect many fractures in a given DFN. The radius of a borehole is small in comparison to the distance between nodes in a FE discretisation of a fracture. This means that the pressure calculated from the FE method close to the borehole can be inaccurate and differ from the analytical solution. In this section the analytical and FE solutions for a pressure field in the vicinity of a pumping borehole are introduced. It is then shown how the two solutions are combined to give a borehole model equation which can be used with the FE method in a DFN model. The analytical solution for steady state flow at a pumping borehole is known as the Thiem solution (Mays 2005). It states that the pressure  $P_r$  at any radial distance  $r$  from a pumping borehole is given by

$$P_r = P_B + \frac{Q_B \rho g}{2\pi T} \ln\left(\frac{r}{r_B}\right), \quad (2.53)$$

where  $\rho$  is the groundwater density,  $g$  is gravitational acceleration,  $T$  is the transmissivity,  $r_B$  is the borehole radius,  $P_B$  is the pressure at the borehole and  $Q_B$  is the borehole flux.

The FE solution to a pumping borehole which intersects a given fracture with a constant transmissivity  $T$  is now considered. This problem is very similar to one described in Pinder and Gray (1977) and is described by the PDE system

$$T \left( \frac{\partial^2 P}{\partial x^2} + \frac{\partial^2 P}{\partial y^2} \right) - Q = 0 \quad \text{in } \Omega = [0 \leq x \leq 2L, 0 \leq y \leq 2L], \quad (2.54)$$

$$Q(x, y) = Q_B (1, 1) \delta(x-1, y-1),$$

where the notation is as before with the addition of  $L$  representing a constant length and  $\delta$  is the Kronecker delta function. The pumping borehole is represented as a point source at  $(1, 1)$  with a flux at the borehole of  $Q_B$ . A subsection of the fracture that surrounds the intersecting borehole is represented by triangular FEs in two dimensions. We consider a node located at the borehole along with four nodes that surround it. This setup is shown in Figure 3. There are four triangular elements I, II, III, IV. From the Thiem solution (2.53) we know that the pressure is constant at a given radius from the borehole. We thus define Dirichlet boundary conditions for the pressure at the four nodes equidistant from the borehole. Accordingly, nodes 1, 2, 4 and 5 are assigned a constant pressure  $P_C$  and the pumping borehole is represented at node 3 as a point sink with flux  $Q_B$ .

Cartesian coordinates are used for the FE formulation, which may seem an odd choice as flow to a pumping borehole is radial as shown by the Thiem solution. The FE method can be formulated in radial coordinates (Pinder and Gray 1977) to calculate radial flow to a borehole. However, we shall use Cartesian coordinates and show that the Cartesian FE solution can be combined with the analytical Thiem solution to model flow at a pumping borehole. In large DFNs the majority of fractures will not be intersected by a borehole and are modelled in Cartesian coordinates. Thus, it is of benefit to model a pumping borehole in Cartesian coordinates so that it is in the same coordinate system as the rest of the DFN.

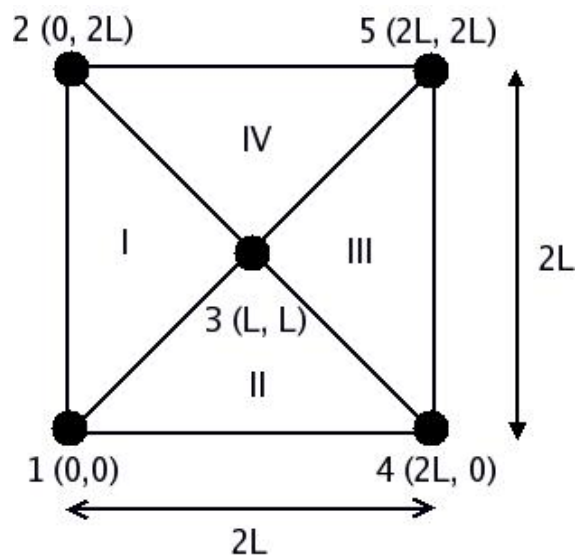


**Figure 3.** FE setup representing a pumping borehole at node 3 on a fracture and the surrounding nodes with discretization length of  $2L$ . Nodes are represented by circles and are shown with their global coordinates in brackets. There are four elements I, II, III and IV.

The FE pressure  $P_{FE}$  at the pumping borehole is given by

$$P_{FE} = P_C + \frac{Q_B}{4T}. \quad (2.55)$$

For full details on the calculation of the FE pressure in equation (2.55) see Pinder and Gray (1977).

Test sites in groundwater modelling are often modelled on a large scale and when using a FE method to model these sites, the discretisation length can be of the order 50m. Figure 4 shows the FE discretisation of a sub-section of a fracture around an intersecting, pumping borehole with a discretisation length of  $2L$ .

Drilled boreholes typically have a radius of approximately 5cm which poses a scale problem considering the FE discretisation length. Figure 5 shows a sketch of how the FE solution struggles to match the Theim solution when the grid spacing is much greater than the borehole radius. The FE pressure  $P_{FE}$  at a borehole needs to be adjusted, so that it gives an accurate measure of the physical pressure  $P_B$  at that borehole.

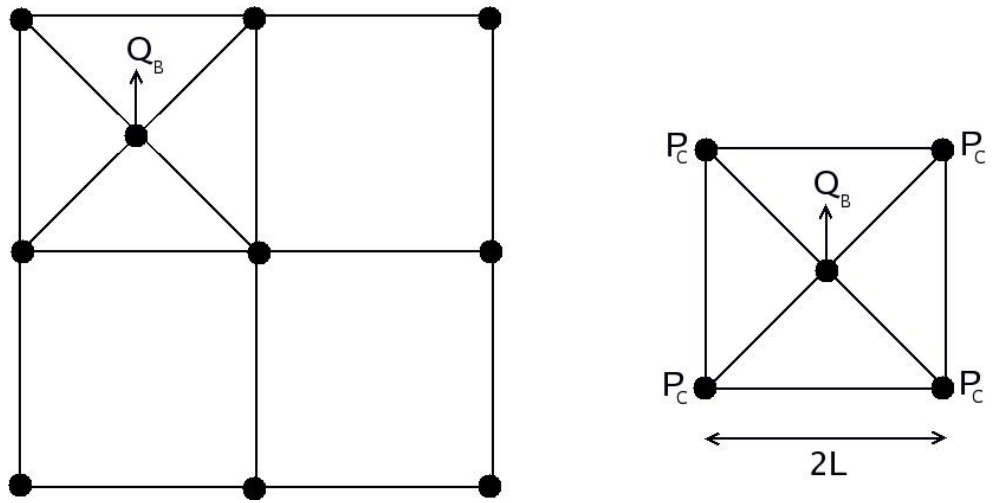


**Figure 4.** The FE grid on a fracture in the vicinity of a pumping borehole with flux  $Q_B$ . The right figure shows the nodes surrounding the borehole node.

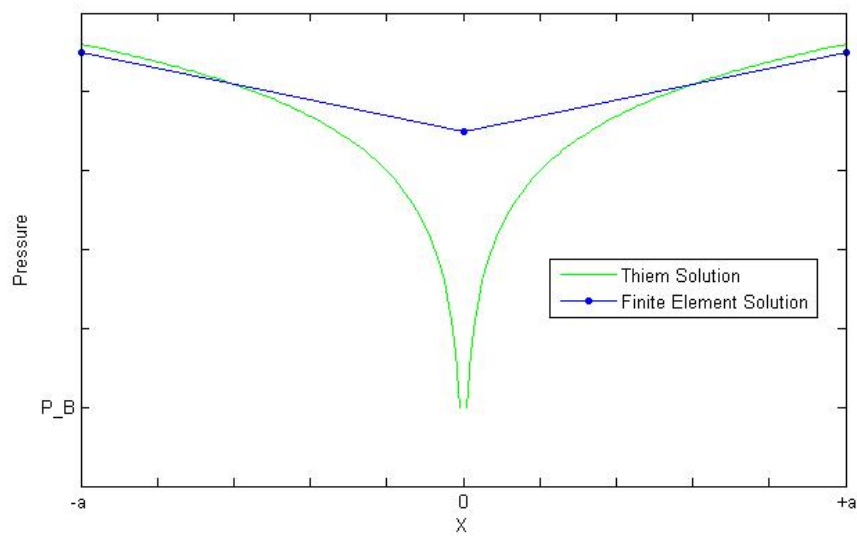


**Figure 5.** Sketch in the  $x$ -axis comparing the Thiem solution to the FE solution at a pumping borehole located at  $x=0$ . In this example the discretisation length used for the FE method is  $a$ .

From the Thiem equation (2.53), the borehole pressure  $P_B$  at a borehole of radius

$r_B$  with a pressure  $P_C$  at radius  $r = \sqrt{2L}$  is

$$P_B = P_C - \frac{Q_B \rho g}{2\pi T} \ln\left(\frac{\sqrt{2L}}{r_B}\right). \quad (2.56)$$

Using equations (2.55) and (2.56), it follows that

$$P_B - P_{FE} = \left(-\frac{1}{4} - \frac{\rho g}{2\pi} \ln\left(\frac{\sqrt{2L}}{r_B}\right)\right) \frac{Q_B}{T}, \quad (2.57)$$

and defining  $\gamma = \left(-\frac{1}{4} - \frac{\rho g}{2\pi} \ln\left(\frac{\sqrt{2L}}{r_B}\right)\right)^{-1}$ ,

$$P_B = P_{FE} + \frac{Q_B}{\gamma T}. \quad (2.58)$$

Equation (2.58) is the borehole model and is used to adjust the FE pressure  $P_{FE}$  calculated at a pumping borehole so that it is given by  $P_B$ . In the discretisation of a DFN model a borehole global node is introduced corresponding to a borehole/fracture intersection. Each borehole node corresponds to a given global node. The set of borehole nodes is denoted by  $B$ . Thus, the FE flow equations (2.51) can be modified to include equation (2.58) and the resulting matrix system is given by

$$\begin{pmatrix} \mathbf{A}_{EE} & \mathbf{A}_{ED} & \mathbf{0} & \mathbf{0} \\ \mathbf{A}_{DE} & \mathbf{A}_{DD} & -\mathbf{I} & \mathbf{0} \\ \mathbf{0} & \mathbf{I} & \mathbf{0} & \mathbf{0} \\ \mathbf{e}_B & \mathbf{0} & \mathbf{0} & \mathbf{I} \end{pmatrix} \begin{pmatrix} \mathbf{P}_E \\ \mathbf{P}_D \\ \mathbf{Q}_D \\ \mathbf{P}_B \end{pmatrix} = \begin{pmatrix} \mathbf{Q}_E \\ \mathbf{0} \\ \mathbf{P}_{D0} \\ \mathbf{R}_B \end{pmatrix}, \quad (2.59)$$

where  $\mathbf{e}_B$  is equal to -1 for all global nodes corresponding to borehole nodes and 0 otherwise and the entries of  $\mathbf{R}_B$  are given by

$$R_{Bi} = \frac{Q_{Bi}}{\gamma_i T_i}, \quad \forall i \in B. \quad (2.60)$$

## 2.4 –ALGORITHM TO CALCULATE THE PRESSURE AT FRACTURE INTERSECTIONS IN A DISCRETE FRACTURE NETWORK USING THE FINITE ELEMENT APPROACH

This section presents an algorithm to calculate the pressure at fracture intersections in a DFN containing a total of  $r$  fractures and  $s$  fracture intersections  $\Gamma_i$ ,  $i = 1, \dots, s$ .

- DO  $i=1, \dots, r$
- Assign a mesh  $\tau_{f_i} \{ \kappa_{f_i} \}$  over  $f_i$  consisting of triangular elements  $\kappa_{f_i}$  and a set  $N_{f_i}$  containing  $n_{f_i}$  local nodes. Calculate local basis functions  $\phi^{f_i}$  on  $f_i$ .

- END DO
  
- DO i=1,...,s
- Discretise the fracture intersection  $\Gamma_i$  into a set  $N_{\Gamma_i}$  containing  $n_{\Gamma_i}$  global nodes.
  - DO j=1,..., $n_{\Gamma_i}$
  - Calculate the global basis function  $\Psi_j$  corresponding to global node  $j \in N_{\Gamma_i}$  over fractures containing global node I using (2.11).
  - END DO
- END DO
  
- Calculate  $\mathbf{A}_{EE}$  and  $\mathbf{A}_{ED}$  defined in (2.49),  $\mathbf{A}_{DE}$  and  $\mathbf{A}_{DD}$  defined in (2.52) and  $\mathbf{R}_B$  defined in (2.60).
  
- Solve the matrix system (2.59) for the pressure at global nodes  $\mathbf{P}_E$  and the adjusted pressure at boreholes  $\mathbf{P}_B$ .

## **2.5 – COMPARISON OF THE BASIS FUNCTION APPROACH TO A STANDARD FINITE ELEMENT APPROACH**

We now compare the global basis function FE approach introduced in this chapter to a standard FE approach. In a standard FE approach the DFN domain is discretised in the same way as the global basis function FE

approach. However, all the basis functions corresponding to nodes are equal to the local basis functions defined in (2.3). The pressure is calculated on all the fractures and the flow boundary condition is enforced on nodes corresponding to fracture intersections, see Quarteroni and Valli (1999). If every global node in the discretisation of a DFN corresponds to a given local node, then the global basis function FE approach is equivalent to a standard FE approach. To show this, we consider the two fractures  $f_1$  and  $f_2$  from the setup described in section 2.1. The global basis function for global node  $I = 1, \dots, n_\Gamma$  over  $f_1$  can be written as

$$\Psi_I^{f_1} = \phi_i^{f_1} + \sum_{\substack{k=1, \\ k \neq i}}^{n_{f_1}} b_{Ik} \phi_k^{f_1}, \quad (2.61)$$

where  $\phi_i^{f_1}$  is the local basis function at local node  $i$  corresponding to global node  $I$  and  $b_{Ik}$  are constant coefficients depending on the geometry of the fracture. The global basis function  $\Psi_I^{f_1}$  is calculated over  $f_1$  by solving

$$\int_{f_1} \nabla \phi_n^{f_1} \cdot T \nabla \Psi_I^{f_1} = 0, \quad n \in N_{f_1}, \quad (2.62)$$

with boundary conditions

$$\begin{aligned} \Psi_I &= 1 \text{ at } I, \\ \Psi_I &= 0, \quad \forall N_\Gamma \neq I. \end{aligned} \quad (2.63)$$

The pressure across  $f_1$  is given by

$$\begin{aligned}
\hat{P} &= \sum_{j=1}^{n_\Gamma} P_j \Psi_j, \\
&= \sum_{j=1}^{n_\Gamma} P_j \left( \phi_j^{f_1} + \sum_{\substack{k=1, \\ k \neq j}}^{n_{f_1}} b_{jk} \phi_k^{f_1} \right), \quad k \in N_{f_1}.
\end{aligned} \tag{2.64}$$

The flow  $Q_I^{f_1}$  at global node  $I = 1, \dots, n_\Gamma$ , from  $f_1$  is given by

$$\begin{aligned}
Q_I^{f_1} &= \int_{f_1} \nabla \Psi_I^{f_1} \cdot \tilde{T}_{f_1} \nabla \hat{P}, \quad i = 1, \dots, n_\Gamma, \\
&= \int_{f_1} \nabla \left( \phi_j + \sum_{\substack{k=1, \\ k \neq j}}^{n_1} b_{jk} \phi_k \right) \cdot \tilde{T}_{f_1} \nabla \hat{P}, \quad i = 1, \dots, n_\Gamma, \quad k \in N_{f_1},
\end{aligned} \tag{2.65}$$

Equation (2.62) can be used to show that the second term in (2.65) is equal to zero, and so equation (2.65) simplifies to

$$Q_I^{f_1} = \int_{f_1} \nabla \phi_i^{f_1} \cdot \tilde{T}_1 \nabla \hat{P}, \quad i = 1, \dots, n_\Gamma. \tag{2.66}$$

Enforcing the conservation of flow boundary condition at global node  $I$  yields

$$\int_{f_1} \nabla \phi_i^{f_1} \cdot \tilde{T}_{f_1} \nabla \hat{P} + \int_{f_2} \nabla \phi_i^{f_2} \cdot \tilde{T}_{f_2} \nabla \hat{P} = 0, \quad i = 1, \dots, n_\Gamma. \tag{2.67}$$

Equation (2.67) is the weak form of the flow boundary condition on a fracture intersection that would be implemented in the standard FE approach (Quarteroni and Valli 1999). Therefore, the basis function FE approach and

the standard FE approach both solve the pressure on individual fractures along with the same condition (2.67) at fracture intersections. It should be noted that this is only the case when every global node has a corresponding local node.

The standard FE approach results in a large sparse stiffness matrix in the matrix system that is to be solved for pressure values. The advantage of using the global basis function approach is that it results in many smaller matrix systems that are to be solved. This structure means that it is easy to use parallel computing when solving the matrix systems. Furthermore, the discretisation of fracture intersections can be coarsened to reduce the total number of operations required to calculate the pressure in the DFN. This is vital for large scale DFNs such as ones we use for test cases.

The global basis function FE approach allows for individual fractures to be discretised into highly refined meshes or coarse meshes. This means that on fracture intersections, there is the possibility that local nodes between the fractures do not match. Thus, on some fracture intersections there are more local nodes than global nodes. This problem is essentially equivalent to that of non-conforming sub-domains. This thesis will not go into the details of non-conforming sub-domains but for a concise description of FE methods that can handle non-conforming domains, see Quarteroni and Valli (1999).

## **3 - DEVELOPMENT OF THE BASIS VECTOR**

### **CONDITIONING METHOD**

Our new conditioning method is developed in a DFN setting. It is based on a previous conditioning method proposed by Cliffe and Jackson (1995; 2000) for conditioning hydraulic conductivities in CPM models on head measurements. Section 3.1 summarises the conditioning method proposed by Cliffe and Jackson (1995; 2000). Section 3.2 then outlines the modifications made to Cliffe and Jackson's method to develop our new conditioning method in a DFN setting. The mathematical formulation of our new conditioning method is then given in the remaining sections of this chapter.

#### **3.1 – SUMMARY OF CLIFFE AND JACKSON'S**

##### **CONDITIONING METHOD**

Cliffe and Jackson (1995; 2000) proposed a method for conditioning hydraulic conductivities  $K$  in CPM models on head measurements. They assumed that a CPM model had been discretised into nodes each of which had an initial value of  $K$  (with units m/s) assigned to it, and they defined  $Y = \log_{10} K$  to be the log of the hydraulic conductivities. The  $Y$  values are defined by their mean and covariance. The starting point for their method is

the observation that when the variability in  $Y$  and the deviations of the head from the mean head field are both small there is a linear relationship between the perturbations of head from the mean head field and the perturbations of  $Y$  from its mean value. As a result of this linear relationship, unconditioned values of  $Y$  can be directly conditioned on head measurements by the formula

$$\mathbf{Y}^C = \mathbf{Y}^U + \mathbf{W}(\mathbf{h}_M - \mathbf{h}_C), \quad (3.1)$$

where  $\mathbf{Y}^C$  is a vector containing the conditioned values of  $Y$ ,  $\mathbf{Y}^U$  is a vector containing the unconditioned values of  $Y$ ,  $\mathbf{h}_M$  is a vector containing  $n$  measured head values,  $\mathbf{h}_C$  is a vector containing the calculated heads at the  $n$  measurement points and  $\mathbf{W}$  denotes a matrix containing a set of  $n$  basis vectors. Each basis vector represents the change to the nodal values of  $Y$  that results in a unit increase in pressure at one measurement point whilst keeping the pressure at the  $n-1$  remaining measurement points constant. These basis vectors are calculated from the system

$$(\mathbf{LCL}^T)\mathbf{W}^T = \mathbf{LC}, \quad (3.2)$$

where  $\mathbf{C}$  is the covariance matrix of  $Y$  values and  $\mathbf{L}$  is the sensitivity matrix which contains the sensitivity values for all the measured pressures with respect to all the different  $Y$  values. The sensitivity is the derivative of a measured pressure value with respect to a  $Y$  value. Thus, it tells us how

much influence the change in each nodal value of  $Y$  will have on a measured pressure.

This conditioning approach can be extended to that of large variability in  $Y$  and large deviations of the head from the mean head field. Here, the  $Y$  values are conditioned using the formula

$$\mathbf{Y}^C = \mathbf{Y}^U + \sum_{i=1}^n \alpha_i \mathbf{W}_i, \quad (3.3)$$

where  $\mathbf{W}_i$  is the basis vector corresponding to measurement point  $i$  and  $\alpha_i$  are coefficients obtained from minimising the least squares error function

$$E(\alpha_i) = \sum_{i=1}^n \frac{(h_{Mi} - h_{Ci}(Y, \alpha))^2}{\sigma_i^2}, \quad (3.4)$$

where  $h_{Mi}$  is the measured head at measurement point  $i$ ,  $h_{Ci}$  is the calculated head at measurement point  $i$  and  $\sigma_i$  is the standard deviation of the measured head at measurement point  $i$ . The standard deviation tells us how reliable we think the measured heads are. Thus, the measurements can be given different weightings using  $\sigma_i$ .

Cliffe and Jackson's conditioning method was tested using a CPM model of the Waste Isolation Pilot Plant (WIPP) in the USA (The U.S. Department of Energy 2010); a potential location for a repository for the disposal of radioactive waste. The CPM model of the site was based on work by Cliffe and Jackson (1993) and Cauffman, LaVenue et al. (1990). Additionally, there were 20 head measurements available at the site (Cauffman and

LaVenue 1990). The  $Y$  field was heterogeneous and was assumed to have an isotropic covariance ( $C$  was a non-diagonal matrix). The model region was approximately 20km by 30km and was modelled using a FE grid. Cliffe and Jackson's conditioning method (1995; 2000) was very successful when conditioning on the available head values. It reduced the root mean square error from 5m to 0.5m.

### **3.2 – OUTLINE OF THE BASIS VECTOR CONDITIONING METHOD**

In this section, the modifications made to Cliffe and Jackson's conditioning method (1995; 2000) to develop our new conditioning method for a DFN setting (with different governing equations) are outlined. Our new conditioning method will be referred to as the basis vector conditioning method. The details of our conditioning method are described fully in later sections. For consistency with the rest of this thesis we consider pressure measurements instead of head measurements. Additionally, when working with fractures, transmissivity is the natural hydraulic parameter to use instead of hydraulic conductivity (Bear 1972). The proposed basis vector conditioning method conditions fracture log transmissivities on measured pressures at the intersection between a borehole and a fracture. The transmissivity is assumed to be constant over the fracture. Therefore, our conditioning method differs from Cliffe and Jackson's (1995; 2000) in that it conditions the log transmissivity of a whole fracture and not the nodal value of hydraulic conductivity. The fracture log transmissivities are used because it ensures that conditioned fracture transmissivities have a positive value

and are physically admissible. It should be noted that log transmissivities are dependent on the units used for transmissivity. In this thesis units of  $\text{m}^2/\text{s}$  are used for fracture transmissivities. The basic approach taken to update fracture log transmissivity values in order that the calculated and measured pressure values agree, in some appropriate sense, is as follows. A simulation is run with an initial distribution of unconditioned fracture log transmissivities. These fracture log transmissivities are the parameters of our model which we wish to change. When there is a small variance in the values of the fracture log transmissivities, a linear relationship between fracture log transmissivities and pressure measurements can be assumed. This allows us to condition the fracture log transmissivities directly multiplying each basis vector by a given coefficient and adding a linear combination of the resulting vectors to the unconditioned log transmissivities (similar to (3.1)). The coefficients are the difference between the calculated and measured pressures at measurement points. The basis vectors represent the change to the log transmissivity of the fractures in the DFN that results in a unit increase in the pressure at one measurement point whilst keeping the pressure constant at the remaining measurement points, and are calculated using (3.2). However, in a DFN setting,  $\mathbf{C}$  in equation (3.2) is defined as the covariance matrix of the fracture log transmissivities and  $\mathbf{L}$  is defined as the sensitivity matrix where the sensitivity is now the derivative of a measured pressure value with respect to a fracture log transmissivity. Thus, in our basis vector conditioning method, sensitivities are calculated using a transmissivity value over a whole fracture and not for a nodal value of hydraulic conductivity as in Cliffe and Jackson (1995; 2000).

It is physically more realistic for the variance in fracture transmissivities to be large and therefore the assumption of a linear relationship between them and the pressure measurements may not be valid. In this case, the same basis vectors are employed, but the coefficients are now determined by minimising an appropriate error function. Thus, the conditioning will proceed iteratively, while the fracture log transmissivities are updated until the error function has reached a suitable convergence criterion. The error function takes into account the difference between measured and calculated (from our numerical simulation) pressure values. It is equivalent to (3.4) with head values replaced by pressure values. The number of coefficients in the model is equal to the number of measurement points. Thus, for large DFNs, the number of model coefficients is much less than the total number of log transmissivity values.

One of the key steps in the conditioning procedure is the calculation of the sensitivities. We require the sensitivity value of every measured pressure value with respect to each fracture log transmissivity. To this end, adjoint methods can be used to calculate the desired sensitivities. Indeed, it is well known that adjoint methods are advantageous when the number of observation points is less than the number of parameters (Chavent 2009). In this thesis large DFNs containing thousands of fractures are to be conditioned on a small number of measured pressure values and thus the number of parameters is much greater than the observation points; therefore, the adjoint method will be very efficient. Non-linear minimisation of the error function is performed by the Levenberg-Marquardt method.

There are no existing methods that condition fracture log transmissivities in a DFN based on measured pressures. A concise description of our basis function

conditioning method is given in the following sections of this chapter. Firstly, in section 3.3, the case of conditioning realisations of the logarithm of the fracture transmissivity  $T$ ,  $X = \log_{10} T$ , on measurements of  $X$  at fractures of a DFN model (this could be either a FE or FD model) is considered where  $X$  is described by its mean and variance. Figure 6 shows an example of a generated DFN; the fractures are coloured according to their transmissivity  $T$ , which is assumed constant across each fracture. Section 3.4 describes the case in which the variability is small and so there is a linear relationship between the perturbations in  $X$  and the measured pressure values. Furthermore, it explains how an unconditioned realisation is conditioned by adding a linear combination of basis vectors corresponding to the measurements and coefficients which are the difference between the measured pressures and the pressures in the realisation. Section 3.5 introduces the adjoint method, then section 3.6 describes how the sensitivity matrix is calculated using this approach; this sensitivity matrix is then used to calculate the corresponding basis vectors. Finally, section 3.7 considers the case of conditioning on pressure measurements when the variability of the fracture log transmissivities is large; this involves the minimisation of a corresponding error function.

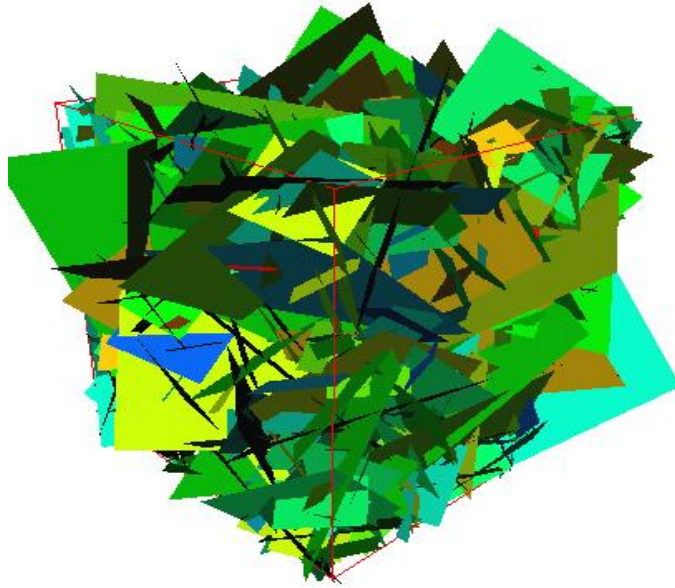


**Figure 6.** Example of a DFN generated within a cubic domain. Fractures are coloured according to their transmissivity value.

### **3.3 – CONDITIONING ON FRACTURE LOG TRANSMISSIVITIES**

The work in this section is based on work by Cliffe and Jackson (1995; 2000) .

This section considers conditioning a DFN model where realisations of fracture log transmissivities  $X$  are generated conditioned on measurements of  $X$  at locations corresponding to the nodes at which  $X$  is generated. These are the nodes of a FE numerical flow model, but could equally have been the nodes of a FD model. Fracture transmissivities are constant on each fracture.

We use a stochastic model to describe the model parameters  $X$  where they are uniquely described by their mean and covariance. The mean of a log transmissivity value  $X_i$  of fracture  $i$  is defined by

$$m_i(X_i) = E[X_i], \tag{3.5}$$

where  $E[\cdot]$  denotes expectation. The covariance of the log transmissivity between two fractures  $i$  and  $j$  is given by

$$C(X_i, X_j) = E[(X_i - m_i)(X_j - m_j)], \quad (3.6)$$

In applications of this stochastic approach, the mean  $m$  and covariance  $C$  are inferred from data. The stochastic approach corresponds to taking  $X$  to be a Gaussian random vector where the joint distribution of  $X$  at any set of points is a multi-variate normal distribution. If we take  $\mathbf{X}$  to be the vector of log transmissivity values  $X$  of each of the  $n$  fractures, i.e.

$$\mathbf{X} = \begin{pmatrix} X_1 \\ X_2 \\ \dots \\ X_n \end{pmatrix}, \quad (3.7)$$

and

$$\mathbf{m} = \begin{pmatrix} m(X_1) \\ m(X_2) \\ \dots \\ m(X_n) \end{pmatrix}, \quad (3.8)$$

to be the mean of the fracture log transmissivities  $X_f$ ,  $f = 1, \dots, n$ , then the probability density function for  $\mathbf{X}$  is given by (Mood, Franklin et al. 1974)

$$\text{pdf}(\mathbf{X}) = \frac{1}{(2\pi)^{n/2} |\mathbf{C}|^{1/2}} \exp\left(-\frac{1}{2}(\mathbf{X}-\mathbf{m})^T \mathbf{C}^{-1}(\mathbf{X}-\mathbf{m})\right), \quad (3.9)$$

where

$$\mathbf{C} = \begin{pmatrix} C(X_1, X_1) & \dots & C(X_1, X_n) \\ \dots & \dots & \dots \\ C(X_n, X_1) & \dots & C(X_n, X_n) \end{pmatrix}, \quad (3.10)$$

is the covariance matrix for  $\mathbf{X}$  between the various fracture log transmissivities and  $|\cdot|$  denotes the determinant.

A realisation of  $\mathbf{X}$  is generated for  $n$  fractures in a DFN model. To simplify the notation, the mean  $m$  of all  $X_f$  values is taken to be zero (it can be added back in at any time in the following analysis if desired) and the vector  $\mathbf{X}$  is partitioned into two parts

$$\mathbf{X} = \begin{pmatrix} \mathbf{X}_1 \\ \mathbf{X}_2 \end{pmatrix}, \quad (3.11)$$

where  $\mathbf{X}_1$  corresponds to the  $m$  fractures for which there are log transmissivity measurements of  $X_f$  (but  $\mathbf{X}_1$  is unconditioned and is not equal to the measurements of  $X_f$ ) and  $\mathbf{X}_2$  corresponds to the  $n-m$  fractures for which there are no measurements. The covariance matrix  $\mathbf{C}$  can be partitioned in a similar way to  $\mathbf{X}$ , giving

$$\mathbf{C} = \begin{pmatrix} \mathbf{C}_{11} & \mathbf{C}_{12} \\ \mathbf{C}_{21} & \mathbf{C}_{22} \end{pmatrix}. \quad (3.12)$$

Here  $\mathbf{C}_{11}$  is the  $m \times m$  covariance matrix for the  $m$  measurement fractures and  $\mathbf{C}_{22}$  is the  $(n-m) \times (n-m)$  covariance matrix for the  $n-m$  fractures where there are no measurements. Unconditioned realisations  $\mathbf{X}^u = \begin{pmatrix} \mathbf{X}_1^u \\ \mathbf{X}_2^u \end{pmatrix}$  can be generated with given mean and covariance values. Consider generating realisations of  $\mathbf{X}$ , that are such that  $\mathbf{X}_1 = \mathbf{X}_1^*$ , where  $\mathbf{X}_1^*$  is the vector of measured values of  $X$ . Due to the fact that  $\mathbf{X}$  is a Gaussian spatial process it will have a multi-variate normal distribution given by (3.9) with the mean vector  $\mathbf{m}$  set to zero. Then, we write the conditional probability density function for  $\mathbf{X}_2$  given measurements  $\mathbf{X}_1 = \mathbf{X}_1^*$  as (Mood, Franklin et al. 1974)

$$\text{pdf}(\mathbf{X}_2 | \mathbf{X}_1) = \frac{\frac{1}{(2\pi)^{n/2} |\mathbf{C}|^{1/2}} \exp\left(-\frac{1}{2} \mathbf{X}^T \mathbf{C}^{-1} \mathbf{X}\right)}{\frac{1}{(2\pi)^{m/2} |\mathbf{C}_{11}|^{1/2}} \exp\left(-\frac{1}{2} \mathbf{X}_1^T (\mathbf{C}_{11})^{-1} \mathbf{X}_1\right)}. \quad (3.13)$$

The aim is to identify the parameters  $\mathbf{X}$  of this distribution. An

$LDL^T$  factorisation is used to factorise the inverse of the covariance matrix  $\mathbf{C}$  as

$$\begin{aligned}
\mathbf{C}^{-1} &\equiv \left[ \begin{pmatrix} \mathbf{I} & \mathbf{0} \\ \mathbf{C}_{21}\mathbf{C}_{11}^{-1} & \mathbf{I} \end{pmatrix} \begin{pmatrix} \mathbf{C}_{11} & \mathbf{0} \\ \mathbf{0} & \mathbf{C}_{22} - \mathbf{C}_{21}\mathbf{C}_{11}^{-1}\mathbf{C}_{12} \end{pmatrix} \begin{pmatrix} \mathbf{I} & \mathbf{C}_{11}^{-1}\mathbf{C}_{12} \\ \mathbf{0} & \mathbf{I} \end{pmatrix} \right]^{-1} \\
&= \begin{pmatrix} \mathbf{I} & \mathbf{C}_{11}^{-1}\mathbf{C}_{12} \\ \mathbf{0} & \mathbf{I} \end{pmatrix}^{-1} \begin{pmatrix} \mathbf{C}_{11} & \mathbf{0} \\ \mathbf{0} & \mathbf{C}_{22} - \mathbf{C}_{21}\mathbf{C}_{11}^{-1}\mathbf{C}_{12} \end{pmatrix}^{-1} \begin{pmatrix} \mathbf{I} & \mathbf{0} \\ \mathbf{C}_{21}\mathbf{C}_{11}^{-1} & \mathbf{I} \end{pmatrix}^{-1} \\
&= \begin{pmatrix} \mathbf{I} & \mathbf{0} \\ \mathbf{C}_{21}\mathbf{C}_{11}^{-1} & \mathbf{I} \end{pmatrix}^{-\text{T}} \begin{pmatrix} \mathbf{C}_{11} & \mathbf{0} \\ \mathbf{0} & \mathbf{C}_{22} - \mathbf{C}_{21}\mathbf{C}_{11}^{-1}\mathbf{C}_{12} \end{pmatrix}^{-1} \begin{pmatrix} \mathbf{I} & \mathbf{0} \\ \mathbf{C}_{21}\mathbf{C}_{11}^{-1} & \mathbf{I} \end{pmatrix}^{-1},
\end{aligned} \tag{3.14}$$

where  $^{-\text{T}}$  denotes the transpose of the inverse. Equation (3.14) makes use of the fact that

$$(\mathbf{C}_{21}\mathbf{C}_{11}^{-1})^{\text{T}} = \mathbf{C}_{11}^{-\text{T}}\mathbf{C}_{21}^{\text{T}} = \mathbf{C}_{11}^{-1}\mathbf{C}_{12}, \tag{3.15}$$

which in turn uses the relationships  $\mathbf{C}_{21}^{\text{T}} = \mathbf{C}_{12}$  and  $\mathbf{C}_{11}^{\text{T}} = \mathbf{C}_{11}$ . Thus, we may write

$$\mathbf{X}^{\text{T}}\mathbf{C}^{-1}\mathbf{X} = \begin{pmatrix} \mathbf{X}_1^{\text{T}} & \mathbf{X}_2^{\text{T}} \end{pmatrix} \begin{pmatrix} \mathbf{I} & \mathbf{0} \\ \mathbf{C}_{21}\mathbf{C}_{11}^{-1} & \mathbf{I} \end{pmatrix}^{-\text{T}} \begin{pmatrix} \mathbf{C}_{11} & \mathbf{0} \\ \mathbf{0} & \mathbf{C}_{22} - \mathbf{C}_{21}\mathbf{C}_{11}^{-1}\mathbf{C}_{12} \end{pmatrix}^{-1} \begin{pmatrix} \mathbf{I} & \mathbf{0} \\ \mathbf{C}_{21}\mathbf{C}_{11}^{-1} & \mathbf{I} \end{pmatrix}^{-1} \begin{pmatrix} \mathbf{X}_1 \\ \mathbf{X}_2 \end{pmatrix}. \tag{3.16}$$

Defining

$$\begin{pmatrix} \mathbf{X}'_1 \\ \mathbf{X}'_2 \end{pmatrix} = \begin{pmatrix} \mathbf{I} & \mathbf{0} \\ \mathbf{C}_{21}\mathbf{C}_{11}^{-1} & \mathbf{I} \end{pmatrix}^{-1} \begin{pmatrix} \mathbf{X}_1 \\ \mathbf{X}_2 \end{pmatrix} = \begin{pmatrix} \mathbf{X}_1 \\ \mathbf{X}_2 - \mathbf{C}_{21}\mathbf{C}_{11}^{-1}\mathbf{X}_1 \end{pmatrix}, \tag{3.17}$$

and inserting (3.17) into (3.16) yields

$$\begin{aligned}\mathbf{X}^T \mathbf{C}^{-1} \mathbf{X} &= \begin{pmatrix} \mathbf{X}'_1 & \mathbf{X}'_2 \end{pmatrix} \begin{pmatrix} \mathbf{C}_{11} & \mathbf{0} \\ \mathbf{0} & \mathbf{C}_{22} - \mathbf{C}_{21} \mathbf{C}_{11}^{-1} \mathbf{C}_{12} \end{pmatrix}^{-1} \begin{pmatrix} \mathbf{X}'_1 \\ \mathbf{X}'_2 \end{pmatrix} \\ &= \mathbf{X}'_1{}^T \mathbf{C}_{11}^{-1} \mathbf{X}'_1 + \mathbf{X}'_2{}^T (\mathbf{C}_{22} - \mathbf{C}_{21} \mathbf{C}_{11}^{-1} \mathbf{C}_{12})^{-1} \mathbf{X}'_2.\end{aligned}\quad (3.18)$$

Now the exponential in the denominator on the right hand side of (3.13) can be cancelled with the term in the exponential in the numerator when it is written in the form of (3.18), resulting from the fact that  $\mathbf{X}'_1{}^T \mathbf{C}_{11}^{-1} \mathbf{X}'_1 = \mathbf{X}_1^T \mathbf{C}_{11}^{-1} \mathbf{X}_1$ . From (3.14) the determinant of the covariance matrix may be written as

$$|\mathbf{C}| = \begin{vmatrix} \mathbf{C}_{11} & \mathbf{0} \\ \mathbf{0} & \mathbf{C}_{22} - \mathbf{C}_{21} \mathbf{C}_{11}^{-1} \mathbf{C}_{12} \end{vmatrix} = |\mathbf{C}_{11}| |\mathbf{C}_{22} - \mathbf{C}_{21} \mathbf{C}_{11}^{-1} \mathbf{C}_{12}|. \quad (3.19)$$

Therefore, the determinant in the denominator of (3.13) can also be cancelled with the corresponding factor in the numerator, as can the factor  $2\pi^{m/2}$ . Thus, the conditional distribution for  $\mathbf{X}_2$  given  $\mathbf{X}_1$  can be written as

$$\begin{aligned}\text{pdf}(\mathbf{X}_2 | \mathbf{X}_1) &= \frac{1}{(2\pi)^{(n-m)/2} |\mathbf{C}_{22} - \mathbf{C}_{21} \mathbf{C}_{11}^{-1} \mathbf{C}_{12}|^{1/2}} \exp\left(-\frac{1}{2} \mathbf{X}'_2{}^T (\mathbf{C}_{22} - \mathbf{C}_{21} \mathbf{C}_{11}^{-1} \mathbf{C}_{12})^{-1} \mathbf{X}'_2\right) \\ &= \frac{1}{(2\pi)^{(n-m)/2} |\mathbf{C}_{22} - \mathbf{C}_{21} \mathbf{C}_{11}^{-1} \mathbf{C}_{12}|^{1/2}} \\ &\quad \exp\left(-\frac{1}{2} (\mathbf{X}_2 - \mathbf{C}_{21} \mathbf{C}_{11}^{-1} \mathbf{X}_1)^T (\mathbf{C}_{22} - \mathbf{C}_{21} \mathbf{C}_{11}^{-1} \mathbf{C}_{12})^{-1} (\mathbf{X}_2 - \mathbf{C}_{21} \mathbf{C}_{11}^{-1} \mathbf{X}_1)\right).\end{aligned}\quad (3.20)$$

This is a multi-variate normal distribution with mean

$$\mathbf{C}_{21}\mathbf{C}_{11}^{-1}\mathbf{X}_1, \quad (3.21)$$

and covariance

$$\mathbf{C}_{22} - \mathbf{C}_{21}\mathbf{C}_{11}^{-1}\mathbf{C}_{12}. \quad (3.22)$$

It can be shown that the probability density function for

$$\mathbf{X}_2^{\bar{C}} = \mathbf{X}_2^u + \mathbf{C}_{21}\mathbf{C}_{11}^{-1}(\mathbf{X}_1^* - \mathbf{X}_1^u), \quad (3.23)$$

is identical to that for  $\mathbf{X}_2$  given  $\mathbf{X}_1 = \mathbf{X}_1^*$  in (3.20) (the notation  $\bar{C}$  has been introduced to distinguish it from the covariance matrix). To show this we denote the mean of  $\mathbf{X}_2^{\bar{C}}$  as  $E[\mathbf{X}_2^{\bar{C}}]$ , then

$$\begin{aligned} E[\mathbf{X}_2^{\bar{C}}] &= E[\mathbf{X}_2^u + \mathbf{C}_{21}\mathbf{C}_{11}^{-1}(\mathbf{X}_1^* - \mathbf{X}_1^u)] \\ &= E[\mathbf{X}_2^u] + \mathbf{C}_{21}\mathbf{C}_{11}^{-1}(E[\mathbf{X}_1^*] - E[\mathbf{X}_1^u]) \\ &= \mathbf{C}_{21}\mathbf{C}_{11}^{-1}\mathbf{X}_1^*. \end{aligned} \quad (3.24)$$

This is the same mean as in (3.21) with  $\mathbf{X}_1 = \mathbf{X}_1^*$ . The covariance of  $\mathbf{X}_2^{\bar{C}}$  is defined as

$$\mathbf{C}(\mathbf{X}_2^{\bar{C}}) = E\left[\left(\mathbf{X}_2^{\bar{C}} - E[\mathbf{X}_2^{\bar{C}}]\right)\left(\mathbf{X}_2^{\bar{C}} - E[\mathbf{X}_2^{\bar{C}}]\right)^T\right]. \quad (3.25)$$

Then using (3.23) and (3.24) this becomes

$$\mathbf{C}(\mathbf{X}_2^{\bar{c}}) = E \left[ \left[ \mathbf{X}_2^u + \mathbf{C}_{21} \mathbf{C}_{11}^{-1} (\mathbf{X}_1^* - \mathbf{X}_1^u) - \mathbf{C}_{21} \mathbf{C}_{11}^{-1} \mathbf{X}_1^* \right] \left[ \mathbf{X}_2^u + \mathbf{C}_{21} \mathbf{C}_{11}^{-1} (\mathbf{X}_1^* - \mathbf{X}_1^u) - \mathbf{C}_{21} \mathbf{C}_{11}^{-1} \mathbf{X}_1^* \right]^T \right] \quad (3.26)$$

which simplifies to

$$\begin{aligned} \mathbf{C}(\mathbf{X}_2^{\bar{c}}) &= E \left[ (\mathbf{X}_2^u - \mathbf{C}_{21} \mathbf{C}_{11}^{-1} \mathbf{X}_1^u) (\mathbf{X}_2^u - \mathbf{C}_{21} \mathbf{C}_{11}^{-1} \mathbf{X}_1^u)^T \right], \\ &= E \left[ \mathbf{X}_2^u (\mathbf{X}_2^u)^T \right] - \mathbf{C}_{21} \mathbf{C}_{11}^{-1} E \left[ \mathbf{X}_1^u (\mathbf{X}_2^u)^T \right] \\ &\quad - \mathbf{C}_{21} \mathbf{C}_{11}^{-1} E \left[ \mathbf{X}_2^u (\mathbf{X}_1^u)^T \right] + \mathbf{C}_{21} \mathbf{C}_{11}^{-1} \mathbf{C}_{21} \mathbf{C}_{11}^{-1} E \left[ \mathbf{X}_1^u (\mathbf{X}_1^u)^T \right]. \end{aligned} \quad (3.27)$$

By using the partitioning of the covariance matrix as defined in (3.12) we can write this as

$$\begin{aligned} \mathbf{C}(\mathbf{X}_2^{\bar{c}}) &= \mathbf{C}_{22} - \mathbf{C}_{21} \mathbf{C}_{11}^{-1} \mathbf{C}_{12} - \mathbf{C}_{21} \mathbf{C}_{11}^{-1} \mathbf{C}_{21} + \mathbf{C}_{21} \mathbf{C}_{11}^{-1} \mathbf{C}_{21} \\ &= \mathbf{C}_{22} - \mathbf{C}_{21} \mathbf{C}_{11}^{-1} \mathbf{C}_{12}, \end{aligned} \quad (3.28)$$

which is the same covariance as (3.22) with. Thus, we have shown that the probability density function for  $\mathbf{X}_2^{\bar{c}}$  given in (3.23) is a Gaussian process with the same mean and covariance as (3.20). Therefore,

$$\mathbf{X}^{\bar{c}} = \begin{pmatrix} \mathbf{X}_1^{\bar{c}} \\ \mathbf{X}_2^{\bar{c}} \end{pmatrix} = \begin{pmatrix} \mathbf{X}_1^* \\ \mathbf{X}_2^u + \mathbf{C}_{21} \mathbf{C}_{11}^{-1} (\mathbf{X}_1^* - \mathbf{X}_1^u) \end{pmatrix}, \quad (3.29)$$

provides the desired conditional realisation for the logarithm of fracture transmissivities  $\mathbf{X}^{\bar{c}}$  conditioned on measured values of the logarithm of fracture transmissivities  $\mathbf{X}_1^*$ .

### 3.4 CONDITIONING ON LINEAR CONSTRAINTS

For ease of notation we take  $\mathbf{P}$  to be a vector of residual pressures at global nodes located at fracture intersections. From hereon any reference to a pressure value is referring to the residual pressure defined by (1.5). For small perturbations in both the pressure and fracture log transmissivities  $\mathbf{X}$ , we can assume that the relationship between these quantities is linear. Thereby, we may condition  $\mathbf{X}$  based on linear constraints. To this end, we write

$$\mathbf{LX} = \mathbf{P}_M, \quad (3.30)$$

where  $\mathbf{L}$  is an  $m \times n$  matrix of full rank representing a linear constraint and  $\mathbf{P}_M$  is an  $m$ -vector containing measured pressure values. The rows of  $\mathbf{L}$  are

independent, so we can find a matrix  $\mathbf{J}$  such that  $\begin{pmatrix} \mathbf{L} \\ \mathbf{J} \end{pmatrix}$  is non-singular. The

matrix  $\mathbf{J}$  is introduced to ensure that  $\begin{pmatrix} \mathbf{L} \\ \mathbf{J} \end{pmatrix}^{-1}$  exists because (as will be seen in the

following analysis)  $\begin{pmatrix} \mathbf{L} \\ \mathbf{J} \end{pmatrix}$  will then fall out of the conditioning expression and

hence the value of  $\mathbf{J}$  is not important. Define

$$\mathbf{P} = \begin{pmatrix} \mathbf{L} \\ \mathbf{J} \end{pmatrix} \mathbf{X}. \quad (3.31)$$

Then the probability density function for  $\mathbf{P}$  is given by

$$\begin{aligned} \text{pdf}(\mathbf{P}) &= \frac{1}{\left| \begin{pmatrix} \mathbf{L} \\ \mathbf{J} \end{pmatrix} \right| (2\pi)^{n/2} |\mathbf{C}|^{1/2}} \exp\left(-\frac{1}{2} \mathbf{X}^T \mathbf{C}^{-1} \mathbf{X}\right) \\ &= \frac{1}{\left| \begin{pmatrix} \mathbf{L} \\ \mathbf{J} \end{pmatrix} \right| (2\pi)^{n/2} |\mathbf{C}|^{1/2}} \exp\left(-\frac{1}{2} \left( \begin{pmatrix} \mathbf{L} \\ \mathbf{J} \end{pmatrix}^{-1} \mathbf{P} \right)^T \mathbf{C}^{-1} \left( \begin{pmatrix} \mathbf{L} \\ \mathbf{J} \end{pmatrix}^{-1} \mathbf{P} \right)\right) \\ &= \frac{1}{\left| \begin{pmatrix} \mathbf{L} \\ \mathbf{J} \end{pmatrix} \right| (2\pi)^{n/2} |\mathbf{C}|^{1/2}} \exp\left(-\frac{1}{2} \mathbf{P}^T \left( \begin{pmatrix} \mathbf{L} \\ \mathbf{J} \end{pmatrix}^{-1} \right)^T \mathbf{C}^{-1} \begin{pmatrix} \mathbf{L} \\ \mathbf{J} \end{pmatrix}^{-1} \mathbf{P}\right) \\ &= \frac{1}{(2\pi)^{n/2} |\mathbf{C}_P|^{1/2}} \exp\left(-\frac{1}{2} \mathbf{P}^T \mathbf{C}_P^{-1} \mathbf{P}\right), \end{aligned} \quad (3.32)$$

where  $\mathbf{C}_P$  is defined as

$$\begin{aligned} \mathbf{C}_P &= \left( \left( \begin{pmatrix} \mathbf{L} \\ \mathbf{J} \end{pmatrix}^{-1} \right)^T \mathbf{C}^{-1} \begin{pmatrix} \mathbf{L} \\ \mathbf{J} \end{pmatrix}^{-1} \right)^{-1} \\ &= \begin{pmatrix} \mathbf{L} \\ \mathbf{J} \end{pmatrix} \mathbf{C} \begin{pmatrix} \mathbf{L} \\ \mathbf{J} \end{pmatrix}^T \\ &= \begin{pmatrix} \mathbf{LCL}^T & \mathbf{LCJ}^T \\ \mathbf{JCL}^T & \mathbf{JCJ}^T \end{pmatrix}. \end{aligned} \quad (3.33)$$

Moreover,

$$|\mathbf{C}_P| = \left| \begin{pmatrix} \mathbf{L} \\ \mathbf{J} \end{pmatrix} \right|^2 |\mathbf{C}|. \quad (3.34)$$

Generating realisations of  $\mathbf{X}$  such that  $\mathbf{LX} = \mathbf{P}_M$  is equivalent to generating realisations of  $\mathbf{P}$  such that  $\mathbf{P}_1 = \mathbf{P}_M$ , where  $\mathbf{P}_1$  is a vector of calculated pressures at measurement points. The conditional realisations that are required,  $\mathbf{P}^{\bar{C}}$ , can be obtained from unconditioned realisations  $\mathbf{P}^U$ . This is done using the method discussed in section 3.3 and using (3.29) so that the conditioned realisations are given by

$$\mathbf{P}^{\bar{C}} = \begin{pmatrix} \mathbf{P}_1^{\bar{C}} \\ \mathbf{P}_2^{\bar{C}} \end{pmatrix} = \begin{pmatrix} \mathbf{P}_M \\ \mathbf{P}_2^U + \mathbf{C}_{P21} \mathbf{C}_{P11}^{-1} (\mathbf{P}_M - \mathbf{P}_1^U) \end{pmatrix}. \quad (3.35)$$

The unconditioned realisations  $\mathbf{P}^U$  can be obtained from unconditioned realisations of  $\mathbf{X}^U$ . We then find from (3.31) and (3.35) that the conditioned realisations are given by

$$\begin{aligned}
\mathbf{LX}^{\bar{c}} &= \mathbf{P}_1^{\bar{c}} = \mathbf{P}_M = \mathbf{P}_1^U + (\mathbf{P}_M - \mathbf{P}_1^U) \\
&= \mathbf{P}_1^U + (\mathbf{LCL}^T)(\mathbf{LCL}^T)^{-1}(\mathbf{P}_M - \mathbf{P}_1^U) \\
&= \mathbf{LX}^U + (\mathbf{LCL}^T)(\mathbf{LCL}^T)^{-1}(\mathbf{P}_M - \mathbf{P}_1^U),
\end{aligned} \tag{3.36}$$

and

$$\begin{aligned}
\mathbf{JX}^{\bar{c}} &= \mathbf{P}_2^{\bar{c}} = \mathbf{P}_2^U + (\mathbf{JCL}^T)(\mathbf{LCL}^T)^{-1}(\mathbf{P}_M - \mathbf{P}_1^U) \\
&= \mathbf{JX}^U + (\mathbf{JCL}^T)(\mathbf{LCL}^T)^{-1}(\mathbf{P}_M - \mathbf{P}_1^U).
\end{aligned} \tag{3.37}$$

Therefore, we can write

$$\begin{pmatrix} \mathbf{L} \\ \mathbf{J} \end{pmatrix} \mathbf{X}^{\bar{c}} = \begin{pmatrix} \mathbf{L} \\ \mathbf{J} \end{pmatrix} \mathbf{X}^U + \begin{pmatrix} \mathbf{L} \\ \mathbf{J} \end{pmatrix} (\mathbf{CL}^T)(\mathbf{LCL}^T)^{-1}(\mathbf{P}_M - \mathbf{P}_1^U), \tag{3.38}$$

and because  $\begin{pmatrix} \mathbf{L} \\ \mathbf{J} \end{pmatrix}$  is non-singular, the desired conditioned realisations are given by

$$\mathbf{X}^{\bar{c}} = \mathbf{X}^U + (\mathbf{CL}^T)(\mathbf{LCL}^T)^{-1}(\mathbf{P}_M - \mathbf{P}_1^U), \tag{3.39}$$

which can be written as

$$\mathbf{X}^{\bar{c}} = \mathbf{X}^U + \mathbf{W}(\mathbf{P}_M - \mathbf{P}_1^U), \tag{3.40}$$

where  $\mathbf{W}$  is an  $n \times m$  matrix given by

$$\mathbf{W} = (\mathbf{C}\mathbf{L}^T)(\mathbf{L}\mathbf{C}\mathbf{L}^T)^{-1}. \quad (3.41)$$

Thus,  $\mathbf{W}$  is obtained by solving the system

$$(\mathbf{L}\mathbf{C}\mathbf{L}^T)\mathbf{W}^T = \mathbf{L}\mathbf{C}. \quad (3.42)$$

The matrix  $\mathbf{W}$  comprises of a set of  $n$  basis vectors each of which corresponds to a given pressure measurement. The basis vector corresponding to a pressure measurement represents the change to the log transmissivity of the fractures in the network that results in a unit increase in the pressure at that measurement point whilst keeping the pressure constant at the remaining measurement points constant. The basis functions may give an exact answer when used in (3.40) if the variance in the fracture transmissivities is small. Non-linear minimization extends this approach to deal with large variability in fracture log transmissivities, and will be discussed in section 3.7. Thus, we can condition an unconditioned realisation of fracture log transmissivities by adding a linear combination of the basis vectors and coefficients given by (3.40). The coefficients of the basis vectors,  $(\mathbf{P}_M - \mathbf{P}_1^U)$ , are the differences between the measured values of pressure and their unconditioned values at measurement points. The matrix  $\mathbf{L}$  is known as the sensitivity matrix. The covariance matrix  $\mathbf{C}$  represents the correlation of the log transmissivities of the fractures in the network.

### 3.5 – INTRODUCTION TO THE ADJOINT METHOD

We consider a model characterised by a set of pressure values  $P_j$ ,  $j = 1, \dots, N$ , where  $N$  is the number of global nodes at fracture intersections that the model is discretised with. The parameters of the model are the fracture log transmissivities  $X_f$ ,  $f = 1, \dots, n$ , where  $n$  is the number of fractures. The equations for the model are written in the form

$$F_i(P; X) = 0, \quad i = 1, \dots, N. \quad (3.43)$$

Suppose one is interested in  $m$  ( $\ll n$ ) measurements or consequences  $G_s(P_j, X_f)$ ,  $s = 1, \dots, m$ , (defined as the difference between calculated and measured pressure values at measurement locations). The quantities of interest are the sensitivities

$$\frac{dG_s}{dX_f}, \quad f = 1, \dots, n, \quad s = 1, \dots, m, \quad (3.44)$$

where index notation has been used and will continue to be used when considering matrix derivatives in this section. Now,

$$\frac{dG_s}{dX_f} = \frac{\partial G_s}{\partial P_j} \frac{\partial P_j}{\partial X_f} + \frac{\partial G_s}{\partial X_f}, \quad f = 1, \dots, n, \quad j = 1, \dots, N, \quad s = 1, \dots, m. \quad (3.45)$$

The last term in (3.45) gives the sensitivity of  $G_s$  to  $X_f$  resulting in an explicit dependence on  $X_f$ , while the first term gives the implicit dependence of  $G_s$  on  $X_f$  from the model. Now differentiating the equations for the model (3.43) with respect to  $X_f$  gives

$$\frac{dF_i}{dX_f} = \frac{\partial F_i}{\partial P_j} \frac{\partial P_j}{\partial X_f} + \frac{\partial F_i}{\partial X_f} = 0, \quad f = 1, \dots, n, \quad i = 1, \dots, N, \quad j = 1, \dots, N, \quad (3.46)$$

and it follows that

$$\frac{\partial P_j}{\partial X_f} = - \left( \frac{\partial F_i}{\partial P_j} \right)^{-1} \frac{\partial F_i}{\partial X_f}, \quad f = 1, \dots, n, \quad i = 1, \dots, N, \quad j = 1, \dots, N. \quad (3.47)$$

Then, substituting (3.47) into (3.45) yields

$$\frac{dG_s}{dX_f} = - \frac{\partial G_s}{\partial P_j} \left( \frac{\partial F_i}{\partial P_j} \right)^{-1} \frac{\partial F_i}{\partial X_f} + \frac{\partial G_s}{\partial X_f}, \quad (3.48)$$

$$f = 1, \dots, n, \quad i = 1, \dots, N, \quad j = 1, \dots, N, \quad s = 1, \dots, m,$$

which may be written in the form

$$\frac{dG_s}{dX_f} = (\theta^T)_{sj} \frac{\partial F_i}{\partial X_f} + \frac{\partial G_s}{\partial X_f}, \quad (3.49)$$

$$f = 1, \dots, n, \quad i = 1, \dots, N, \quad j = 1, \dots, N, \quad s = 1, \dots, m,$$

where

$$\begin{aligned} (\theta^T)_{sj} &= -\frac{\partial G_s}{\partial P_j} \left( \frac{\partial F_i}{\partial P_j} \right)^{-1}, \\ i &= 1, \dots, N, \quad j = 1, \dots, N, \quad s = 1, \dots, m. \end{aligned} \quad (3.50)$$

Rearranging terms gives

$$\begin{aligned} (\theta^T)_{sj} \frac{\partial F_i}{\partial P_j} &= -\frac{\partial G_s}{\partial P_j}, \\ i &= 1, \dots, N, \quad j = 1, \dots, N, \quad s = 1, \dots, m. \end{aligned} \quad (3.51)$$

Equation (3.50) defines the adjoint  $(\theta^T)_{sj}$ , and this can be inserted into equation (3.49) to calculate the sensitivities. The key reason for introducing the adjoint is that it is computationally cheaper to calculate sensitivities using the adjoint approach when  $m \ll n$  than using a direct approach such as a finite difference approximation. The term  $\frac{dG_s}{dX_f}$  can be evaluated from a single solve of (3.51)

which is independent of the number of fractures  $n$ , followed by a single matrix-matrix product calculated in (3.49). Other direct methods such as a finite difference approximation of  $\frac{dG_s}{dX_f}$  require the solution of (3.44)  $n$  times. Hence in this setting where  $m \ll n$ , the adjoint method is computationally cheaper than other direct methods.

### 3.6 - CALCULATION OF THE PRESSURE SENSITIVITIES IN A DISCRETE FRACTURE NETWORK

There will be  $m$  pressure measurements obtained at different boreholes across the model domain where the inflow is specified and we suppose that the vector of consequences at measurement points  $G_s$ ,  $s = 1, \dots, m$ , is given by

$$\begin{aligned} G_s &= P_s^B - P_{Ms} \\ &= P_s^B + \frac{Q_{Bs}}{\gamma_s T_s} - P_{Ms} , \end{aligned} \tag{3.52}$$

where  $P_s^B$ ,  $s = 1, \dots, m$ , are borehole pressures,  $T_s$ ,  $s = 1, \dots, m$ , are fracture transmissivities at the measurement points,  $Q_{Bs}$ ,  $s = 1, \dots, m$ , are borehole fluxes and  $\gamma_s$ ,  $s = 1, \dots, m$ , are geometric constants all defined in the borehole model (2.53). The consequence was chosen to be given by (3.52) because this corresponds to the data available to us from test sites. The consequence could equally be a flow or transmissivity measurement.

Given pressures  $P_i$ ,  $i = 1, \dots, N$ , at  $N$  global nodes, and  $T_f$ ,  $f = 1, \dots, n$ , constant transmissivities corresponding to  $n$  fractures, the weak form of the flow equation defined in (2.47) (without splitting the Dirichlet boundary nodes) at global nodes, is

$$F_j = \sum_{i=1}^N \left\{ \int_f \nabla \Psi_j \cdot \tilde{T}_f \nabla \Psi_i P_i + \int_{\Upsilon} \Psi_j Q_j \right\} = 0, \quad (3.53)$$

$$f = 1, \dots, n, \quad i = 1, \dots, N, \quad j = 1, \dots, N,$$

where  $\Upsilon$  is the boundary where the flux  $Q$  is defined,  $\Psi_j$  are the FE global basis

functions and the pressure has been approximated as  $\hat{P} = \sum_{i=1}^N \Psi_i P_i$ . Differentiating

(3.53) with respect to  $P_i$  we may write

$$\frac{\partial F_j}{\partial P_i} = \sum_{i=1}^N \int_f \nabla \Psi_j \cdot \tilde{T}_f \nabla \Psi_i, \quad (3.54)$$

$$f = 1, \dots, n, \quad i = 1, \dots, N, \quad j = 1, \dots, N.$$

Similarly,

$$\frac{\partial F_j}{\partial X_f} = \sum_{i=1}^N \left\{ \int_f \nabla \Psi_j \cdot \left( \frac{1}{\rho g} \frac{\partial T_f}{\partial X_f} \right) \nabla \Psi_i P_i \right\}, \quad (3.55)$$

$$f = 1, \dots, n, \quad i = 1, \dots, N, \quad j = 1, \dots, N.$$

The partial derivatives of the consequences (3.52) with respect to the log transmissivities  $X_f$  are

$$\frac{\partial G_s}{\partial X_f} = - \frac{\ln 10 Q_{Bs} \delta_{sf}}{\gamma_s T_f}, \quad (3.56)$$

$$f = 1, \dots, n, \quad s = 1, \dots, m.$$

Furthermore,

$$\frac{\partial G_s}{\partial P_j} = \delta_{sj} , \quad (3.57)$$

$$j = 1, \dots, N, \quad s = 1, \dots, m .$$

Then, using (3.51), (3.54) and (3.57) the equation for the adjoint becomes

$$\theta_{sj}^T \sum_{i=1}^N \int_f \nabla \Psi_j \cdot (\tilde{T}_f \nabla \Psi_i) = -\delta_{sj} , \quad (3.58)$$

$$f = 1, \dots, n, \quad i = 1, \dots, N, \quad j = 1, \dots, N, \quad s = 1, \dots, m .$$

where  $\theta_{sj}^T$  denotes the transpose of the adjoint. This then gives us a defining equation for the transpose of the adjoint,  $\theta_{sj}^T$ , corresponding to measurement point  $s$ . The adjoint is approximated in the same way as the pressure, namely

$$\hat{\theta} = \sum_{i=1}^N \Psi_i \theta_i . \quad (3.59)$$

The sensitivities can now be calculated using (3.49), (3.55), (3.56) and (3.59)

$$\begin{aligned} \frac{dG_s}{dX_f} &= \theta_{sj}^T \left\{ \sum_{i=1}^N \left( \int_f \nabla \Psi_j \cdot \left( \frac{\partial \tilde{T}_f}{\partial X_f} \nabla \Psi_i P_i \right) \right) \right\} - \frac{\ln 10 Q_{Bs} \delta_{sf}}{\gamma_s T_f} \\ &= \int_f \sum_{i=1}^N \left( \nabla \hat{\theta}_s^T \cdot \left( \frac{\partial \tilde{T}_f}{\partial X_f} \nabla \Psi_i P_i \right) \right) - \frac{\ln 10 Q_{Bs} \delta_{sf}}{\gamma_s T_f} \\ &= \int_f \sum_{i=1}^N \nabla \hat{\theta}_s^T \ln 10 \tilde{T}_f \cdot (\nabla \Psi_i P_i) - \frac{\ln 10 Q_{Bs} \delta_{sf}}{\gamma_s T_f} \end{aligned}$$

$$= \int_f \nabla \hat{\theta}_s^T \ln 10 \tilde{T}_f \cdot (\nabla \hat{P}) - \frac{\ln 10 Q_{Bs} \delta_{sf}}{\gamma_s T_f} \quad (3.60)$$

$$f = 1, \dots, n, \quad j = 1, \dots, N, \quad s = 1, \dots, m$$

The integral term in (3.60) can be calculated using a numerical quadrature technique while the second term is easily evaluated. The sensitivity values calculated in (3.60) can be modified to take into account multiple fracture intersections to a borehole, which provide alternative flow routes. This modification is explained in Appendix A.

### 3.7 – CONDITIONING ON PRESSURES WHEN VARIABILITY IS LARGE

So far, only the case of small variability of the fracture transmissivities and small deviations of the pressure from the mean pressure field have been considered. However, such assumptions are not valid due to the many uncertainties in the fracture transmissivities. Therefore, the situation of large variability of the fracture log transmissivities and large deviations of the pressure from the mean pressure field is considered. Here, the unconditioned fracture log transmissivity values are denoted by the vector  $\mathbf{X}^U$  and basis vectors  $\mathbf{W}_{sf}$ ,  $s = 1, \dots, m$ ,  $f = 1, \dots, n$  are computed as in section 3.4. An update to the log

transmissivities is evaluated assuming the following relationship suggested by Cliffe and Jackson (1995; 2000):

$$\mathbf{X} = \mathbf{X}^U + \sum_{s=1}^m \alpha_s \mathbf{W}_{sf} ,$$

$$\begin{pmatrix} X_1 \\ \dots \\ X_n \end{pmatrix} = \begin{pmatrix} X_1^U \\ \dots \\ X_n^U \end{pmatrix} + \left\{ \alpha_1 \begin{pmatrix} W_{11} \\ \dots \\ W_{1n} \end{pmatrix} + \alpha_2 \begin{pmatrix} W_{21} \\ \dots \\ W_{2n} \end{pmatrix} + \dots + \alpha_m \begin{pmatrix} W_{s1} \\ \dots \\ W_{sn} \end{pmatrix} \right\} , \quad (3.61)$$

where  $m$  is the number of pressure measurements,  $n$  the number of fractures and  $\alpha_s$  are coefficients which are to be determined. Initially, the values of  $\alpha_s$  are set to zero or they can be set to the difference between the calculated and measured pressures in which case (3.61) corresponds to (3.40). This updating formula is used to recalculate the pressure in the DFN and then the vector of consequences  $G_s(P, \alpha)$ . The fracture log transmissivities,  $\mathbf{X}$ , are calculated as in (3.61) and are dependent on the coefficients  $\alpha_s$ ; the pressures  $P_i, i = 1, \dots, N$ , are also dependent on  $\alpha_s$ . The coefficients  $\alpha_s$  are chosen so that they minimise a weighted sum of squares of the discrepancies between calculated and measured pressures, namely,

$$E(\alpha_s) = \sum_{s=1}^m \frac{G_s(P^R, \alpha_s)^2}{\sigma_s^2} , \quad (3.62)$$

where  $\sigma_s$  is a the standard deviation of the measurement of the pressure at the measurement point  $s$ .

The pressure in our DFN model depends non-linearly on  $\alpha_s$ , therefore minimisation of (3.62) will proceed in an iterative manner. There are many different algorithms for non-linear minimisation; here we use the Levenberg-Marquardt method to efficiently minimise the error  $E(\alpha_s)$ . The Levenberg-Marquardt algorithm requires the derivatives

$$\frac{\partial E}{\partial \alpha_k} = \sum_{s=1}^m \frac{2G_s}{\sigma_s^2} \frac{\partial G_s}{\partial \alpha_k}, \quad k = 1, \dots, m, \quad (3.63)$$

and

$$\frac{\partial^2 E}{\partial \alpha_k \partial \alpha_l} = \sum_{s=1}^m \frac{1}{\sigma_s^2} \left[ \frac{\partial G_s}{\partial \alpha_k} \frac{\partial G_s}{\partial \alpha_l} \right], \quad l = 1, \dots, m, \quad k = 1, \dots, m, \quad (3.64)$$

for the  $s$  measurement points. The term  $\frac{\partial G_s}{\partial \alpha_f}$  can be calculated for a fracture  $f$

by using the chain rule with the sensitivity values. The increments of the coefficients  $\delta \alpha_s$  are calculated by solving the system

$$\gamma_{kl} \delta \alpha_k = \beta_k, \quad l = 1, \dots, m, \quad k = 1, \dots, m, \quad (3.65)$$

where

$$\beta_k = \frac{\partial E}{\partial \alpha_k}, \quad k = 1, \dots, m, \quad (3.66)$$

and

$$\gamma_{jk} = \frac{\partial^2 E}{\partial \alpha_j \partial \alpha_k} + \delta_{jk} \lambda, \quad j, k = 1, \dots, m, \quad (3.67)$$

where  $\lambda$  is a parameter initially set to a small value which will change by a factor of ten with each iteration and  $\delta$  is the Kronecker delta function. Here,  $\lambda$  controls whether the Levenberg-Marquardt method corresponds to a steepest decent method or a Newton method for the minimisation at each iteration. For more details on the Levenberg Marquardt method, see Press, Flannery et al. (1986).

There are two different approaches that can be taken for the minimisation. In the first approach the sensitivities are updated with each iteration of the minimisation

procedure. This means that the terms  $\frac{\partial G}{\partial \alpha}$  in (3.63) and (3.64) are updated with

each iteration. In the second approach the sensitivities are not updated. We use the terminology updating in this thesis to mean that the sensitivities are updated with each iteration. The conditioning algorithm is as follows:

1. Compute the initial log transmissivity field  $\mathbf{X}^U$ , and calculate an initial error from (3.62).
2. Calculate the sensitivities using (3.60).
3. Calculate the basis vectors using (3.42).
4. Select an initial guess for the coefficients  $\alpha_s$ .

5. Update  $\mathbf{X}$  using (3.61).
6. Re-calculate pressures with new  $\mathbf{X}$  value.
7. If required, update the new derivatives in (3.63) and (3.64). Recalculate  $\gamma$  and  $\beta$ .
8. Calculate new increment for the coefficients  $\delta\alpha_s$  from (3.65).
9. If error (3.62) has converged then stop. If error has not been reduced then increase  $\lambda$  by a factor of 10 and return to 6. If the error has been reduced then decrease  $\lambda$  by a factor of 10 and update  $\mathbf{X}(\alpha_s)$  to  $\mathbf{X}(\alpha_s + \delta\alpha_s)$  and return to 6.

## 4 – RESULTS OF THE BASIS VECTOR CONDITIONING METHOD

Throughout the remainder of this thesis the conditioning method described in chapter 3 will be referred to as the basis vector conditioning method. It was implemented in NAPSAC, an existing FE code for solving flow problems in a DFN. Four simple test cases were initially used to test the basis vector conditioning method. These test cases contained deterministically placed fractures with simple geometry. For each simple test case a target transmissivity (or target transmissivities if there was more than one fracture) was specified (which gives a corresponding measured pressure). To test the basis vector conditioning method, the target transmissivity was perturbed, and the number of iterations needed to return to the target transmissivity (and match the measured pressure) was determined. Each test case was conditioned separately with and without updating. As explained in chapter 3, updating means that the sensitivities are updated with each iteration of the minimisation procedure.

Finally, the basis vector conditioning method was used to condition a DFN model of a potential site for nuclear waste disposal in Finland which was generated based on field data. This DFN model contains 501 fractures with 9 pressure measurements. Based on results from the simple test cases, the basis function conditioning method was run with updating.

All results in this chapter were obtained by using initial coefficient values  $\alpha_0 = \mathbf{0}$  in step 4 of the conditioning algorithm given in chapter 3. It was found that

when using the basis vector conditioning method with initial coefficient values  $\alpha_0 = \mathbf{P}^B - \mathbf{P}_M$ , where  $\mathbf{P}^B$  is a vector of borehole pressures at measurement points and  $\mathbf{P}_M$  is a vector of measured pressures, an improvement in the match to measured pressures was obtained. However this match was not as good as the match to measured pressures obtained by using initial coefficients  $\alpha_0 = \mathbf{0}$  with the basis vector conditioning method.

#### 4.1 – SIMPLE TEST CASES

For all the simple test cases the problem domain is a cube of 10m by 10m by 10m. Fractures are placed inside the cubic domain with individual fractures and fracture intersections being discretised. Boundary conditions are defined on the cube faces as either a pressure, flux or no-flow boundary condition. The absolute error is defined as

$$\text{Absolute Error} = \sqrt{\sum_{s=1}^m \frac{[P_s^B - P_{M_s}]^2}{\sigma_s^2}}, \quad (4.1)$$

for  $m$  measurement points, where  $P_{M_s}$  is the measured pressure at measurement point  $s$  and  $P_s^B$  is the calculated pressure at measurement point  $s$  and  $\sigma_s$  is the standard deviation of the pressure measurement at measurement point  $s$ . It is assumed that all pressure measurements are independent and have equal standard deviation; accordingly  $\sigma_s$  is set equal to 1 for  $s = 1, \dots, m$ . In other words, we

assume that all the pressure measurements are equally accurate and weight them equally. The basis vector conditioning method is stopped when the absolute error is less than 1 (less than 0 in a log plot).

#### 4.1.1 - TEST CASE 1

Test case 1 consists of a borehole intersecting a single fracture, shown in Figure 7. There is a constant flux of  $1.0E-7m^2/s$  assigned to the left face of the cubic domain as a boundary condition. The right face of the cubic domain has a constant pressure value of  $0Pa$  while the remaining faces of the domain have no flow boundary conditions. The borehole is a non-pumping borehole. An initial transmissivity value of  $1.1E-6m^2/s$  was taken and the target transmissivity was set to  $1.0E-6m^2/s$ .

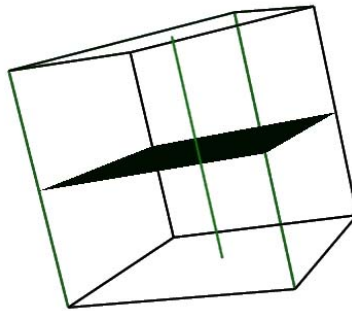


**Figure 7.** Domain of test case 1 with a borehole intersecting a single fracture.

The log of the absolute error is plotted against the iteration of the Levenberg-Marquardt algorithm (used to minimise the absolute error) in Figure 8. It shows that the log of the absolute error decays linearly with each iteration. The initial

transmissivity used was  $1.1\text{E-}6\text{m}^2/\text{s}$ , which is close to the target transmissivity of  $1.0\text{E-}6\text{m}^2/\text{s}$  and is a reason for the fast convergence.

To test the basis vector conditioning method further initial guesses of the fracture transmissivity up to 3 orders of magnitude from the target transmissivity were used. Test case 1 was conditioned separately with and without updating (defined in Chapter 3 to be the updating of the sensitivities with each iteration of the minimisation procedure). Table 1 shows the number of iterations required to converge to the target transmissivity of  $1.0\text{E-}6\text{m}^2/\text{s}$  with and without updating, where the number of iterations required without updating are shown in brackets. It can be seen that when updating is used, the absolute error converges in a respectable number of iterations for all the initial transmissivities. However, we observe that the convergence of the algorithm may be adversely affected when no updating is employed. Indeed, in this case, the absolute error will converge for initial transmissivity values smaller than the target transmissivity, but typically require a large number of iterations. Furthermore, test case 1 fails to converge for an initial transmissivity of  $1.1\text{E-}3\text{m}^2/\text{s}$  and greater without updating.

In this simple one fracture case, the pressure at the measurement point is inversely proportional to the fracture transmissivity. The measured pressure is  $5.0\text{E+}4\text{Pa}$  (corresponding to the target fracture transmissivity of  $1.0\text{E-}6\text{m}^2/\text{s}$ ) and thus the absolute error can be analytically plotted against fracture transmissivity, as shown in Figure 9. Without updating the fracture transmissivity is changed by a small increment with each iteration. When the gradient of the absolute error is large (as it is for transmissivities ranging from  $1.0\text{E-}8\text{m}^2/\text{s}$  to  $1.0\text{E-}5\text{m}^2/\text{s}$ , shown in Figure 9) this still produces a significant change in the absolute error. However, when the gradient of the absolute error is small

(transmissivity values over approximately  $1.0\text{E-}3\text{m}^2/\text{s}$  in Figure 9) there is no significant change in absolute error and the method may converge to a solution far from the minimum.

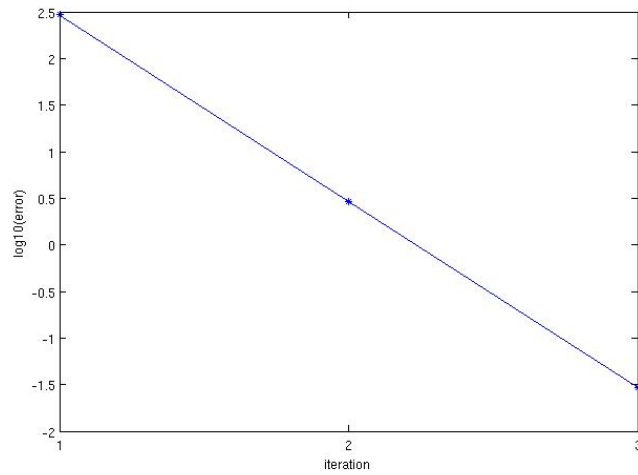


**Figure 8.** Convergence of the log base 10 of the absolute error with each iteration of the Levenberg-Marquardt method for test case 1 with an initial transmissivity of  $1.1\text{E-}6\text{m}^2/\text{s}$  and target transmissivity of  $1.0\text{E-}6\text{m}^2/\text{s}$ .

Initial Transmissivity ( m <sup>2</sup> /s )	Number of iterations to convergence
1.1E-2	15 (N.C.)
1.1E-3	13 (N.C.)
1.1E-4	11 (22)
1.1E-5	9 (15)
1.1E-6	2 (3)
1.1E-7	6 (92)
1.1E-8	8 (1004)

**Table 1.** Number of iterations taken to converge to the measured pressure corresponding to a target fracture transmissivity of 1.0E-6m<sup>2</sup>/s for different initial transmissivity values for test case 1. The number of iterations required without updating are shown in brackets. N.C. denotes no convergence.

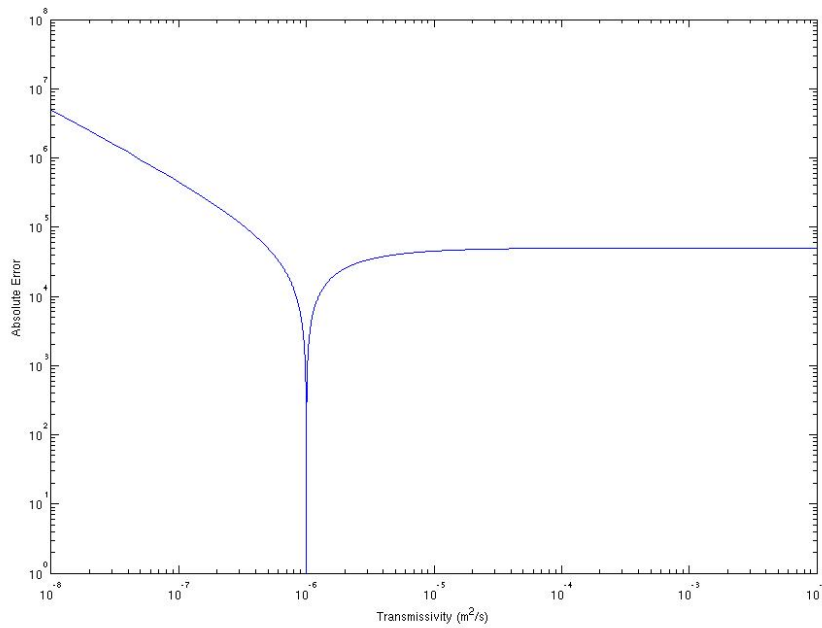


**Figure 9.** Analytic plot of the absolute error against fracture transmissivity at the measurement point for test case 1.

#### 4.1.2 - TEST CASE 2

Test case 2 has the same domain as test case 1, as shown in Figure 7, with a borehole intersecting a single fracture. However, the boundary conditions differ; in test case 2 the borehole is a pumping borehole with a flux of  $1.0E-5m^3/s$  and there is a constant pressure boundary condition of  $0Pa$  on all of the faces of the cubic domain that are in contact with the fracture.

A plot of the log of the error against each iteration of the Levenberg-Marquardt method is shown in Figure 10 for an initial transmissivity guess of  $1.1E-6m^2/s$ . It shows the absolute error converges to the target transmissivity of  $1.0E-6m^2/s$ . Figure 10 indicates a linear relationship between the log of the error and the iteration of the Levenberg Marquardt method when an initial transmissivity of  $1.1E-6m^2/s$  was used. Table 2 shows the convergence of the absolute error for different initial transmissivities for test case 2. This test case shows similar convergence properties to test case 1 when updating, with the error converging in a respectable number of iterations for all choices of the initial transmissivities. However, the convergence of the basis vector conditioning method is poor without updating. Indeed, as in test case 1 the pressure at the measurement point is inversely proportional to the fracture transmissivity and Figure 11 plots the absolute error at the measurement point against the fracture transmissivity.

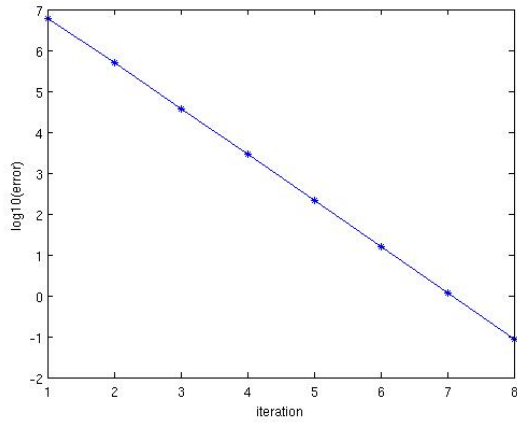


**Figure 10.** Convergence of the log base 10 of the absolute error with each iteration of the Levenberg-Marquardt method for test case 2 with an initial transmissivity of  $1.1\text{E-}6\text{m}^2/\text{s}$  and target transmissivity of  $1.1\text{E-}6\text{m}^2/\text{s}$ .

Initial Transmissivity ( $\text{m}^2/\text{s}$ )	Number of iterations to convergence
1.1E-2	15 (N.C.)
1.1E-3	13 (N.C.)
1.1E-4	11 (N.C.)
1.1E-5	9 (N.C.)
1.1E-6	2 (8)
1.1E-7	6 (94)
1.1E-8	8 (1043)

**Table 2.** Number of iterations taken to converge to the measured pressures corresponding to a target fracture transmissivity of  $1.0\text{E-}6\text{m}^2/\text{s}$  for different initial transmissivity values for test case 2.

The number of iterations required without updating are shown in brackets. N.C. denotes no convergence.

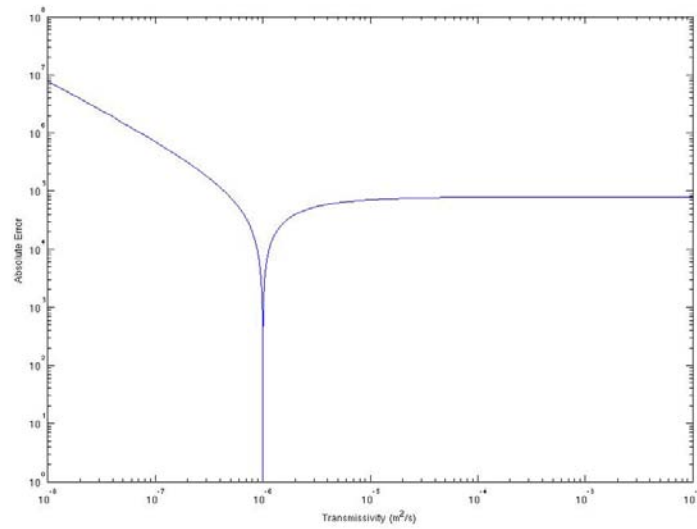


**Figure 11.** Analytic plot of the absolute error against fracture transmissivity at the measurement point for test case 2.

#### 4.1.3 - TEST CASE 3

The domain of test case 3 is shown in Figure 12 with three unconnected fractures intersecting separate boreholes. There is a specified flux of  $1.0\text{E-}5\text{m}^3/\text{s}$  at each borehole. The pressure is set to 0Pa on all faces of the cubic domain and 3 individual borehole intersections are used on each fracture.

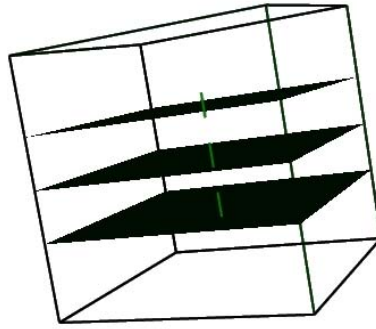


**Figure 12.** The Domain of test case 3 with 3 unconnected fractures each intersecting a borehole. The boreholes are shown as green lines in the middle of each fracture.

The initial fracture transmissivities were  $1.1\text{E-}6\text{m}^2/\text{s}$ ,  $2.1\text{E-}6\text{m}^2/\text{s}$  and  $3.1\text{E-}6\text{m}^2/\text{s}$ . The basis vector conditioning method converged to the target transmissivities of  $1.0\text{E-}6\text{m}^2/\text{s}$ ,  $2.0\text{E-}6\text{m}^2/\text{s}$  and  $3.0\text{E-}6\text{m}^2/\text{s}$ , respectively. Figure 13 shows the convergence of the absolute error with each iteration. Table 3 shows the number of iterations required for the absolute error to converge for different initial transmissivities. Again, when using updating, the absolute error converges in a respectable number of iterations. Without updating the absolute error converges for values of initial transmissivity smaller than the target transmissivity but requires a large number of iterations. It fails to converge with initial transmissivity values of  $1.1\text{E-}3\text{m}^2/\text{s}$ ,  $2.1\text{E-}3\text{m}^2/\text{s}$ ,  $3.1\text{E-}3\text{m}^2/\text{s}$  and larger. An analytic plot of the absolute error contribution against fracture transmissivity for each individual fracture is shown in Figure 14.

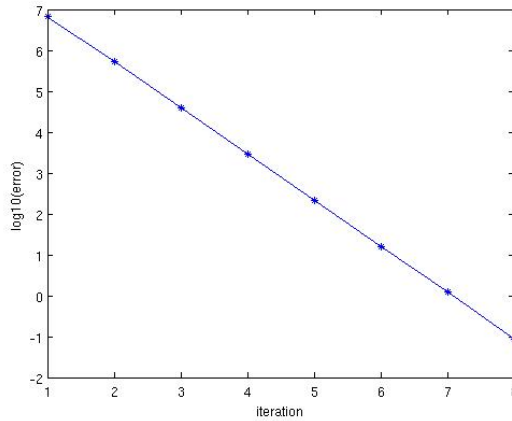


**Figure 13.** Convergence of the log base 10 of the absolute error with each iteration of the Levenberg-Marquardt method for test case 3 with initial transmissivities of (1.1E-6, 2.1E-6, 3.1E-6)m<sup>2</sup>/s for the 3 fractures to target transmissivities of (1.0E-6, 2.0E-6, 3.0E-6)m<sup>2</sup>/s.

Initial Transmissivity ( m <sup>2</sup> /s )	Number of iterations to convergence
1.1E-2, 2.1E-2, 3.1E-2	15 (N.C.)
1.1E-3, 2.1E-3, 3.1E-3	13 (N.C.)
1.1E-4, 2.1E-4, 3.1E-4	11 (26)
1.1E-5, 2.1E-5, 3.1E-5	9 (19)
1.1E-6, 2.1E-6, 3.1E-6	3 (8)
1.1E-7, 2.1E-7, 3.1E-7	6 (74)
1.1E-8, 2.1E-8, 3.1E-8	8 (927)

**Table 3.** Number of iterations taken to converge to the measured pressures corresponding to target transmissivities of (1.0E-6, 2.0E-6, 3.0E-6)m<sup>2</sup>/s for different initial transmissivity values for test case 3. Iterations required without updating are shown in brackets. N.C. denotes no convergence.

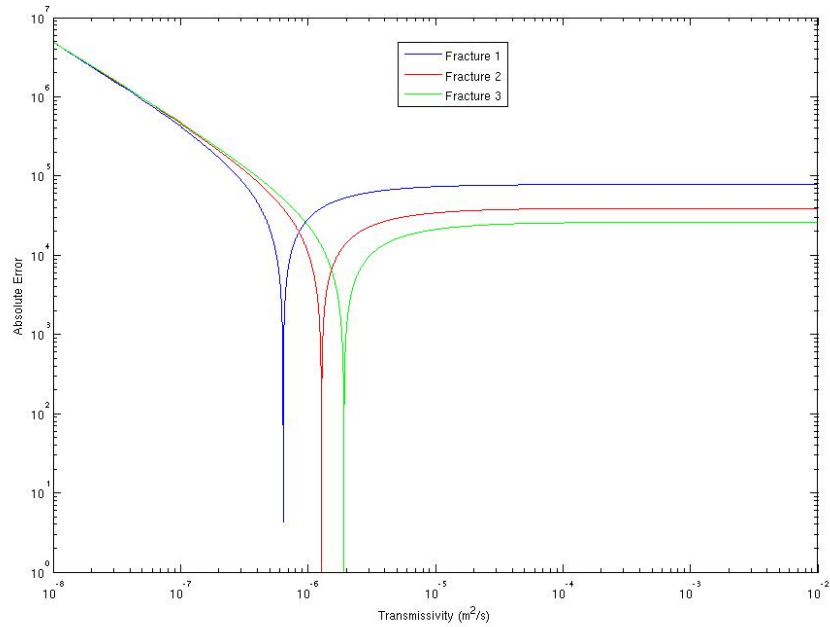


**Figure 14.** Analytic plot of the absolute error contribution against fracture transmissivity at the measurement point for each of the three fractures in test case 2.

#### 4.1.4 - TEST CASE 4

Test case 4 is the first test case where the fractures are connected. Figure 15 shows the domain with 3 fractures, two of which are intersected by separate boreholes; these boreholes are non-pumping boreholes. There is a pressure boundary condition of 0Pa on the right face of the cubic domain, a flux boundary condition of  $1.0E-7m^3/s$  on the left face and no flow boundary conditions on the remaining faces. When the initial transmissivities are  $(1.1E-6, 2.1E-6, 3.1E-6) m^2/s$  they converge to the solution transmissivities of  $(1.0E-6, 2.0E-6, 3.0E-6) m^2/s$ , respectively, and this convergence is shown in Figure 16; it shows a very similar linear decay of the log error to that seen in the previous test cases.

Table 4 shows the absolute error convergence for different initial fracture transmissivities. It can be seen that updating again yields a great reduction in the number of iterations required for the absolute error to converge for all the initial transmissivities considered, in comparison to the case when no updating is employed.

The pressure at the first measurement point is inversely proportional to all three fracture transmissivities and the pressure at the second measurement point is inversely proportional to the third fracture transmissivity.

Figure 17 shows a log plot of the absolute error against the transmissivities of the first and second fractures with the transmissivity of the third fracture held at a constant value of  $3.0E-6\text{m}^2/\text{s}$ . Similar plots are obtained when holding the first fracture transmissivity constant and when holding the second fracture transmissivity constant.

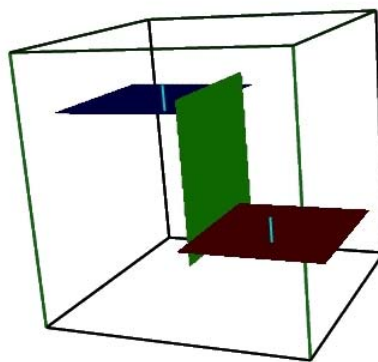


**Figure 15.** Domain of test case 4 with 3 connected fractures. Boreholes (shown in light blue) intersect the fractures connected to the left and right faces of the cube in the plot.

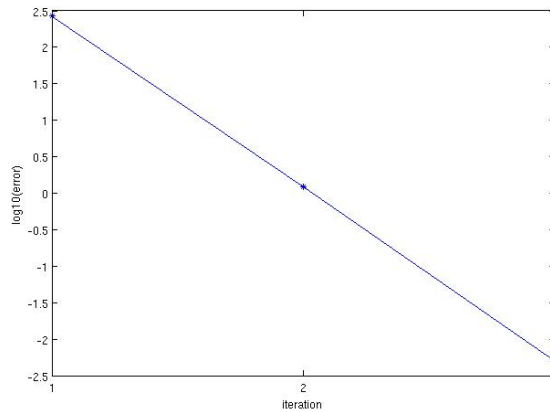


**Figure 16.** Convergence of the log base 10 of the absolute error with each iteration of the Levenberg-Marquardt method for test case 4 with an initial transmissivity of  $1.1\text{E-}6\text{m}^2/\text{s}$ .

Initial Transmissivity ( $\text{m}^2/\text{s}$ )	Number of iterations to convergence
1.1E-2, 2.1E-2, 3.1E-2	19 (38)
1.1E-3, 2.1E-3, 3.1E-3	19 (33)
1.1E-4, 2.1E-4, 3.1E-4	17 (24)
1.1E-5, 2.1E-5, 3.1E-5	10 (17)
1.1E-6, 2.1E-6, 3.1E-6	2 (3)
1.1E-7, 2.1E-7, 3.1E-7	6 (106)
1.1E-8, 2.1E-8, 3.1E-8	8 (1205)

**Table 4.** Number of iterations taken to converge to the measured pressures corresponding to target transmissivities of  $(1.0\text{E-}6, 2.0\text{E-}6, 3.0\text{E-}6)\text{m}^2/\text{s}$  for different initial transmissivity values for test case 4 without updating. Iterations required without updating are shown in brackets.

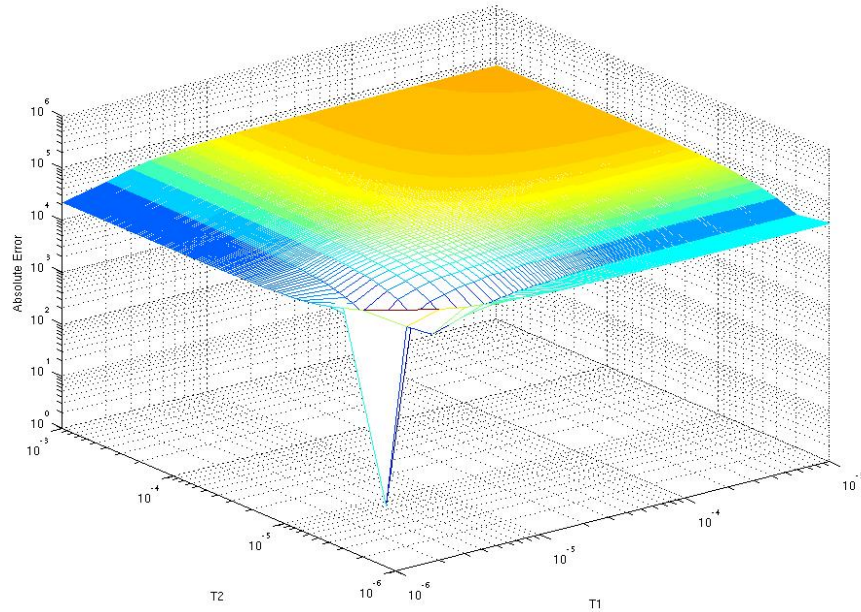


**Figure 17.** Log plot of the absolute error against the first and second fracture transmissivities with the third fracture transmissivity held constant at  $3.0E-6m^2/s$ .

#### 4.1.3.1 - MULTIPLE SOLUTIONS IN TEST CASE 4

Test case 4 is the first test case where the possibility of multiple solutions arises.

Using notation from chapter 3, the log transmissivities are updated in the form

$$\mathbf{X} = \mathbf{X}^U + \sum_{i=1}^m \alpha_i \mathbf{W}_i, \quad (4.2)$$

for  $m$  pressure measurements. For test case 4 this can be written as

$$\begin{aligned}
X_1 &= X_1^U + \alpha_1 W_{11} + \alpha_2 W_{21} , \\
X_2 &= X_2^U + \alpha_1 W_{12} + \alpha_2 W_{22} , \\
X_3 &= X_3^U + \alpha_1 W_{13} + \alpha_2 W_{23} .
\end{aligned} \tag{4.3}$$

By substitution of  $\alpha_2$ ,  $X_1$  and  $X_2$  can be written in terms of  $\alpha_1$

$$\begin{aligned}
X_1 &= X_1^U + \alpha_1 W_{11} + \frac{W_{21}}{W_{22}} (X_3 - X_3^U - \alpha_1 W_{13}) \\
&= X_1^U + \frac{W_{21} (X_3 - X_3^U)}{W_{23}} + \left( W_{11} + \frac{W_{21} W_{13}}{W_{23}} \right) \alpha_1 \\
&= C_1 + \Phi_1 \alpha_1 ,
\end{aligned} \tag{4.4}$$

where  $C_1 = X_1^U + \frac{W_{21} (X_3 - X_3^U)}{W_{23}}$  and  $\Phi_1 = \left( W_{11} + \frac{W_{21} W_{13}}{W_{23}} \right)$ . Similarly,

$$\begin{aligned}
X_2 &= X_2^U + \alpha_1 W_{12} + \frac{W_{22}}{W_{23}} (X_3 - X_3^U - \alpha_1 W_{13}) \\
&= X_2^U + \frac{W_{22} (X_3 - X_3^U)}{W_{23}} + \left( W_{12} + \frac{W_{22} W_{13}}{W_{23}} \right) \alpha_1 \\
&= C_2 + \Phi_2 \alpha_1 ,
\end{aligned} \tag{4.5}$$

where  $C_2 = X_2^U + \frac{W_{22} (X_3 - X_3^U)}{W_{23}}$  and  $\Phi_2 = \left( W_{12} + \frac{W_{22} W_{13}}{W_{23}} \right)$ . Thus, we see that

$$X_2 = \left( C_2 - \frac{\Phi_2}{\Phi_1} C_1 \right) + \frac{\Phi_2}{\Phi_1} X_1 . \tag{4.6}$$

As shown by (4.6) the log-transmissivities  $X_1$ ,  $X_2$  of fractures 1 and 2, respectively, are linearly dependent on each other while  $X_3$  is uniquely determined from the pressure boundary condition. In fact, the value of the initial guesses of the log-transmissivities  $X_1^U$  and  $X_2^U$  will affect the values of the coefficients  $C_1$  and  $C_2$  that are selected and thus affect the final values for  $X_1$  and  $X_2$ . This is illustrated in Figure 18 which shows the relationship between  $X_1$  and  $X_2$  for different initial values of  $X_1^U$  and  $X_2^U$ .  $X_1$  and  $X_2$  are always linearly related with the same gradient and it is the initial guesses  $X_1^U$  and  $X_2^U$  that essentially shift the plots in the  $X_1 - X_2$  axis. The crosses on these lines show where the absolute error is minimized using these initial guesses. Figure 19 further illustrates this by plotting these acceptable transmissivity values against the absolute error. Again it can be seen that the acceptable transmissivity lines intersect the absolute error at different points.

This shows that when using the basis vector conditioning method our prior beliefs of fracture log transmissivities determine the values of conditioned log transmissivities. The ill-posed nature of the problem is also evident with multiple solutions existing.

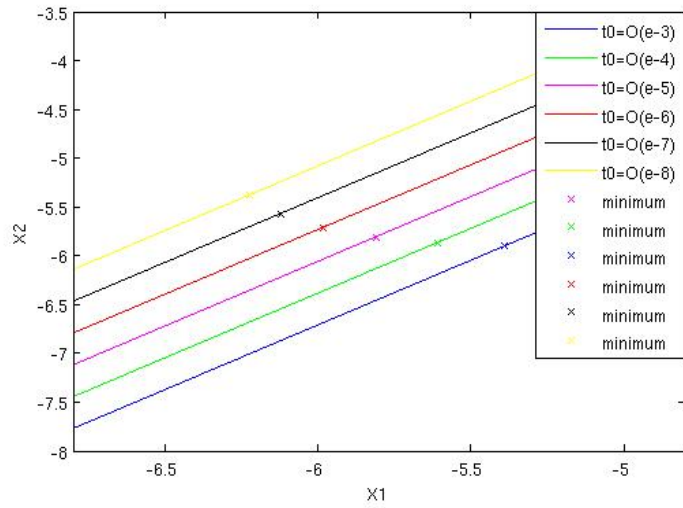


**Figure 18.** Plot of possible values of log transmissivity  $X_1$  and log transmissivity  $X_2$  for different orders of magnitude of the initial log transmissivities  $X_1^U$  and  $X_2^U$ .  $t_0=O(e-a)$  denotes  $t_0=(1.1E-a, 2.1E-a, 3.1E-a)m^2/s$  for  $a=3,\dots,8$ . Crosses denotes the values of  $X_1$  and  $X_2$  that minimise the absolute error.

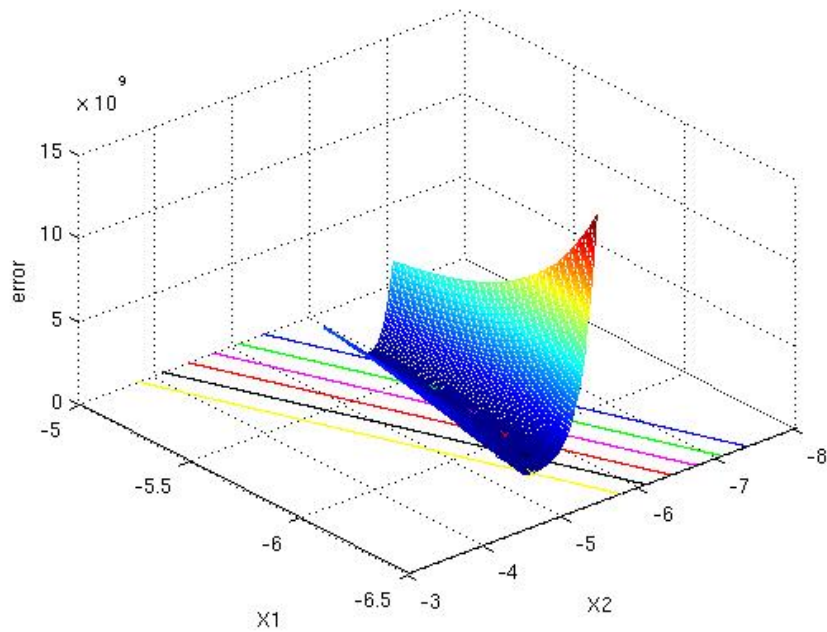


**Figure 19.** Plot of possible values of log transmissivity  $X_1$  and log transmissivity  $X_2$  for different guesses of the initial transmissivities  $X_1^U$ ,  $X_2^U$  intersecting the absolute error.

## 4.2 OLKILOUTO TEST CASE 1

In this section a DFN model of a potential site for nuclear waste disposal in Finland is used as a test case. The site itself is an island called Olkiluoto which lies in the Baltic Sea and is approximately 10 km<sup>2</sup> in size. Based on an environmental report of potential sites (Posiva OY 1999), it is planned to construct an underground repository in the centre of the island. The site has been characterised through various surface and subsurface measurements. A lot of data is available describing the subsurface geology of Olkiluoto island (Ahokas and Koskinen April 2005). Boreholes have been drilled at locations spread across the site and provide pressure measurements at given depths. Pumping tests undertaken on these boreholes give an idea of approximate transmissivity properties of fracture zones located between the drilled boreholes. The location of major fracture zones have been inferred from seismic scanning whereby a seismic source (usually at the surface) produces seismic waves that can be picked up by receivers placed down boreholes. Seismic waves will refract at the interface between different materials and thus give a picture of the surrounding geologic structure.

Data from the Olkiluoto site (Ahokas and Koskinen April 2005) was implemented in NAPSAC to produce a DFN model of the site (Frampton, Cvetkovic et al. February 2008) which we call Olkiluoto test case 1. This DFN model contains 13 fracture sets that were generated based on pumping test results and seismic scanning which gave fracture density, orientation and length estimates. A total of

501 fractures are contained in the different fracture sets. The domain of Olkilouto test case 1 which contains the fracture sets is approximately 7800m by 7800m by 1000m. The fracture transmissivities in fracture zones were assumed to be homogeneous; that is the transmissivity of each fracture contained in a fracture zone is constant. Measured pressure values are obtained at measurement points at 9 boreholes. The depth of the measurement points range from approximately  $z=-97\text{m}$  to  $z=-377\text{m}$ . Figure 20 shows the boundaries of the domain of Olkilouto test case 1. The boundary conditions of the model are as follows. The top surface at  $z=0\text{m}$  has head equal to elevation. This surface is not uniform and its elevation varies, therefore head varies on the top surface. The lateral sides which are in contact with the Baltic Sea have head set to zero. The bottom surface at  $z=-1000\text{m}$  has a no-flow boundary condition. Therefore, a pressure gradient exists between the top surface and the lateral sides of the domain, that results in a flow of groundwater.

The model has been simplified by only modelling borehole measurement points instead of including complete boreholes that are intersected by multiple fractures. This means that fractures are not connected by any boreholes.

Figure 21 shows the location of the borehole measurement points and the geometry of the 501 fractures; these fractures are coloured according to their transmissivity value. The fracture network is shown at the same scale and orientation as the domain boundaries in Figure 20. The reason for two separate figures is that the domain boundaries hide the fractures when they are plotted together.

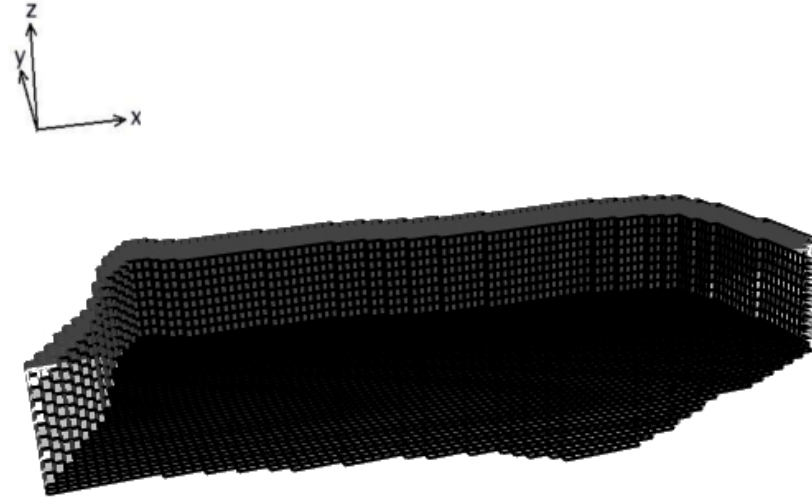


**Figure 20.** Domain boundaries of Olkiluoto test case 1.

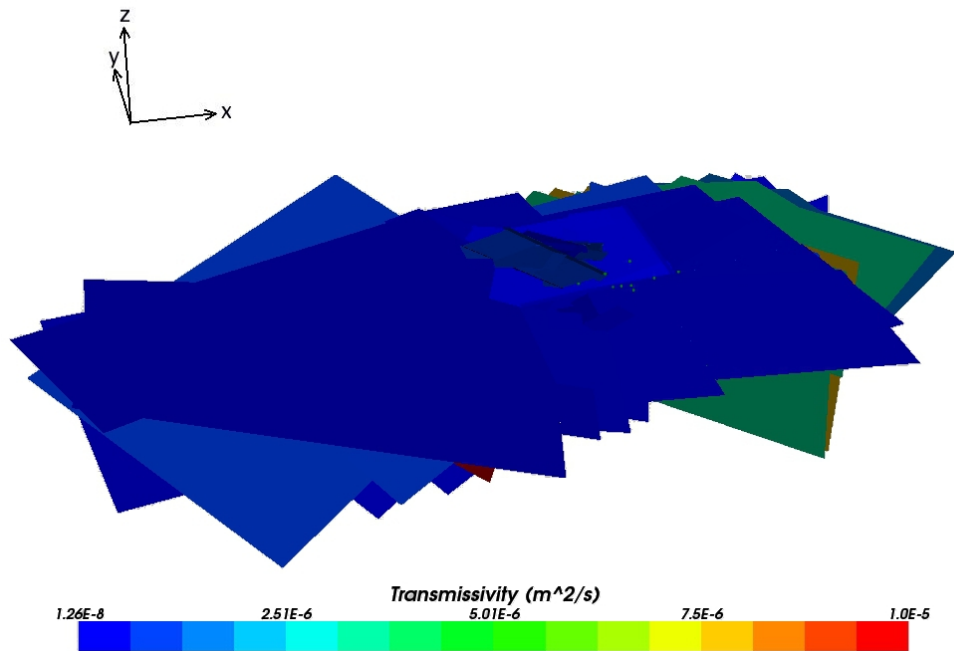


**Figure 21.** Domain of Olkiluoto test case 1 containing 11 fracture sets coloured by fracture transmissivity and 9 borehole measurement points shown as purple dots.

The fractures comprise of thirteen different fracture zones whose geometry and transmissivities have been determined from field data. Figure 22 to Figure 34

show the location of each fracture zone compared to the borehole measurement points. The fracture zones are shown at the same scale and orientation as Figure 20 and Figure 21. Again the fractures are coloured according to their transmissivity value. It should be noted that the fracture transmissivity is constant for all fractures in an individual fracture zone. Fracture sets 1, 2, 3 and 7 are in close proximity to the measurement points and consist of small fractures. The remaining fracture sets contain fractures of greater length which are spread across the domain and extend further away from the measurement points than the first four fracture sets introduced. Fractures sets 4, 5, 7, 12 and 13 are in direct contact with some of the borehole measurement points.

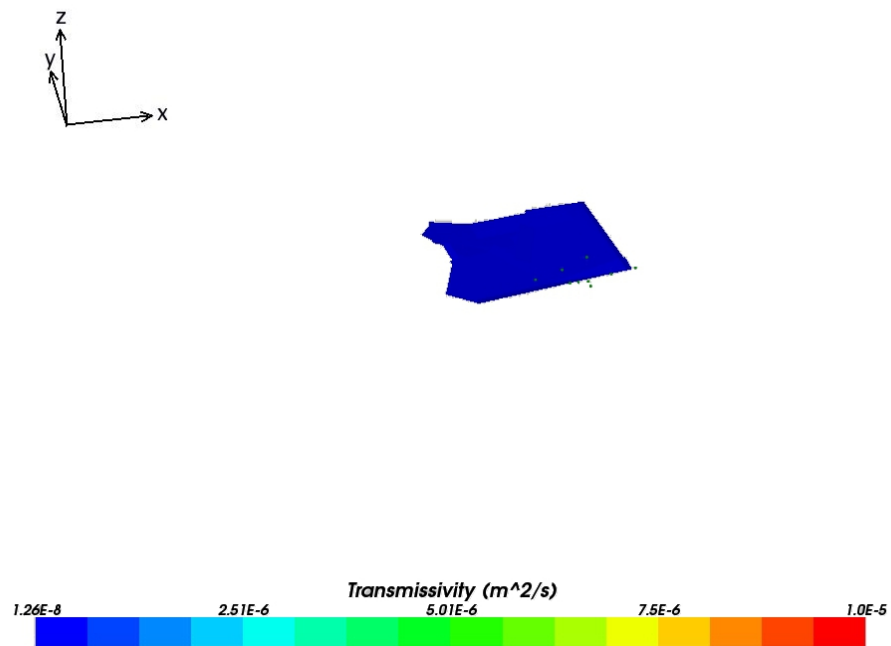


**Figure 22.** Location of the measurement points and fracture set 1 in Olkiluoto test case 1.

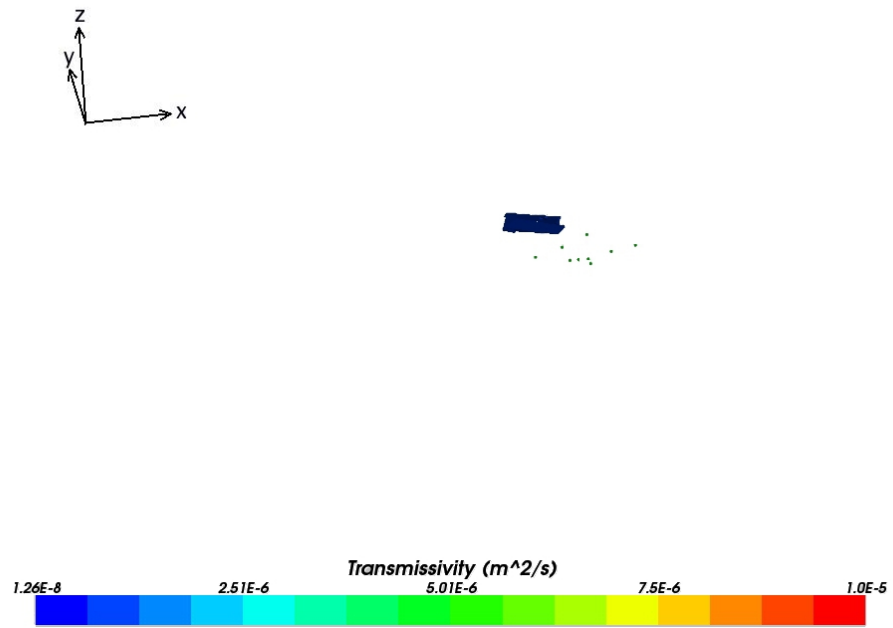


**Figure 23.** Location of the measurement points and fracture set 2 in Olkiluoto test case 1.

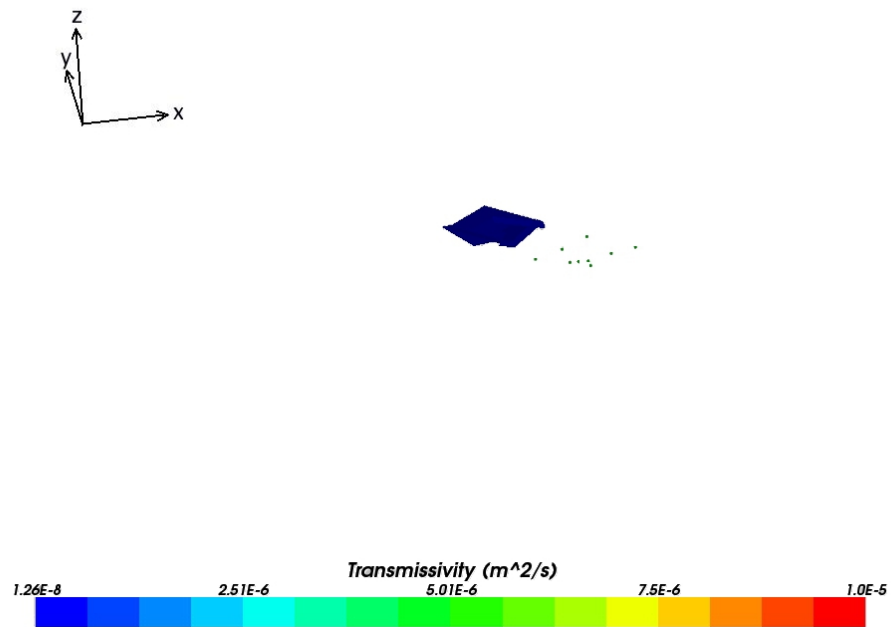


**Figure 24.** Location of the measurement points and fracture set 3 in Olkiluoto test case 1.

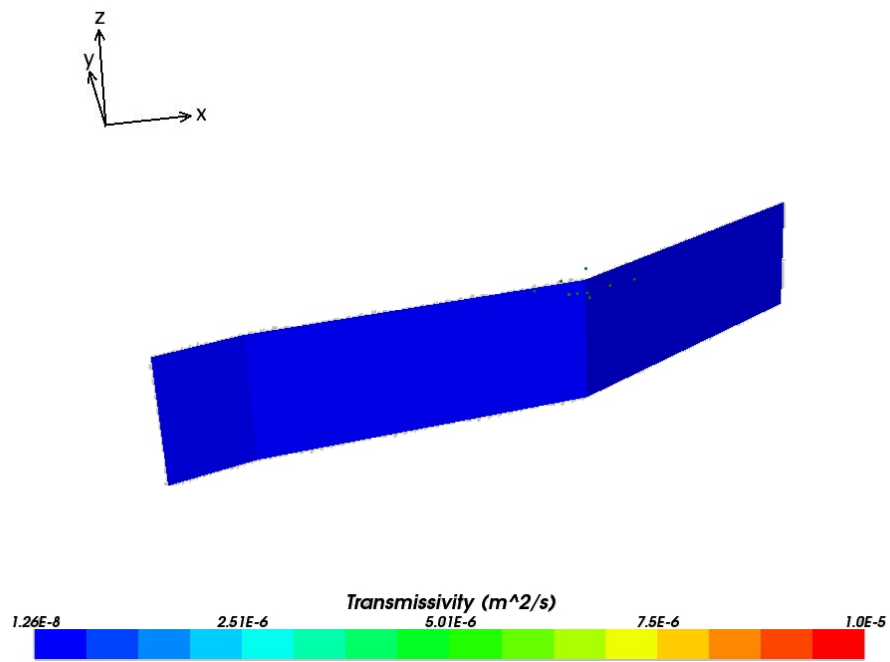


**Figure 25.** Location of the measurement points and fracture set 4 in Olkiluoto test case 1.

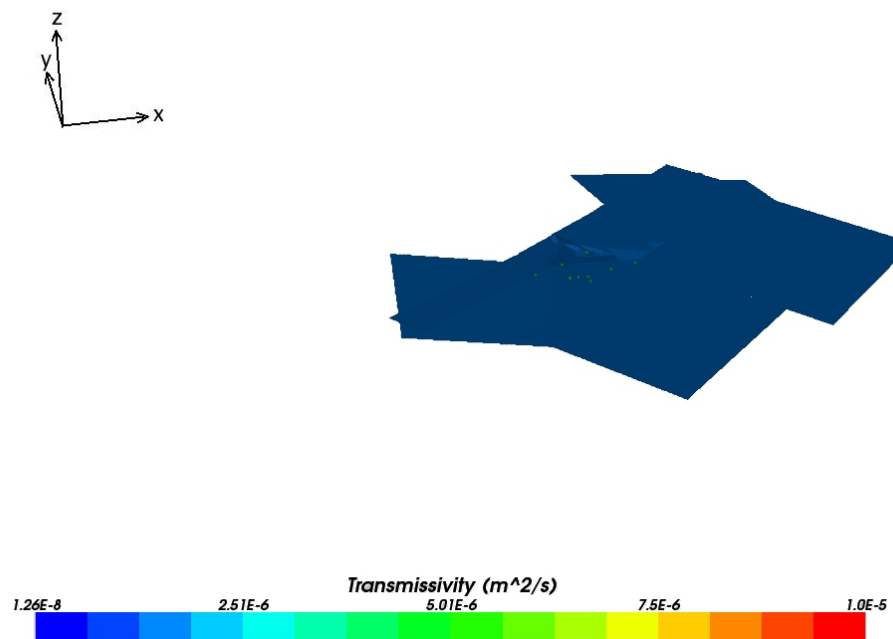


**Figure 26.** Location of the measurement points and fracture set 5 in Olkiluoto test case 1.

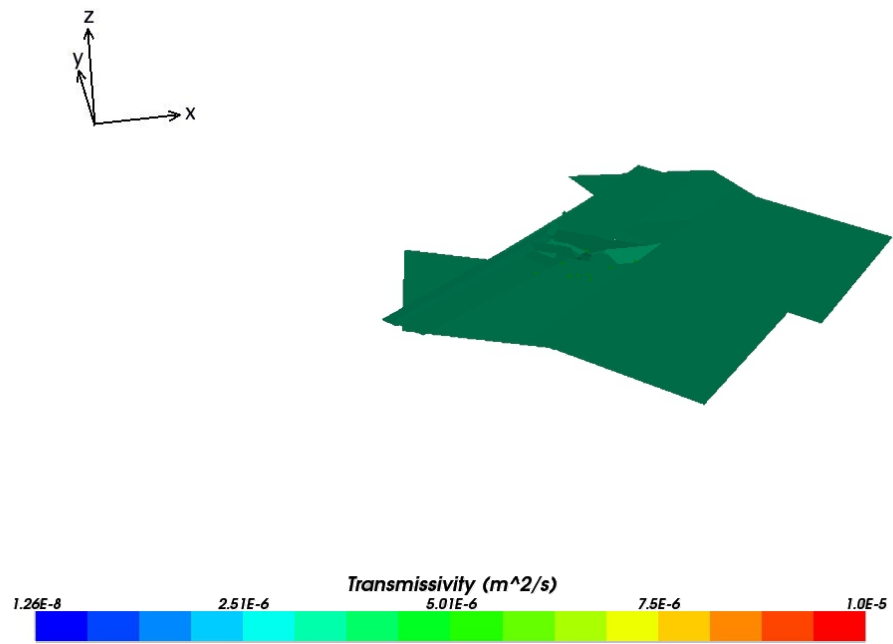


**Figure 27.** Location of the measurement points and fracture set 6 in Olkiluoto test case 1.

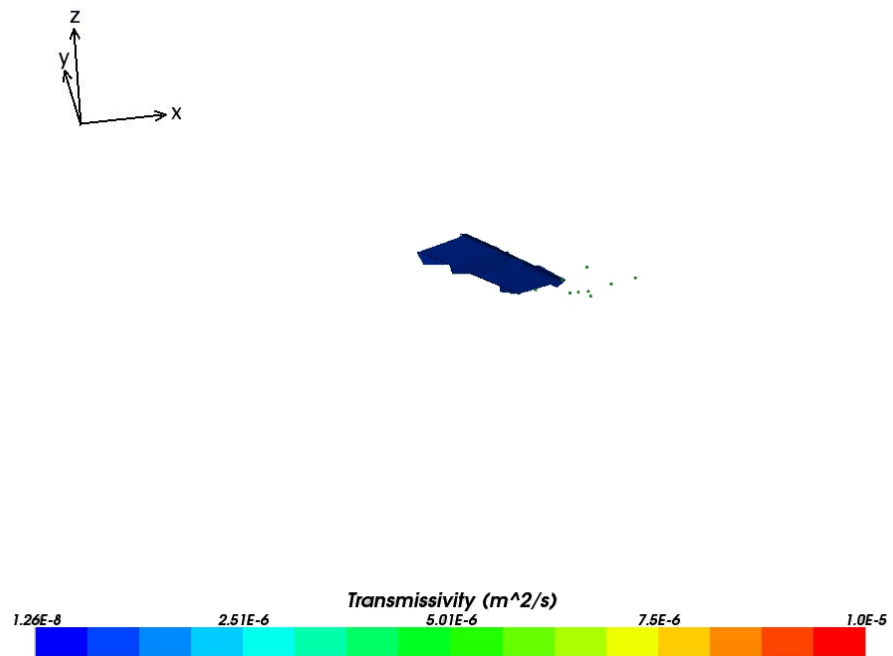


**Figure 28.** Location of the measurement points and fracture set 7 in Olkiluoto test case 1.

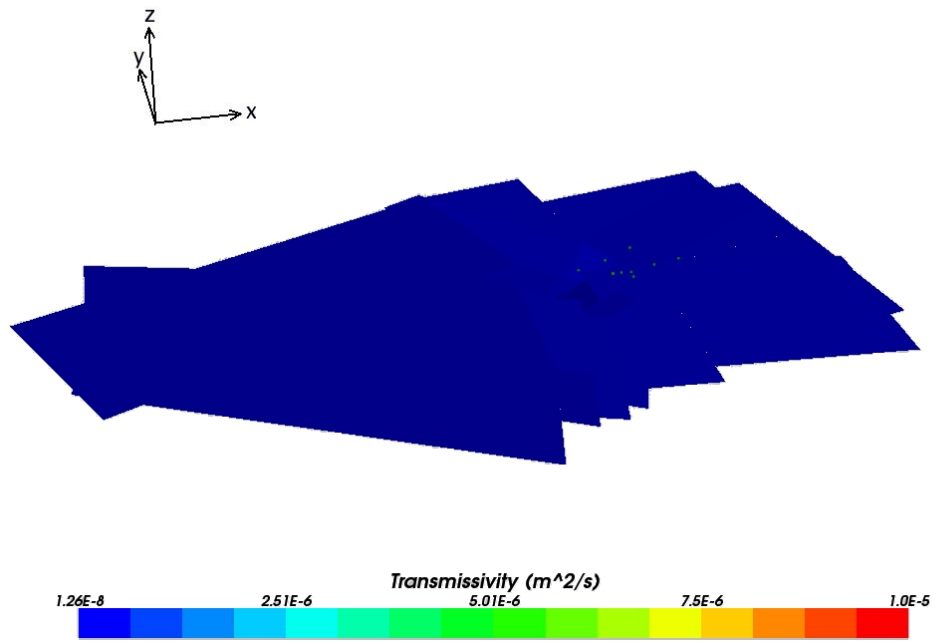


**Figure 29.** Location of the measurement points and fracture set 8 in Olkiluoto test case 1.

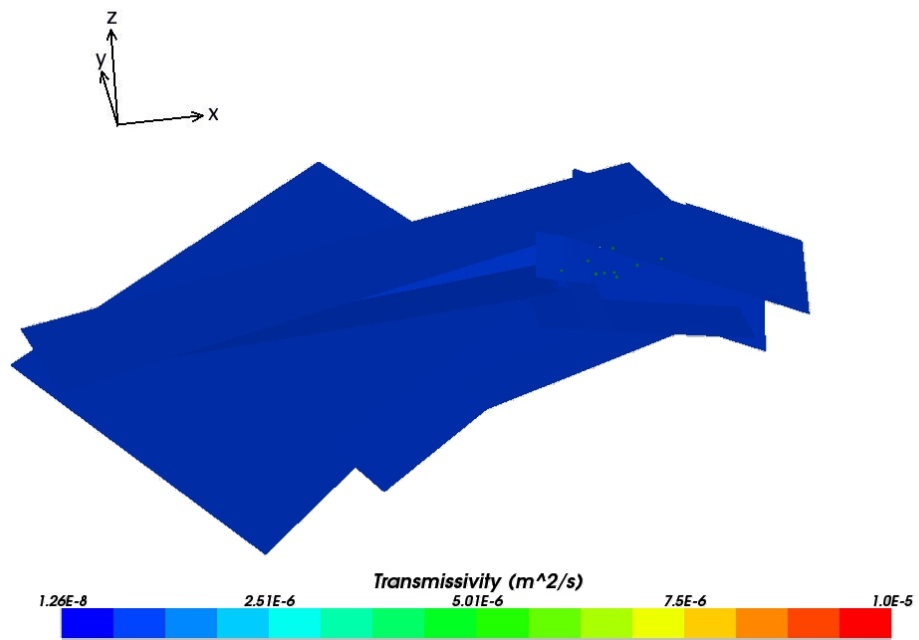


**Figure 30.** Location of the measurement points and fracture set 9 in Olkiluoto test case 1.

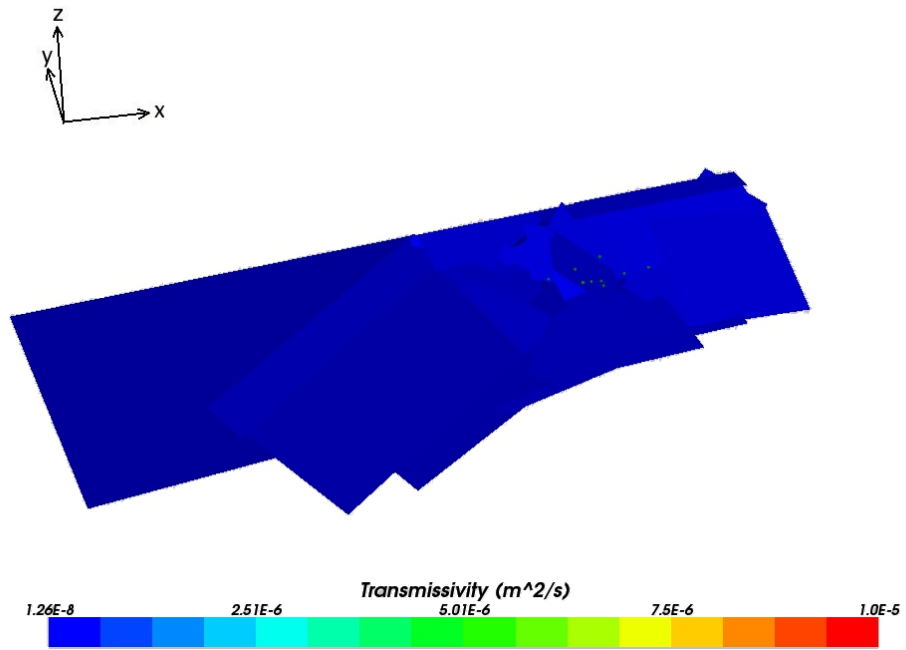


**Figure 31.** Location of the measurement points and fracture set 10 in Olkiluoto test case 1.

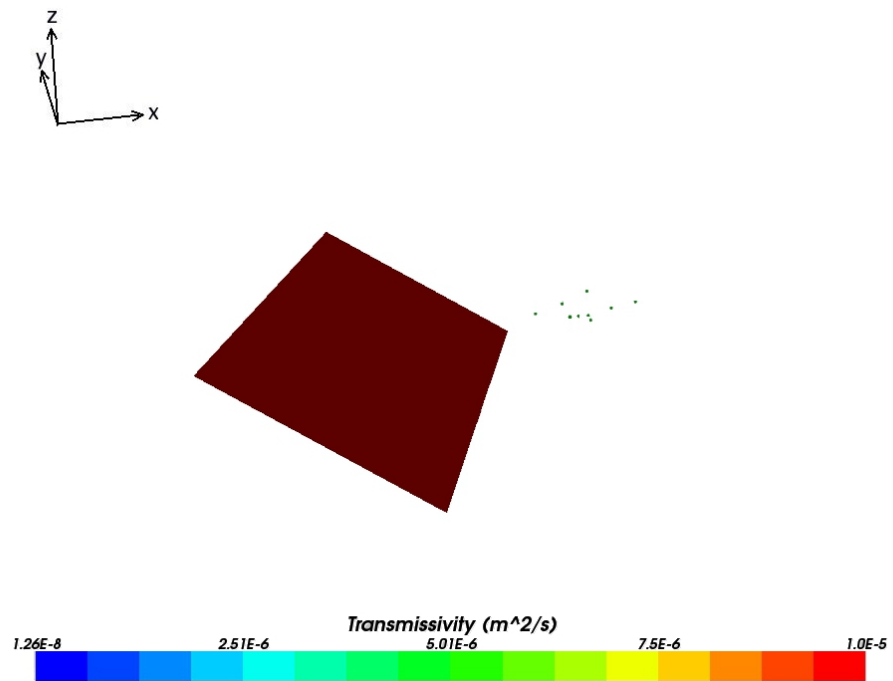


**Figure 32.** Location of the measurement points and fracture set 11 in Olkiluoto test case 1.

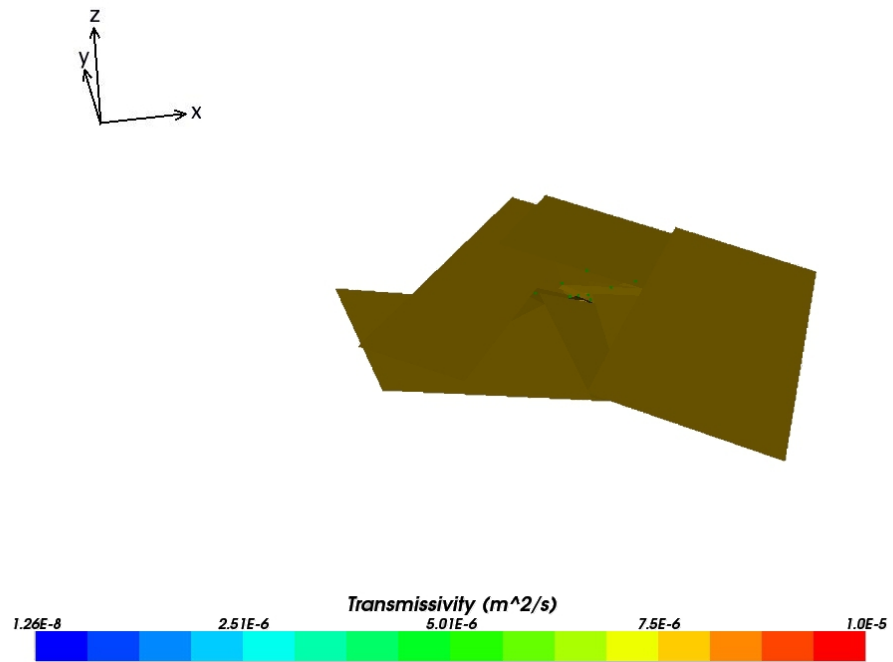


**Figure 33.** Location of the measurement points and fracture set 12 in Olkiluoto test case 1.

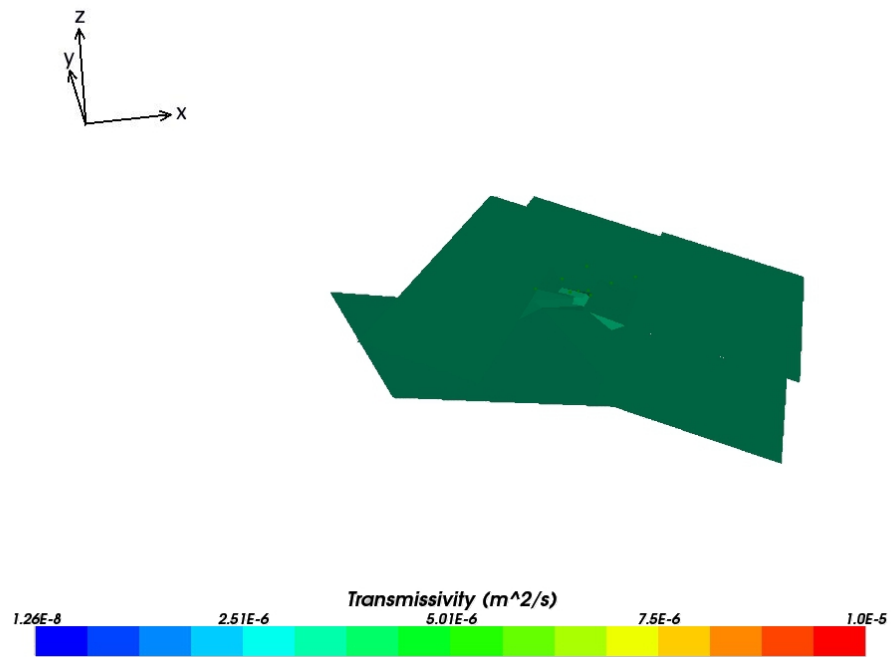


**Figure 34.** Location of the measurement points and fracture set 13 in Olkiluoto test case 1.

When NAPSAC is used to calculate pressures at the boreholes using the set of fractures shown in Figure 22 to Figure 34 with unconditioned transmissivities, the pressures do not agree very well with the measured pressure values. It should be noted that Frampton, Cvetkovic et al.(February 2008) performed a basic trial and error approach to calibration of fracture transmissivities in Olkiluoto test case 1 on pressure measurements assuming homogeneous fracture sets; however, this failed to give a good match to the measured pressures. In fact, all conditioning methods introduced in this thesis give a better match to measured pressures than the trial and error approach used on Olkiluoto test case 1. Our aim here is to get the pressure values calculated at measurement points to agree (or match as closely as possible) with the measured pressures. The basis vector conditioning method was applied and updating was used (based on the results from the simple test cases). From hereon in updating has been used on all of the following calculations.

After application of the basis vector conditioning method, the conditioned pressures gave a closer match to the measured pressures, but not an exact match. Figure 35 compares the conditioned pressure to the measured pressure and initial unconditioned pressure at all the measurement points. The pressures in Figure 35 represent the deviation of the residual pressure from atmospheric pressure. The datum point for the measurements was taken to be at  $z=0\text{m}$ . Therefore, the value of  $Z$  used in the calculation of head (1.4) and residual pressure (1.5) is negative at all the measurement points. It can be seen that the conditioned pressures give a closer match to the measured pressure at every measurement point compared to the unconditioned pressures. Figure 36 plots the absolute error against the iteration number of the Levenberg-Marquardt method. The absolute error

converges to a constant value by the 10<sup>th</sup> iteration. Indeed, after the first iteration the absolute error does not change by a significant amount. Along with the absolute error defined in (4.1) we define the relative error as

$$\text{Relative Error} = \frac{1}{m} \sum_{s=1}^m \frac{|P_s^B - P_{M_s}|}{P_{M_s}}, \quad (4.7)$$

for the  $m$  measurement points, where  $|\cdot|$  denotes the absolute value. Table 5 shows the initial absolute and relative errors between the unconditioned pressures and the measured pressures, together with the final respective values between the conditioned pressures and measured pressures. With 501 parameters being changed to agree with 9 measurement values it is likely that there will be many local minima. During the optimisation process the Levenberg-Marquardt method may well get stuck in one of these minima.

Initial Absolute Error	Final Absolute Error	Initial Relative Error	Final Relative Error
1.1128E+5	6.2327E+4	0.6828	0.3574

**Table 5.** The initial absolute error and relative error between the measured pressures and the unconditioned pressures, compared to the final absolute error and relative error between the conditioned and measured pressures.

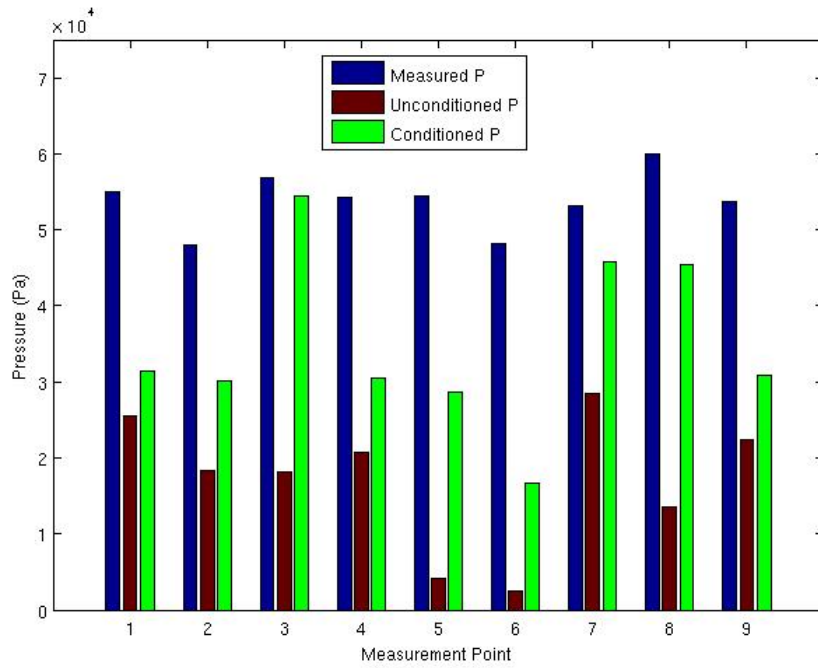


**Figure 35.** The measured pressures, unconditioned pressures and conditioned pressures for the nine measurement points for Olkiluoto test case 1.

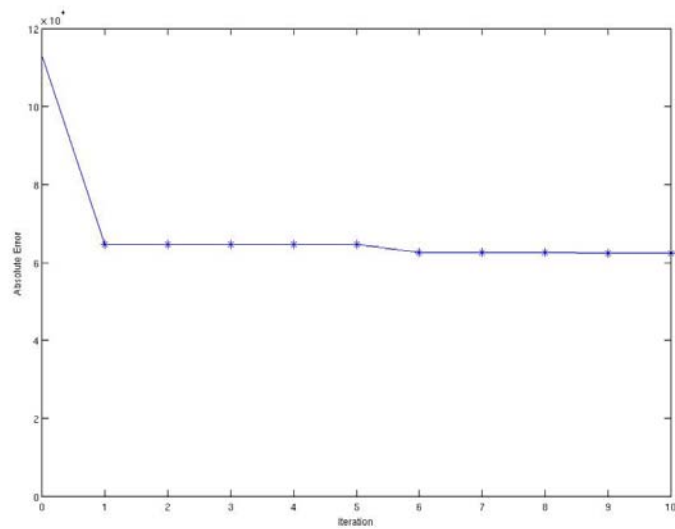


**Figure 36.** Absolute error against iteration of the Levenberg-Marquardt for Olkiluoto test case 1.

Two techniques were considered in an to attempt to avoid local minima. Firstly, in order to improve the match to the measured pressures, the fracture

transmissivities that result in the conditioned pressures in Figure 35 were taken as the initial fracture transmissivities. The method was then started from the local minimum it previously found where the value of  $\lambda$  in the Levenberg Marquardt method (3.67) was set back to its original value. It was hoped that the first iteration of the Levenberg-Marquardt may manage to move away from this local minimum. With these conditioned transmissivities the whole conditioning process was restarted (recalculate adjoints, sensitivities, perform Levenberg-Marquardt method etc.). Unfortunately, this approach did not improve the match to measured pressures.

Additionally, a numerical homotopy was considered; the details of which are now summarised. The conditioning proceeds in the same manner as the basis vector conditioning method, however, the measured pressures on which the fracture transmissivities are conditioned on are changed at a number of steps. As in the basis vector conditioning method, the vector of all fracture log transmissivity values  $\mathbf{X}$  is updated using the formula

$$\mathbf{X} = \mathbf{X}^U + \sum_{i=1}^m \alpha_i \mathbf{W}_i . \quad (4.8)$$

Each measured pressure used in the homotopy method  $P_{HM}(i)$  at  $i = 1, \dots, m$  range from  $P^U(i) \leq P_{HM}(i) \leq P_M(i)$ , where  $P^U(i)$  are the unconditioned pressures shown in Figure 35 and  $P_M(i)$  are the measured pressures shown in Figure 35. This pressure range was used because all the conditioned pressures were less than the measured pressures. The basis vector conditioning method is first used to condition pressures  $\mathbf{P}_{HM}$  close to the unconditioned pressures, where  $\mathbf{P}_{HM}$  is the

vector of all homotopy measured pressures. A final value of weights  $\alpha$  is obtained and used to calculate  $\mathbf{X}$ , as defined in (3.61). This process is repeated at the next step with the new  $\mathbf{X}$  conditioned on  $\mathbf{P}_{\text{HM}}$  values closer to  $\mathbf{P}_M$ , where  $\mathbf{P}_M$  is the vector of all measured pressures. Thus, the basis vector conditioning method is used to condition the log transmissivities  $\mathbf{X}$  on  $\mathbf{P}_{\text{HM}}$  values that approach  $\mathbf{P}_M$  with each step. The following algorithm describes the numerical homotopy method used:

- Select number of steps  $\mu$  between  $\mathbf{P}^U$  and  $\mathbf{P}_M$ .

- Set  $\mathbf{X} = \mathbf{X}^U$ .

- DO  $i=1, \dots, \mu$

$$\text{-Calculate } \mathbf{P}_{\text{HM}} = \left(1 - \frac{i}{\mu}\right) \mathbf{P}^U + \frac{i}{\mu} \mathbf{P}_M.$$

- Use the basis vector conditioning method to condition  $\mathbf{X}$  using  $\mathbf{P}_{\text{HM}}$  to obtain conditioned weights  $\alpha_i^C$  and conditioned log transmissivities  $\mathbf{X}_i^C$  using (4.8).

- Set  $\alpha_{i+1} = \alpha_i^C$  and  $\mathbf{X}_{i+1} = \mathbf{X}_i^C$ .

- END DO

The values of the numerical homotopy conditioned pressures obtained differed from those obtained from the basis vector conditioning method but they did not improve the match to the measured pressures. Thus, the numerical homotopy was unsuccessful in improving the results of the basis vector conditioning method.

#### 4.2.1 - SENSITIVITY ANALYSIS

The sensitivities calculated give an indication of how much each fracture transmissivity affects the calculated pressures. A large sensitivity means that a fracture transmissivity has a great influence on the calculated pressure. Figure 37 to Figure 45 show the sensitivity of each fracture transmissivity in the Olkiluoto test case 1 for each of the 9 measurement points. The fractures have been arranged into their different fracture sets that make up the model (as shown in Figure 22 to Figure 34). It can be seen that some fracture sets affect the calculated pressures far more than others. In fact, fracture sets 8 and 9, have only a small influence on the calculated pressure at the measurement points.

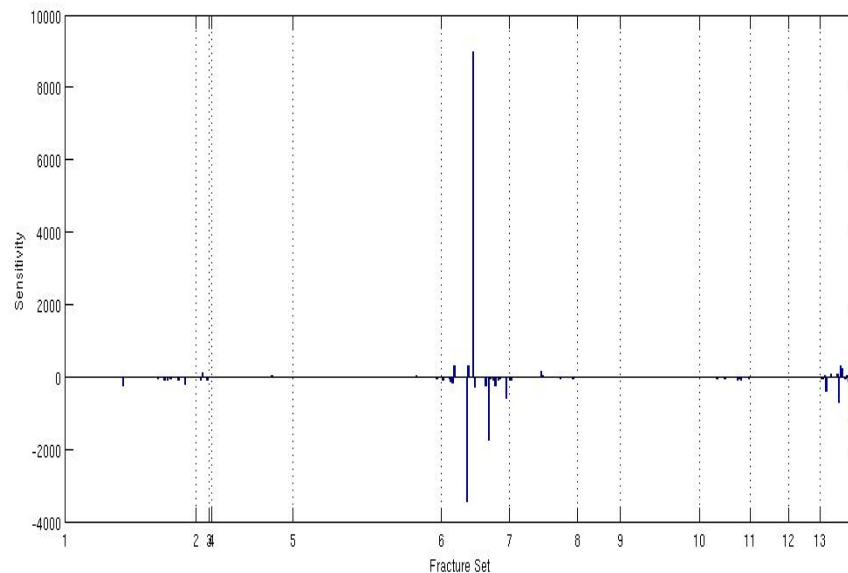


**Figure 37.** Sensitivity values corresponding to fractures belonging to the different fracture sets for measurement point 1.

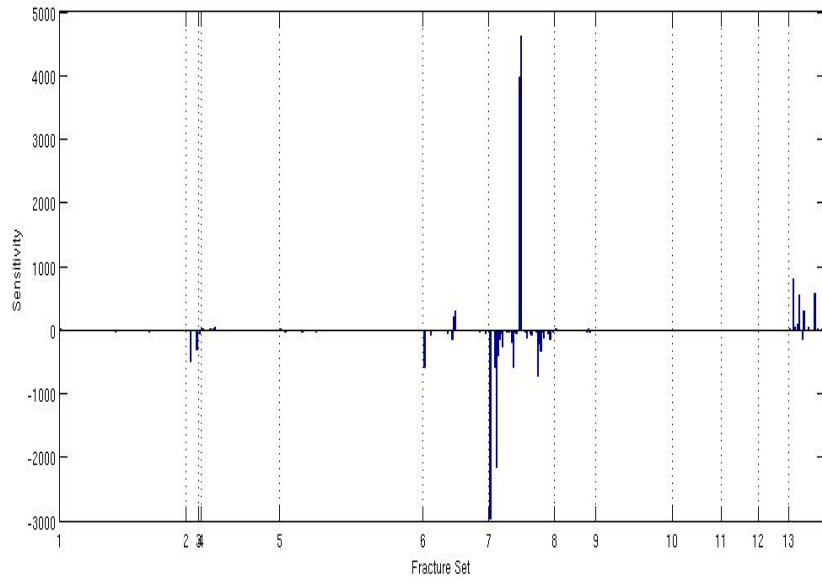


**Figure 38.** Sensitivity values corresponding to fractures belonging to the different fracture sets for measurement point 2.

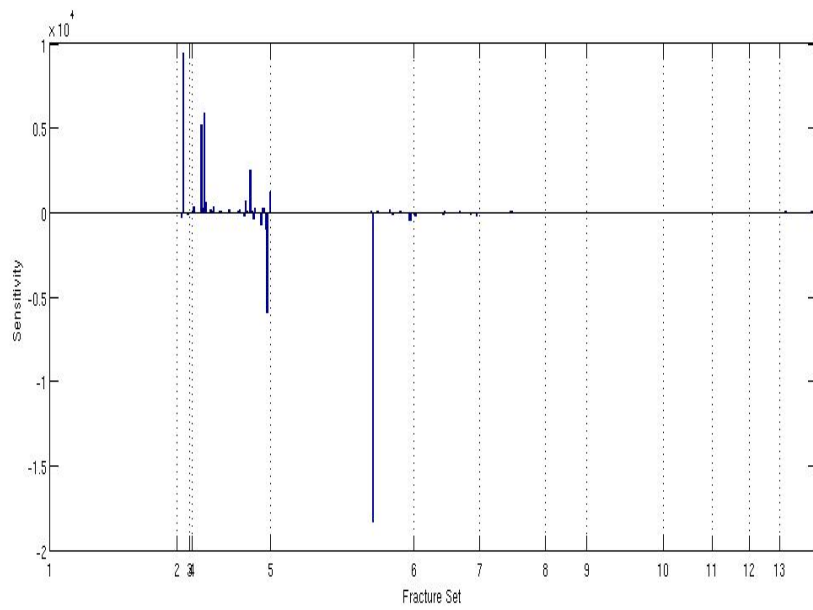


**Figure 39.** Sensitivity values corresponding to fractures belonging to the different fracture sets for measurement point 3.

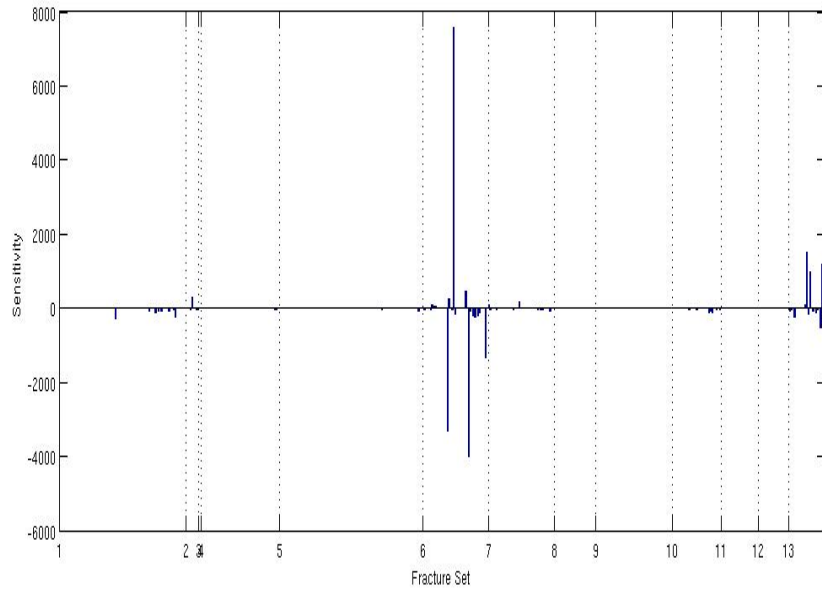


**Figure 40.** Sensitivity values corresponding to fractures belonging to the different fracture sets for measurement point 4.

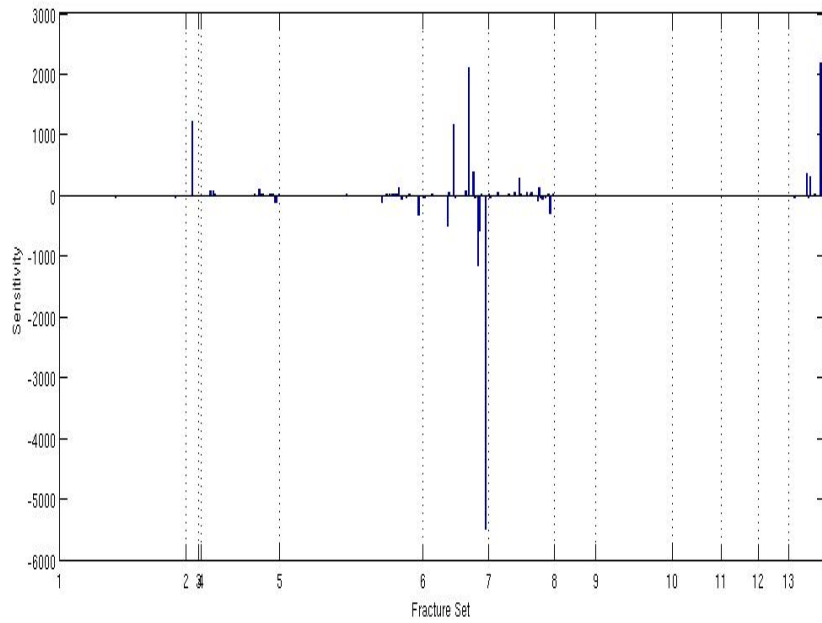


**Figure 41.** Sensitivity values corresponding to fractures belonging to the different fracture sets for measurement point 5.

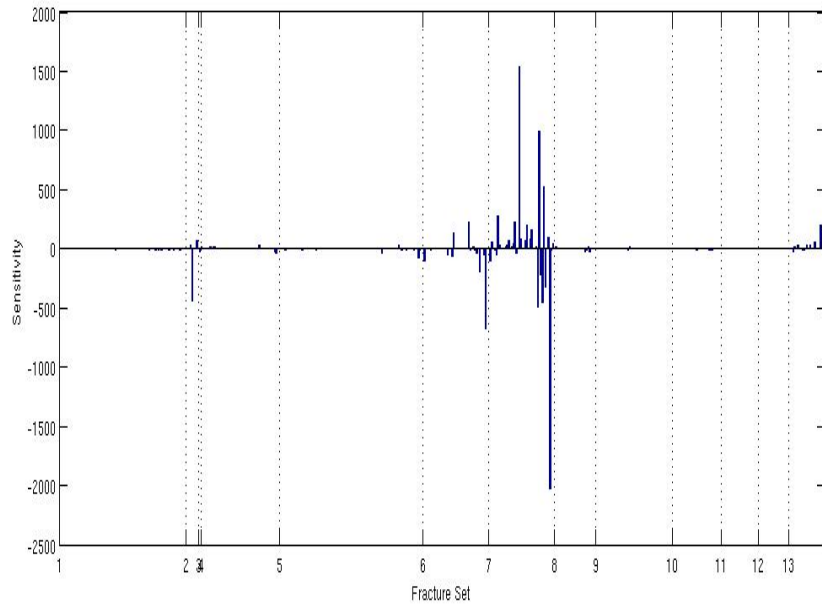


**Figure 42.** Sensitivity values corresponding to fractures belonging to the different fracture sets for measurement point 6.

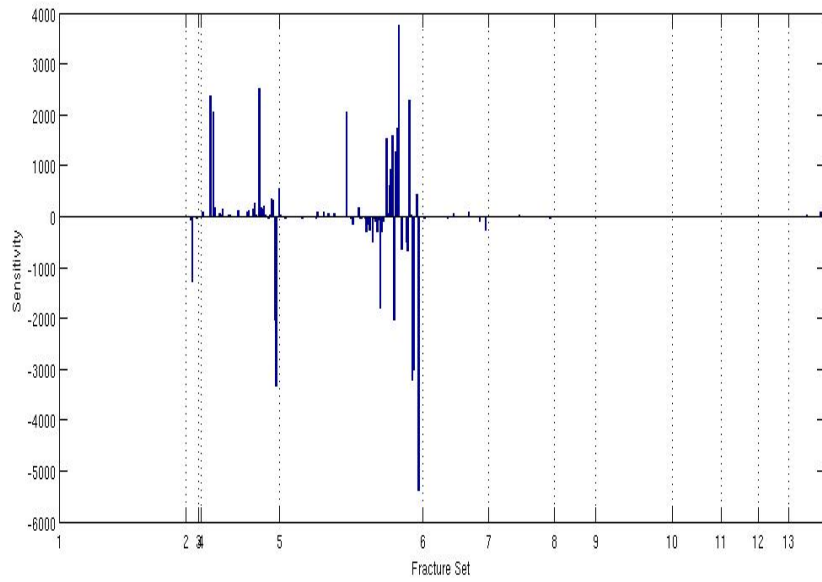


**Figure 43.** Sensitivity values corresponding to fractures belonging to the different fracture sets for measurement point 7.

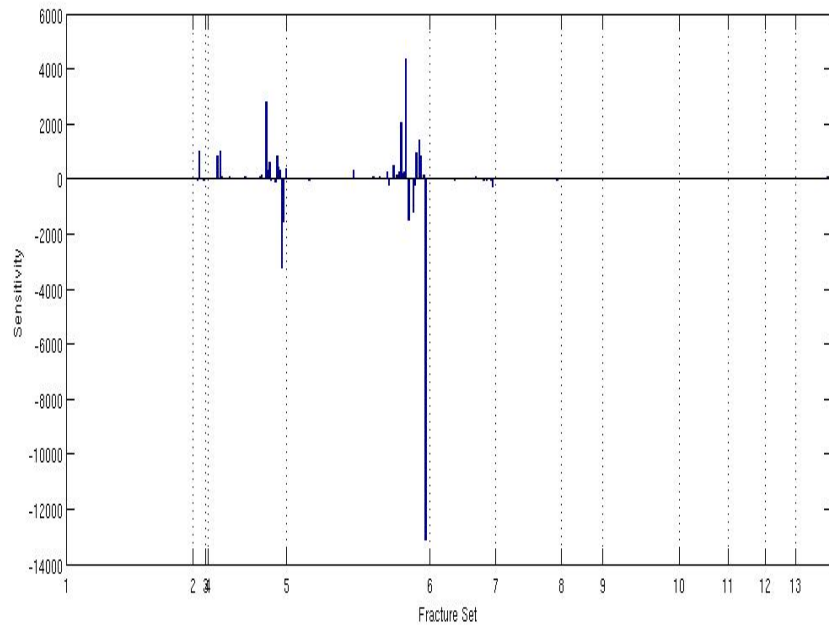


**Figure 44.** Sensitivity values corresponding to fractures belonging to the different fracture sets for measurement point 8.

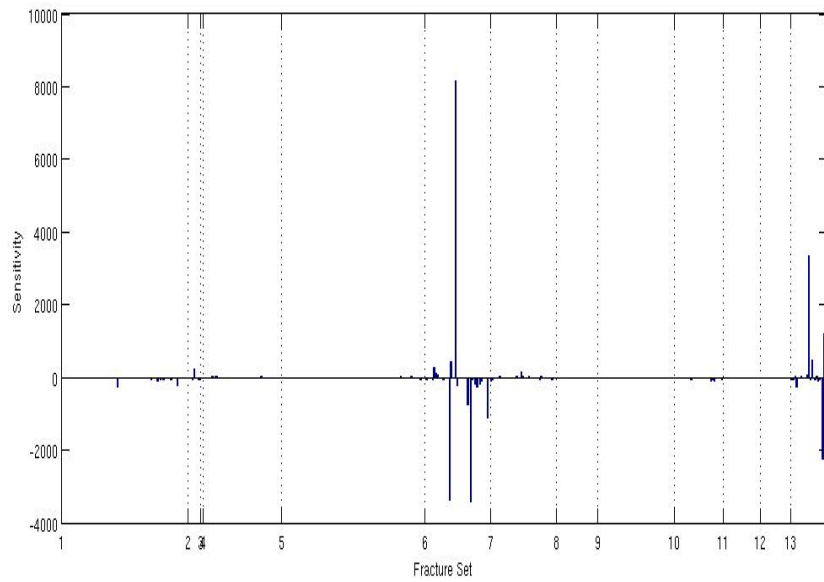


**Figure 45.** Sensitivity values corresponding to fractures belonging to the different fracture sets for measurement point 9.

#### 4.2.2 – CONDITIONED FRACTURE TRANSMISSIVITIES

The conditioned values of the fracture transmissivities for the Olkiluoto test case 1 are plotted in Figure 46 to Figure 58 for each fracture set. The conditioned fracture transmissivities are compared to the unconditioned fracture transmissivities that were homogeneous on each fracture set. The homogeneous unconditioned fracture transmissivities in the figures are represented by a line at a constant log transmissivity value. The conditioned transmissivities of each fracture are shown as bars and the deviation from their unconditioned value can be seen.

Fracture sets 6, 7, 12, and 13 are the only fractures sets that exhibit a major change between the conditioned and unconditioned fracture transmissivities. The lack of change in the other fracture sets can be explained by the small sensitivity values of the fracture transmissivities in the sets, that can be seen in section 4.2. Fracture set 6 contains two small conditioned fracture transmissivities. There are two fracture transmissivities two orders of magnitude greater than their unconditioned values in fracture set 7. Fracture set 12 contains one very small conditioned fracture transmissivity. Fracture set 13 has the most noticeable change in conditioned fracture transmissivities from the unconditioned fracture transmissivities. There are two very large conditioned fracture transmissivities of order  $1E+0$  and  $1E+1$  and one very small value. Additionally there is a lot of change over many orders of magnitude in the remaining conditioned fracture transmissivities compared to the unconditioned fracture transmissivities.

Assuming the cubic law holds the largest conditioned fracture transmissivity corresponds to a fracture aperture value of approximately 2.5cm. While this value

is higher than would be expected it is not physically unreasonable. It may well indicate that instead of a single fracture there exists a cluster of fractures in the area with high transmissivities.

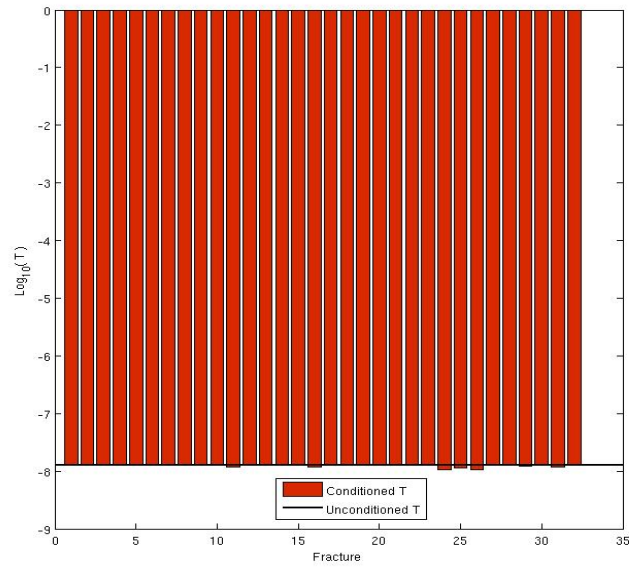


**Figure 46.** Conditioned fracture log transmissivities for fracture set 1. The unconditioned fracture log transmissivities have the value of -7.90 for all fractures and are shown as a black line.

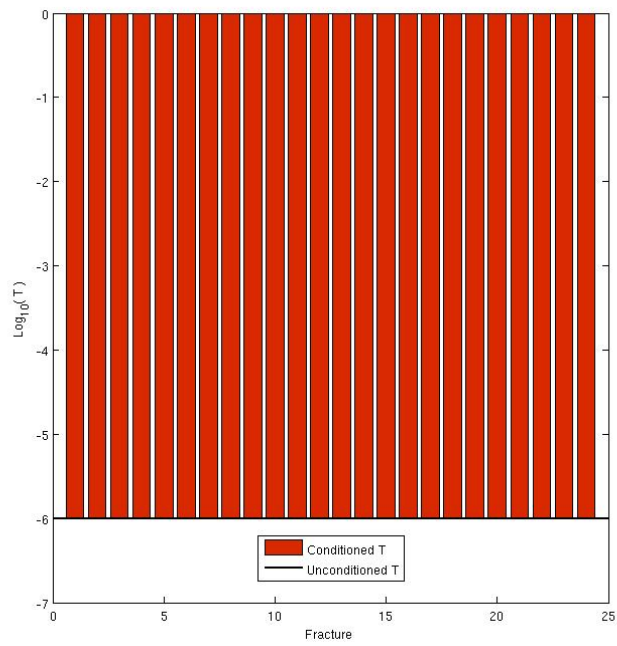


**Figure 47.** Conditioned fracture log transmissivities for fracture set 2. The unconditioned fracture log transmissivities have the value of -6.0006 for all fractures and are shown as a black line.

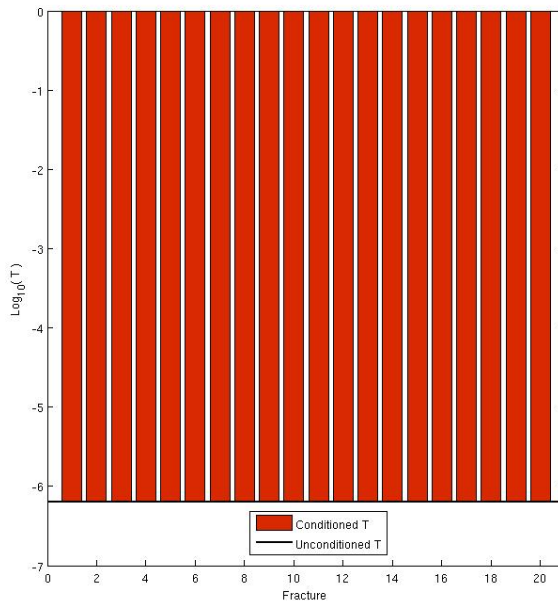


**Figure 48.** Conditioned fracture log transmissivities for fracture set 3. The unconditioned fracture log transmissivities have the value of -6.20 for all fractures and are shown as a black line.

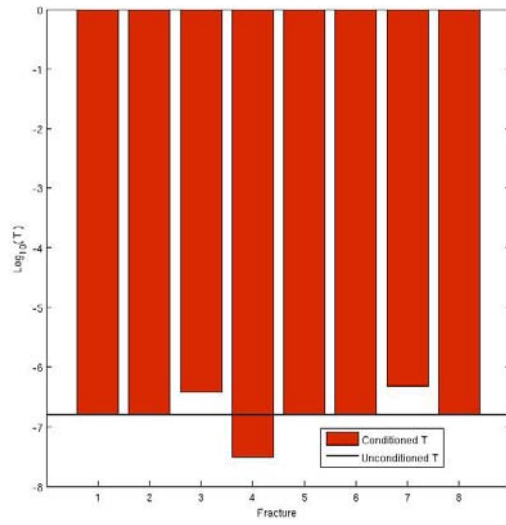


**Figure 49.** Conditioned fracture log transmissivities for fracture set 4. The unconditioned fracture log transmissivities have the value of -6.7999 for all fractures and are shown as a black line.

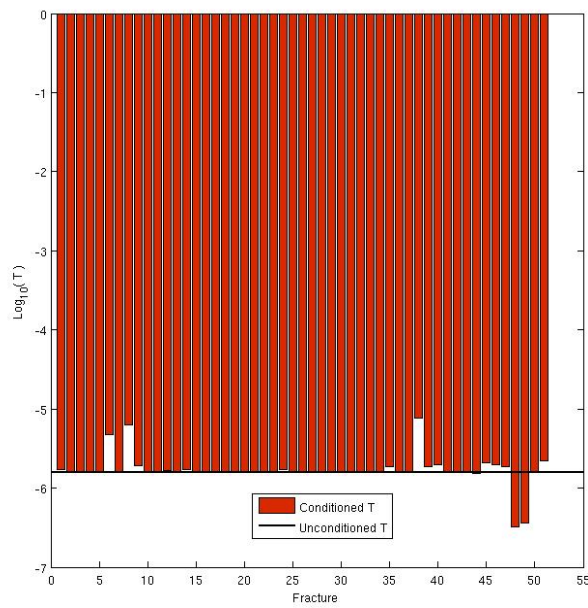


**Figure 50.** Conditioned fracture log transmissivities for fracture set 5. The unconditioned fracture log transmissivities have the value of -5.7999 for all fractures and are shown as a black line.

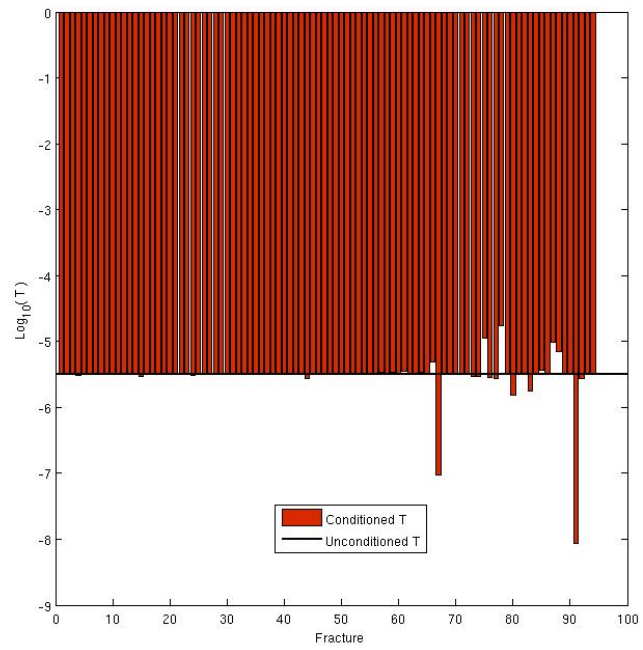


**Figure 51.** Conditioned fracture log transmissivities for fracture set 6. The unconditioned fracture log transmissivities have the value of -5.4998 for all fractures and are shown as a black line.

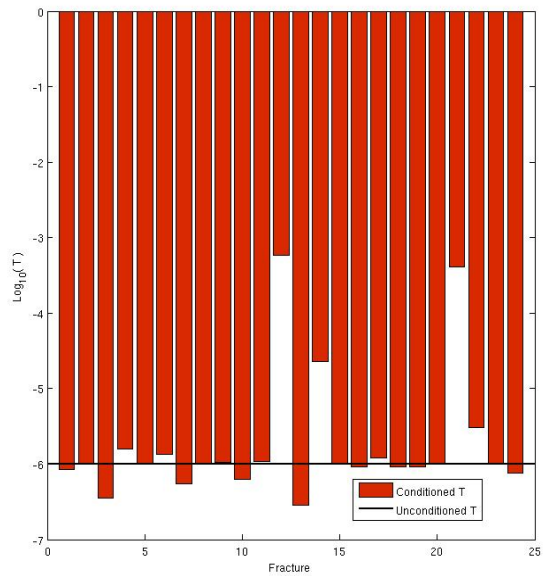


**Figure 52.** Conditioned fracture log transmissivities for fracture set 7. The unconditioned fracture log transmissivities have the value of -6.0006 for all fractures and are shown as a black line.

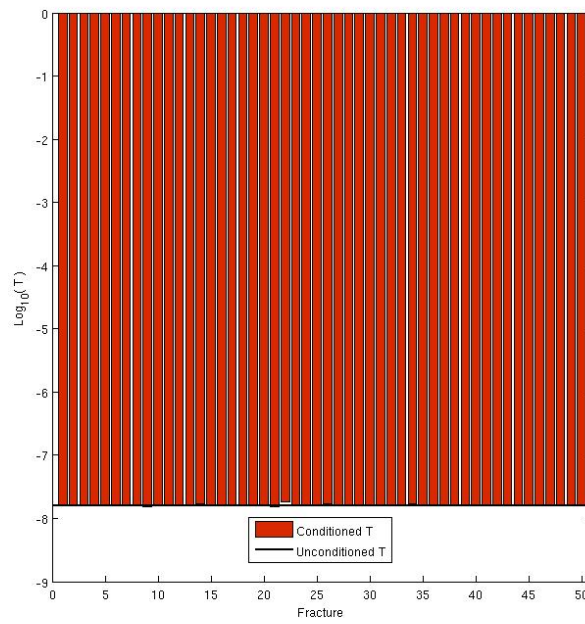


**Figure 53.** Conditioned fracture log transmissivities for fracture set 8. The unconditioned fracture log transmissivities have the value of -7.8002 for all fractures and are shown as a black line.

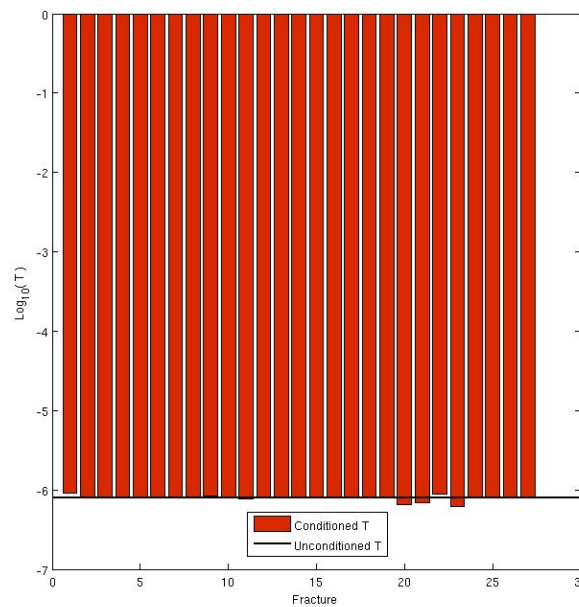


**Figure 54.** Conditioned fracture log transmissivities for fracture set 9. The unconditioned fracture log transmissivities have the value of -6.0999 for all fractures and are shown as a black line.

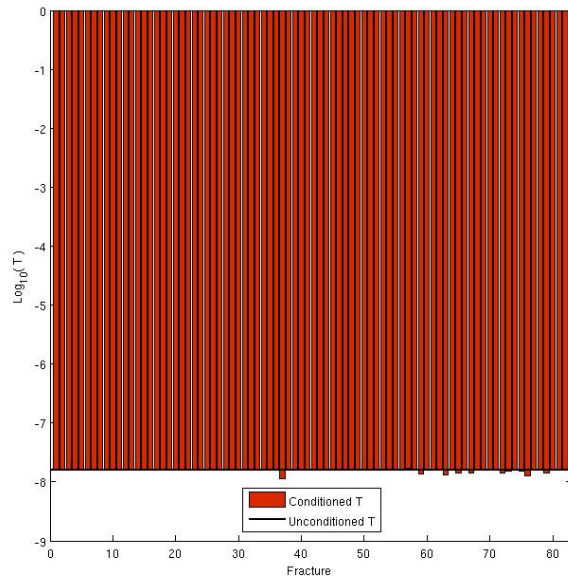


**Figure 55.** Conditioned fracture log transmissivities for fracture set 10. The unconditioned fracture log transmissivities have the value of -7.8002 for all fractures and are shown as a black line.

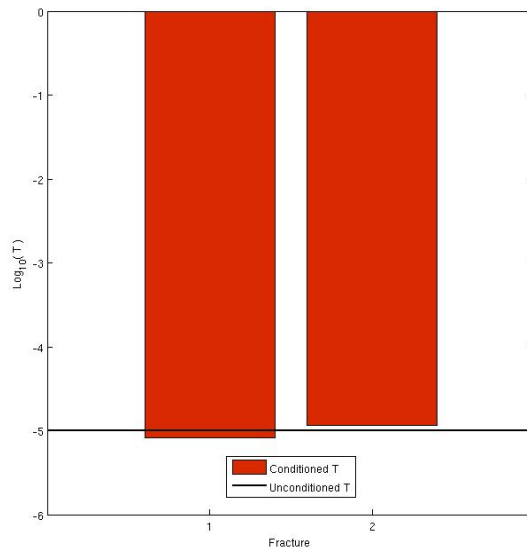


**Figure 56.** Conditioned fracture log transmissivities for fracture set 11. The unconditioned fracture log transmissivities have the value of -5.0 for all fractures and are shown as a black line.

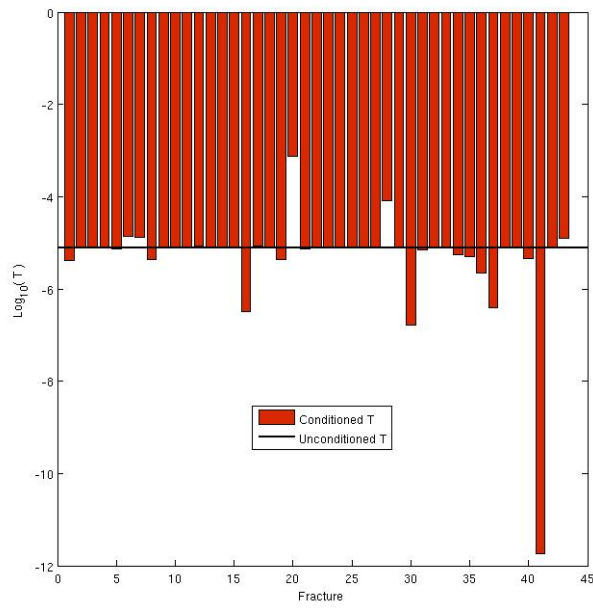


**Figure 57.** Conditioned fracture log transmissivities for fracture set 12. The unconditioned fracture log transmissivities have the value of -5.1110 for all fractures and are shown as a black line.

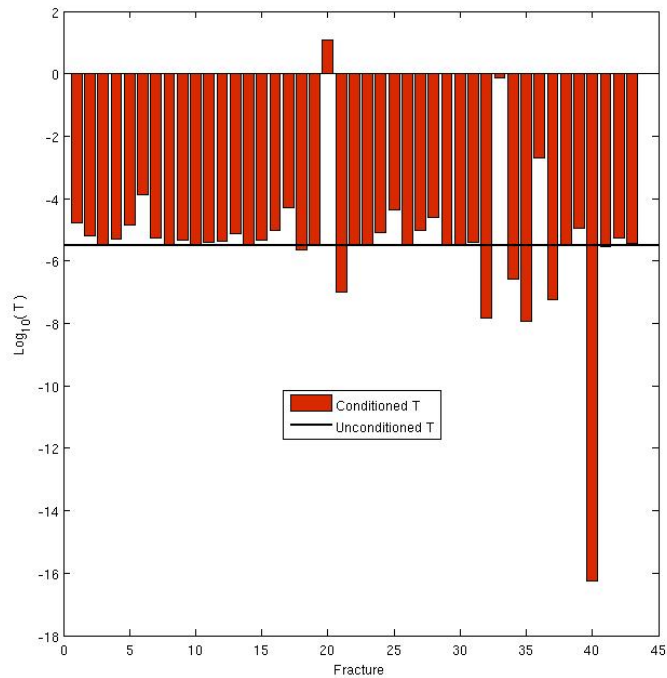


**Figure 58.** Conditioned fracture log transmissivities for fracture set 13. The unconditioned fracture log transmissivities have the value of -5.4998 for all fractures and are shown as a black line.

#### 4.2.3 - CONDITIONING ON DIFFERENT SETS OF FRACTURE TRANSMISSIVITIES

The basis vector conditioning method gives an improved match to the measured pressures but not a close match. The aim of this section is to find out if the basis vector conditioning method can match measured pressures when the unconditioned pressures are sufficiently close to the measured pressures for the Olkiluoto test case 1. To do this a different set of measured pressures were used. The basis vector conditioning method was then used on Olkiluoto test case 1. The new pressure measurements were obtained by generating random fracture transmissivities for each of the fractures. Pressures were obtained at each of the measurement points corresponding to the randomly chosen fracture transmissivities. These pressures were used as measured pressure values to condition the original fracture transmissivities on because we know it is possible for these measured pressures to be matched. Note that the geometry of the fractures was not changed. Fracture transmissivities were generated from a log-normal distribution of

$$P(T) = \frac{1}{\sigma\sqrt{2\pi T}} e^{-\frac{(\log_{10} T - M)^2}{2\sigma^2}}, \quad (4.9)$$

where  $T$  is the fracture transmissivity,  $M$  is the mean of  $\log_{10} T$  and  $\sigma$  is the standard deviation of  $\log_{10} T$ . Four different sets of fracture transmissivities for the 501 fractures were generated using different mean transmissivities and standard deviations of the associated normal distribution of the transmissivities (4.9); these are shown in Table 6.

Case	$\mu$	$sd$
A	2.0E-6	1.0E-6
B	2.0E-5	1.0E-6
C	2.0E-3	1.0E-6
D	2.0E-5	1.0E-3

**Table 6.** The mean transmissivity and standard deviation of the associated normal distribution of the fracture transmissivities for the four generated fracture sets.

Thus,  $M = \log_{10} \mu$ , and  $sd$  is the standard deviation of the associated normal distribution of transmissivities. Figure 59 shows the pressure values at each measurement point corresponding to each of the cases from Table 6 compared to the unconditioned pressures shown in Figure 35. Cases A, B and C are close to the unconditioned pressure values; Case D differs by a greater amount. Note that there is no conditioning involved in Figure 59. Another point to note is that the pressures from all the randomly generated fracture transmissivities are much closer to the unconditioned pressures than the measured pressures in Figure 35.

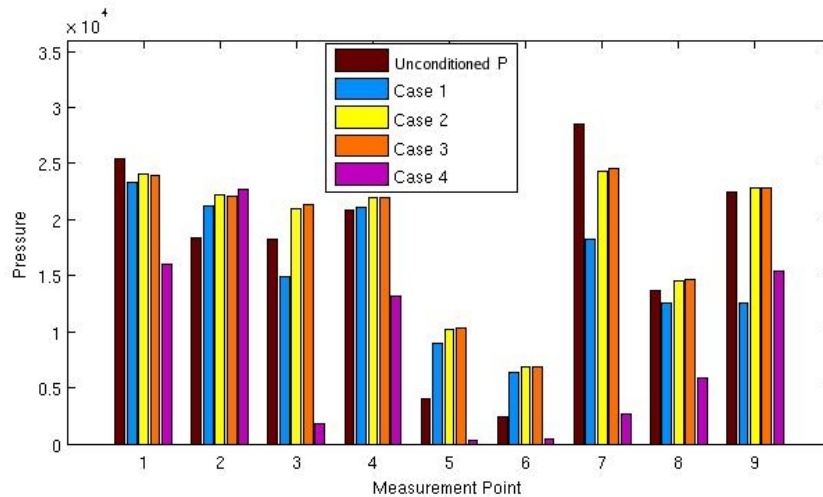


**Figure 59.** Pressure values at each measurement point corresponding to the unconditioned transmissivities and the 4 cases of randomly generated transmissivities from log-normal distributions.

The fracture transmissivity values corresponding to the unconditioned pressures from Figure 35 were used as initial fracture transmissivities; these were then conditioned using the pressures from the four different cases from Table 6 and shown in Figure 59 as measured pressure values.

The conditioned pressures agreed exactly with the pressure values calculated in cases A, B and C. The conditioned pressures did not agree exactly with the pressures obtained from case D, but gave a very close match. Figure 60 shows the pressures obtained from cases A, B, C and D compared to the conditioned pressure for cases A, B, C and D at each measurement point. Table 7 shows the initial absolute error and relative error, final absolute error and relative error and the number of Levenberg-Marquardt iterations required for each of the cases. The results of this section suggest that the basis vector conditioning method can converge to measured pressure values when they are close to the unconditioned pressures. However, when the measured pressures differ greatly from the

unconditioned pressures, the resulting conditioned pressures do not give a good match to the measured pressures. As will be seen in chapter 6, the conditioned fracture transmissivities corresponding to the measured pressures in the Olkiluoto test case 1 differ greatly from the unconditioned fracture transmissivities. On this evidence, the basis vector method does not give a good match to the measured pressures when the unconditioned pressures differ greatly from the measured pressures.

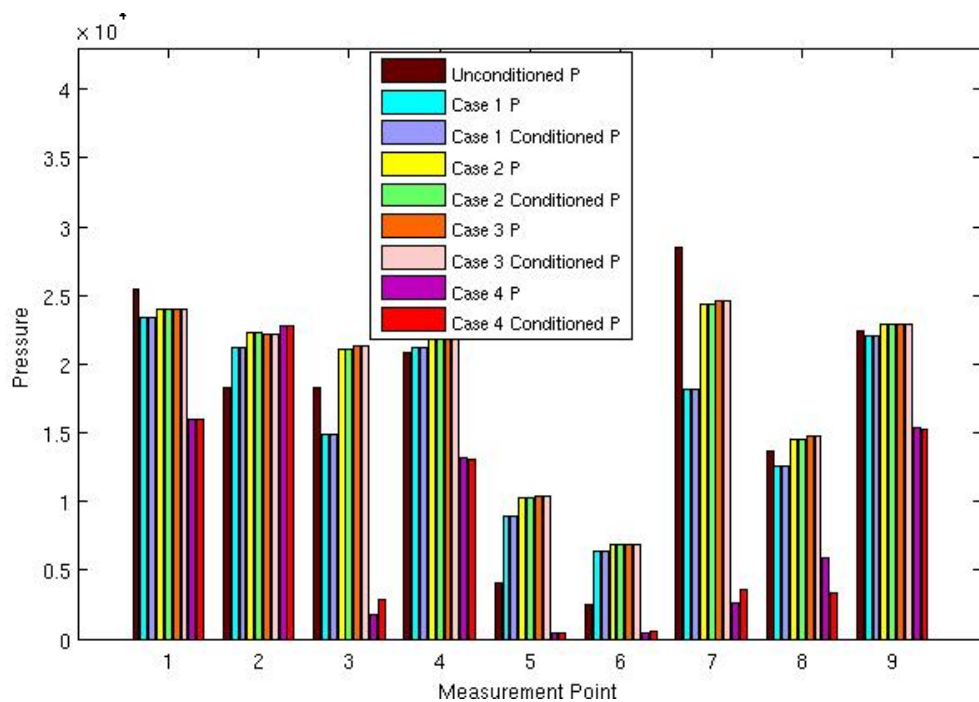


**Figure 60.** Conditioned pressure values compared to the pressure that is to be matched corresponding to each test case set of transmissivities (generated using the data in Table 6) for each measurement point.

Case	Initial Absolute Error	Final Absolute Error	Initial Relative Error	Final Relative Error	Number of Iterations
A	1.3063E+4	0.54	0.2542	0	10
B	1.0978E+4	0.69	0.2089	0	9
C	1.0206E+4	0.35	0.2153	0	10
D	3.5117E+4	2.9203E+3	4.1238	0.1915	24

**Table 7.** The initial absolute error, the final absolute error, the initial relative error, the final relative error and the number of iterations of the Levenberg Marquardt algorithm required to converge to the final absolute error, shown for each of the generated fracture transmissivity cases.

### 4.3 - CHAPTER SUMMARY AND CONCLUSIONS

A new conditioning method has been developed for DFNs based on previous work undertaken on CPMs which we have referred to as the basis vector conditioning method. The practical driver for the work was the need to reproduce measurements of pressure in a DFN based on limited measurement points. The basis vector conditioning method conditions fracture transmissivities on measured

pressure values. This algorithm was tested on a number of simple test cases, as well as on a test case based on data from a real site.

When the term updating was used it meant the sensitivity values were updated in each iteration of the minimisation procedure. When updating was employed in the conditioning of simple test cases, the absolute error converged (the value of the final absolute error was less than 1Pa) in a relatively small number of iterations so that the calculated and measured pressures were in agreement. Without updating it was found that convergence would always occur if the initial fracture transmissivities were up to three orders of magnitude less than the solution transmissivity. However, a large number of iterations were typically required for small initial fracture transmissivities. When an initial fracture transmissivity was three orders of magnitude greater than the solution transmissivity, the method failed to converge for the first three test cases; the method converged for the fourth test case for all initial values used. It appears that the convergence of the basis vector conditioning method is dependent on the geometry of the fractures and the boundary conditions employed, especially if updating is not being exploited.

The basis vector conditioning method was used on a test case based on data from a potential site for nuclear waste disposal in Finland consisting of 501 fractures with 9 measured pressure values (Olkiluoto test case 1). There was a considerable improvement in the match to the measured pressures, when compared to the unconditioned pressure values at every measurement point, though the conditioned pressures did not agree exactly with the measured pressure values, as we would most likely expect.

When looking at the sensitivities of the pressure at measurement points with respect to fracture transmissivities, it was seen that some fracture sets affect the calculated pressures far more than others. In fact, some of the fracture sets have almost no influence on the calculated pressure at any of the measurement points. The conditioned fracture transmissivities ranged over many orders of magnitude. Some fracture sets showed very little change from the conditioned and unconditioned fracture transmissivities. Fracture set 13 showed the greatest change with two conditioned fracture transmissivities taking large values while the rest of the fracture transmissivities in this set varied greatly in their conditioned values.

In an effort to improve the agreement of calculated pressures with measured pressures, a homotopy method was investigated. However, the homotopy method did not improve the match given by the basis vector conditioning method. Additionally, the fracture transmissivity values that corresponded to the conditioned pressures were used as initial fracture transmissivities and the basis vector conditioning method was re-run. This gave no improvement in the match to measured pressures.

The results in this chapter pose the question of why there are discrepancies between the measured and conditioned pressures. Is the basis vector conditioning method inaccurate or is the underlying conceptual model to blame for these discrepancies? First let us consider our basis vector conditioning method. A likely problem is that the conditioning method is converging to a local minimum. Thus, the lack of agreement to measured pressure values may occur because the initial 501 fracture transmissivity values are not sufficiently close to the unknown target transmissivities which yield the measured pressures; resulting in the Levenberg

Marquardt method getting stuck in a local minimum. This motivated us to consider a case with known ‘measured’ pressure values for a particular set of fracture transmissivities. In this case, these pressures were used as measured pressure values on which to condition our original fracture transmissivities; the geometry of the fractures was not changed.

Four different cases were studied with fracture transmissivities being generated from log-normal distributions with different means and variances. The resulting pressures for the four cases were used as measured pressures for the purposes of conditioning. The conditioning method led to pressures that matched the measured pressures exactly for three of the cases considered. In the final test case, where the transmissivity distribution had a large variance, the pressures computed by the basis vector conditioning agreed well to the (computed) measured pressures.

It appears that the basis vector conditioning method works well when the initial unconditioned pressures are sufficiently close to the measured pressures. However it struggles when the measured pressures differ greatly from the unconditioned pressures.

Based on the results in this chapter it is inconclusive if the lack of a match to the measured pressures was due to the conceptual model or the basis vector conditioning method that was employed. For now let us suppose that the basis vector conditioning method is not responsible for the observed discrepancies between the measured and conditioned pressures. What are the potential causes of these discrepancies?

The lack of a match to measured pressures can suggest that a DFN model is less adequate for the site than a CPM approach. In the case that a DFN is an

appropriate conceptual model, the fact that the fracture transmissivities are assumed to be uncorrelated can also be a source of the observed discrepancies. Furthermore, modelling fractures with a constant transmissivity (using a parallel plate model of the fracture) is a potential cause of discrepancies between conditioned and unconditioned pressures.

The geometry of the DFN and the boundary conditions employed will affect the values of the unconditioned pressure values and the range of possible pressure values.

Instead of changing the conceptual model that was used we focus on the conditioning method. To this end, in the next chapter we develop a Bayesian conditioning method for application to the Olkiluoto test case 1.

## 5 – BAYESIAN CONDITIONING METHOD

In this chapter a Bayesian conditioning method is developed in an attempt to improve the conditioning results obtained from the basis vector conditioning method. A mathematical formulation of the Bayesian conditioning method is given and results from conditioning fracture transmissivities on measured pressures using two large scale test cases are also shown.

### 5.1 - MATHEMATICAL FORMULATION OF THE BAYESIAN CONDITIONING METHOD

As in the basis vector conditioning method, it is assumed that the transmissivity is constant over each fracture. The vector of fracture log transmissivities is denoted by  $\mathbf{X}$  and  $\mathbf{m}$  denotes the vector of mean fracture log transmissivities.  $\mathbf{X}$  is assumed to have a prior Gaussian distribution, defined as

$$f(\mathbf{X}) = \mathbf{A}_1 \exp\left\{-\frac{1}{2}(\mathbf{X}-\mathbf{m})^T \mathbf{C}^{-1}(\mathbf{X}-\mathbf{m})\right\}, \quad (5.1)$$

where the matrix  $\mathbf{C}$  is the covariance matrix of the fracture log transmissivities  $\mathbf{X}$  and  $\mathbf{A}_1$  is a constant vector. The fracture log transmissivities  $\mathbf{X}$  may or may not be correlated. Furthermore, the measured pressures are assumed to be known to within some measurement error  $\varepsilon$  and it is assumed they are independent,

normally distributed random variables with possibly different standard deviations for each measurement. The pressures calculated (by NAPSAC) at a measurement point  $\mathbf{P}_C$  are a function of the fracture log transmissivities. This can be written as

$$\mathbf{F}(\mathbf{X}) = \mathbf{P}_C, \quad (5.2)$$

where  $\mathbf{F}(\mathbf{X})$  is the vector of calculated pressure values at measurement points as a function of the fracture log transmissivities  $\mathbf{X}$ . It is assumed that the measured pressures  $\mathbf{P}_M$  are equal to the sum of the mean values of the measured pressures  $\bar{\mathbf{P}}_M$  and a vector of measurement errors  $\boldsymbol{\varepsilon}$ , i.e.

$$\mathbf{P}_M = \bar{\mathbf{P}}_M + \boldsymbol{\varepsilon}. \quad (5.3)$$

Bayes theorem (Lee 1997) can be used to write down the posterior distribution for  $\mathbf{X}$  defined as

$$f(\mathbf{X}|\mathbf{P}_M) = \frac{f(\mathbf{P}_M|\mathbf{X})f(\mathbf{X})}{f(\mathbf{P}_M)}, \quad (5.4)$$

where, for a pair of events  $\mathbf{a}$  and  $\mathbf{b}$ ,  $f(\mathbf{a}|\mathbf{b})$  is defined as the probability density function of the event  $\mathbf{a}$  given the hypotheses  $\mathbf{b}$ . The structure of  $f(\cdot)$  is determined by the term in its brackets. For example, the  $f(\cdot)$  terms that appear in (5.4) are all different functions. The term  $f(\mathbf{X})$  is the prior distribution of

fracture log transmissivities defined in (5.1), while the term  $f(\mathbf{P}_M | \mathbf{X})$  is the likelihood function and is given by

$$f(\mathbf{P}_M | \mathbf{X}) = \mathbf{A}_2 \exp \left\{ -\frac{1}{2} (\mathbf{F}(\mathbf{X}) - \mathbf{P}_M)^T \boldsymbol{\Sigma}^{-1} (\mathbf{F}(\mathbf{X}) - \mathbf{P}_M) \right\}, \quad (5.5)$$

where  $\mathbf{A}_2$  is a constant vector, the matrix  $\boldsymbol{\Sigma}$  is the covariance matrix of the error in the measured pressures  $\boldsymbol{\varepsilon}$  and will be a diagonal matrix if the measured pressures are independent. Our interpretation of Bayes' theorem is that it expresses our posterior beliefs (our beliefs after we have obtained the pressure measurement data) about  $\mathbf{X}$  taking into account our prior beliefs of  $\mathbf{X}$  expressed by the distribution of  $\mathbf{X}$  given by (5.1) and the data available, which are pressure measurements related to  $\mathbf{X}$  as given by (5.5). The normalisation constant  $f(\mathbf{P}_M)$  is unknown, but using (5.1), (5.4) and (5.5) we can state

$$f(\mathbf{X} | \mathbf{P}_M) \propto \exp \left( -\frac{1}{2} (\mathbf{X} - \mathbf{m})^T \mathbf{C}^{-1} (\mathbf{X} - \mathbf{m}) \right) \exp \left( -\frac{1}{2} (\mathbf{F}(\mathbf{X}) - \mathbf{P}_M)^T \boldsymbol{\Sigma}^{-1} (\mathbf{F}(\mathbf{X}) - \mathbf{P}_M) \right). \quad (5.6)$$

The mode of a probability distribution function such as (5.6) is the value at which it attains its maximum value and can be found by solving  $\frac{df(\mathbf{X} | \mathbf{P}_M)}{d\mathbf{X}} = \mathbf{0}$ . The mode of (5.6) finds the most probable set of fracture transmissivities that yield the given measured pressures. The exponential function is monotonic so it is also true

that the posterior mode for  $\mathbf{X}$  occurs when  $\frac{d}{d\mathbf{X}}\left\{\ln\left(f\left(\mathbf{X}|\mathbf{P}_M\right)\right)\right\} = \mathbf{0}$  and it follows

from (5.6) that, at the mode of  $f\left(\mathbf{X}|\mathbf{P}_M\right)$ ,

$$\frac{d}{d\mathbf{X}}\left\{-\left[\left(\frac{1}{2}\left(\mathbf{X}-\mathbf{m}\right)^T\mathbf{C}^{-1}\left(\mathbf{X}-\mathbf{m}\right)\right)+\left(\frac{1}{2}\left(\mathbf{F}\left(\mathbf{X}\right)-\mathbf{P}_M\right)^T\boldsymbol{\Sigma}^{-1}\left(\mathbf{F}\left(\mathbf{X}\right)-\mathbf{P}_M\right)\right)\right]\right\} = \mathbf{0} . \quad (5.7)$$

Using the product rule for vectors

$$\frac{d}{d\mathbf{X}}\left(\frac{1}{2}\left(\mathbf{X}-\mathbf{m}\right)^T\mathbf{C}^{-1}\left(\mathbf{X}-\mathbf{m}\right)\right) = \frac{1}{2}\left(\mathbf{X}-\mathbf{m}\right)^T\left(\mathbf{C}^{-1}+\mathbf{C}^{-T}\right), \quad (5.8)$$

and similarly

$$\frac{d}{d\mathbf{X}}\left(\frac{1}{2}\left(\mathbf{F}\left(\mathbf{X}\right)-\mathbf{P}_M\right)^T\boldsymbol{\Sigma}^{-1}\left(\mathbf{F}\left(\mathbf{X}\right)-\mathbf{P}_M\right)\right) = \frac{1}{2}\left(\mathbf{F}\left(\mathbf{X}\right)-\mathbf{P}_M\right)^T\left(\boldsymbol{\Sigma}^{-1}+\boldsymbol{\Sigma}^{-T}\right)\frac{d\mathbf{F}}{d\mathbf{X}} . \quad (5.9)$$

Thus, the mode of the posterior distribution  $f\left(\mathbf{X}|\mathbf{P}_M\right)$  can be found when

$$\left(\mathbf{X}-\mathbf{m}\right)^T\left(\mathbf{C}^{-1}+\mathbf{C}^{-T}\right)+\left(\mathbf{F}\left(\mathbf{X}\right)-\mathbf{P}_M\right)^T\left(\boldsymbol{\Sigma}^{-1}+\boldsymbol{\Sigma}^{-T}\right)\frac{d\mathbf{F}}{d\mathbf{X}} = \mathbf{0} . \quad (5.10)$$

For the case where both  $\mathbf{C}$  and  $\boldsymbol{\Sigma}$  are diagonal matrices (assuming uncorrelated fracture transmissivities) (5.10) simplifies to

$$(\mathbf{X} - \mathbf{m})^T \mathbf{C}^{-1} + (\mathbf{F}(\mathbf{X}) - \mathbf{P}_M)^T \boldsymbol{\Sigma}^{-1} \frac{d\mathbf{F}}{d\mathbf{X}} = \mathbf{0} . \quad (5.11)$$

Equation (5.10) can be solved using the Newton method (for a description of this method, see, for example, Bonnans, Gilbert et al.(2006) ) to compute the posterior mode of  $\mathbf{X}$ . We define the left hand side of (5.10) to be

$$\mathbf{G}(\mathbf{X}) \equiv (\mathbf{X} - \mathbf{m})^T (\mathbf{C}^{-1} + \mathbf{C}^{-T}) + (\mathbf{F}(\mathbf{X}) - \mathbf{P}_M)^T (\boldsymbol{\Sigma}^{-1} + \boldsymbol{\Sigma}^{-T}) \frac{d\mathbf{F}}{d\mathbf{X}} = \mathbf{0} . \quad (5.12)$$

The Newton method generates a sequence for updating the log transmissivities  $\mathbf{X}_k$  at the  $k^{\text{th}}$  iteration by the recurrence formula

$$\mathbf{X}_{k+1} = \mathbf{X}_k + \mathbf{d}_k , \quad (5.13)$$

where  $\mathbf{d}_k$  solves equation (5.12) linearised at  $\mathbf{X}_k$  given by

$$\mathbf{G}(\mathbf{X}_k) + \mathbf{G}'(\mathbf{X}_k) \mathbf{d}_k = \mathbf{0} , \quad (5.14)$$

where  $\mathbf{G}'(\mathbf{X}_k) = \frac{d\mathbf{G}(\mathbf{X}_k)}{d\mathbf{X}_k}$ . If  $\mathbf{G}'(\mathbf{X}_k)$  is non-singular

$$\mathbf{d}_k = -\mathbf{G}'(\mathbf{X}_k)^{-1} \mathbf{G}(\mathbf{X}_k) . \quad (5.15)$$

Now  $\mathbf{G}'(\mathbf{X}_k)$  is given by

$$\mathbf{G}'(\mathbf{X}_k) = (\mathbf{C}^{-1} + \mathbf{C}^{-T}) + \left( \frac{d\mathbf{F}}{d\mathbf{X}_k} \right)^T (\boldsymbol{\Sigma}^{-1} + \boldsymbol{\Sigma}^{-T}) \frac{d\mathbf{F}}{d\mathbf{X}_k} + (\mathbf{F}(\mathbf{X}_k) - \mathbf{P}_M)^T (\boldsymbol{\Sigma}^{-1} + \boldsymbol{\Sigma}^{-T}) \frac{d^2\mathbf{F}}{d\mathbf{X}_k^2}. \quad (5.16)$$

In minimisation problems such as ours it is common (Press, Flannery et al. 1986)

to drop the  $\frac{\partial^2\mathbf{F}}{\partial\mathbf{X}_k^2}$  term from (5.16). Thus, from hereon we use the approximation

$$\mathbf{G}'(\mathbf{X}_k) \approx (\mathbf{C}^{-1} + \mathbf{C}^{-T}) + \left( \frac{d\mathbf{F}}{d\mathbf{X}_k} \right)^T (\boldsymbol{\Sigma}^{-1} + \boldsymbol{\Sigma}^{-T}) \frac{d\mathbf{F}}{d\mathbf{X}_k}. \quad (5.17)$$

The algorithm to condition fracture log transmissivities  $\mathbf{X}$  on pressure measurements  $\mathbf{P}_M$  solves the system

$$\mathbf{G}(\mathbf{X}) = (\mathbf{X} - \mathbf{m})^T (\mathbf{C}^{-1} + \mathbf{C}^{-T}) + (\mathbf{F}(\mathbf{X}) - \mathbf{P}_M)^T (\boldsymbol{\Sigma}^{-1} + \boldsymbol{\Sigma}^{-T}) \frac{d\mathbf{F}}{d\mathbf{X}} = \mathbf{0} \text{ using the}$$

approximation  $\mathbf{G}'(\mathbf{X}) = (\mathbf{C}^{-1} + \mathbf{C}^{-T}) + \left( \frac{d\mathbf{F}}{d\mathbf{X}} \right)^T (\boldsymbol{\Sigma}^{-1} + \boldsymbol{\Sigma}^{-T}) \frac{d\mathbf{F}}{d\mathbf{X}}$  is as follows:

### Bayesian Conditioning Algorithm

1 – Take the initial set of fracture log transmissivities  $\mathbf{X}_0 = \mathbf{m}$  and set  $k = 0$ .

2 - Compute  $\mathbf{G}(\mathbf{X}_k)$  and  $\mathbf{G}'(\mathbf{X}_k)$ .

3 - Compute the increment  $\mathbf{d}_k$  from the system  $\mathbf{G}'(\mathbf{X}_k)\mathbf{d}_k = -\mathbf{G}(\mathbf{X}_k)$ .

4 - Update the fracture log transmissivities  $\mathbf{X}_{k+1} = \mathbf{X}_k + \mathbf{d}_k$ .

5 - Calculate the new pressure values  $\mathbf{F}(\mathbf{X}_{k+1})$ .

6 - Update the sensitivities  $\frac{d\mathbf{F}(\mathbf{X}_{k+1})}{d\mathbf{X}_{k+1}}$  using the adjoint method from chapter 3.

7 - If the convergence criteria has been met then stop. Otherwise set  $k=k+1$  and return to 2.

Essentially, as the variance in the pressure measurements is increased, the matrix  $\Sigma^{-1}$  approaches zero and the measured pressure values are of less importance in the conditioning procedure. Thus, as the variance of the pressure measurements increases the log transmissivities  $\mathbf{X}$  will tend to their prior distribution.

## 5.2 – BAYESIAN CONDITIONING USING OLKILUOTO TEST CASE 1

The Bayesian conditioning method was used to condition  $n = 501$  fracture transmissivities on  $m = 9$  measured pressure values obtained at borehole/fracture intersections as described in the Olkiluoto test case 1 in chapter 4.

For the results obtained in this chapter, it is assumed that each pressure measurement is independent and all measurements have the same standard deviation in the measured pressure. Thus, the covariance matrix,  $\Sigma$ , of the error in the pressure measurements takes the form

$$\Sigma = \sigma_p^2 \mathbf{I}_m, \quad (5.18)$$

where  $\mathbf{I}_m$  is the  $(m \times m)$  identity matrix and the variance  $\sigma_p^2$  is defined at a pressure measurement point  $i$  as

$$\sigma_p^2 = C(P_M^i, \bar{P}_M^i) = E\left[(P_M^i - \bar{P}_M^i)(P_M^i - \bar{P}_M^i)\right]. \quad (5.19)$$

Pressure measurements are of the order 1.0E+4Pa, therefore physically we would expect the variance to be less than the order of  $(1.0E+4)^2 = 1.0E+8$ .

As in chapter 4, when studying the Olkiluoto test case 1, it is assumed that the fracture transmissivities are uncorrelated and accordingly that the covariance

matrix  $\mathbf{C}$  of the fracture log transmissivities is set equal to the  $(n \times n)$  identity matrix  $\mathbf{I}_n$ . It was found that the final absolute error obtained from the Bayesian conditioning method was dependent on the value of the variance in the pressure measurements  $\sigma_p^2$ . Table 8 compares the final absolute errors and relative errors of the basis vector conditioning method to the Bayesian conditioning method with different values of the variance in the pressure measurements  $\sigma_p^2$ , in addition, it shows the number of iterations required for the algorithm to converge for each conditioning method.

Conditioning method	Final Absolute Measure	Final Relative Error	Number of Iterations
Basis vector conditioning method	6.2327E+4	0.3574	8
Bayesian ( $\sigma_p^2=1.0E+0$ )	6.4532E+4	0.3689	1
Bayesian ( $\sigma_p^2=1.0E+1$ )	6.4532E+4	0.3689	1
Bayesian ( $\sigma_p^2=1.0E+2$ )	6.4527E+4	0.3689	1
Bayesian ( $\sigma_p^2=1.0E+3$ )	4.1522E+4	0.1866	15
Bayesian ( $\sigma_p^2=1.0E+4$ )	6.4518E+4	0.3688	1
Bayesian ( $\sigma_p^2=1.0E+5$ )	4.9403E+4	0.2717	26
Bayesian ( $\sigma_p^2=1.0E+6$ )	5.4049E+4	0.3010	33
Bayesian ( $\sigma_p^2=1.0E+7$ )	4.8304E+4	0.2416	12
Bayesian ( $\sigma_p^2=1.0E+8$ )	7.1635E+4	0.4318	1
Bayesian ( $\sigma_p^2=1.0E+9$ )	9.4867E+4	0.5676	3
Bayesian ( $\sigma_p^2=1.0E+10$ )	1.1011E+5	0.6659	1

**Table 8.** Comparison of the conditioning methods on the Olkiluoto test case 1, where the initial absolute error is 1.1128E+5 and the initial relative error is 0.6828.

The absolute error is plotted against the variance of the pressure measurements  $\sigma_p^2$  in Figure 61. It can be seen that the absolute error is at a minimum when the variance in the pressure measurements is  $\sigma_p^2=1.0E+3$ . The relative error is plotted against the variance of the pressure measurements in Figure 62. It can be seen that the final absolute error and relative error start to increase as the variance in the

pressure measurements  $\sigma_p^2$  increases above a value of  $1.0E+8$ . This represents the point at which the standard deviation of the pressure measurements is of the same magnitude of the pressure measurements themselves.

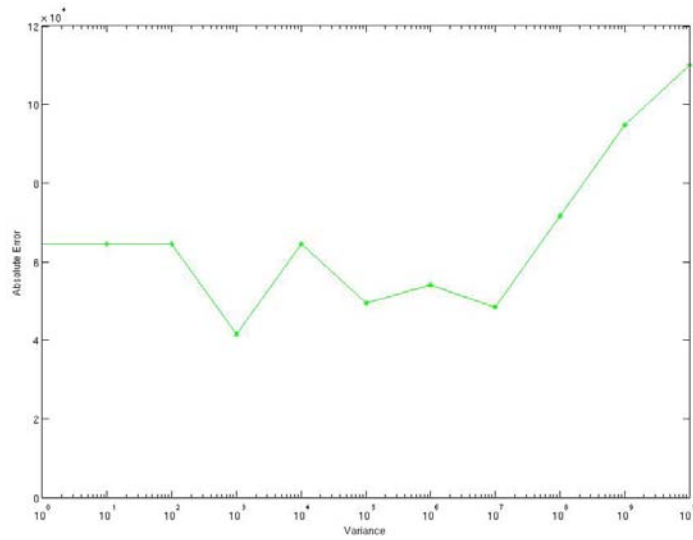


**Figure 61.** Absolute error against the variance  $\sigma_p^2$  of the pressure measurements.

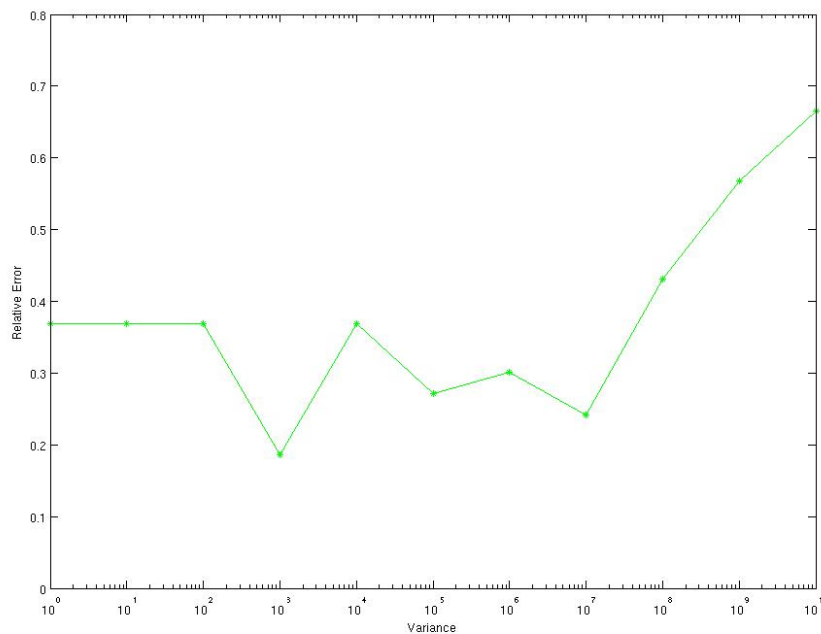


**Figure 62.** Relative error against standard deviation  $\sigma_p$  of the pressure measurements.

## 5.2.1 – DEVELOPMENT OF A NUMERICAL ALGORITHM TO IMPROVE RESULTS FROM THE BAYESIAN CONDITIONING METHOD

A numerical algorithm was developed to improve the match to the measured pressures given by the Bayesian conditioning method. A given set of initial fracture transmissivities was taken and separate runs of the Bayesian conditioning method were performed with different variance values  $\sigma_p^2$  of the measured pressures, with the covariance matrix  $\Sigma$  of the pressure measurement errors equal to  $\sigma_p^2 \mathbf{I}_n$ . By changing the value of  $\sigma_p^2$  used in the Bayesian conditioning method, different conditioned fracture transmissivity sets are obtained with corresponding final absolute error. The fracture transmissivity set which produced the smallest absolute error was selected and used as initial fracture transmissivities in the next step of the algorithm. Thus, the Bayesian conditioning method is applied again with new initial transmissivity values for a range of  $\sigma_p^2$  values. The numerical algorithm is as follows:

### Algorithm A

- 1 - Set initial fracture log transmissivity values  $\mathbf{X} = \mathbf{X}_0$  and set  $i = 1$ .
- 2 - Run the Bayesian conditioning algorithm for step  $i$  on log transmissivities  $\mathbf{X}$  with variance  $\sigma_p^2$  of the pressure measurements ranging from 1.0E+0 to 1.0E+10 as in Table 8 (each variance value corresponds to a separate run as they are held constant when using Newton's method).

3 - Take conditioned log transmissivity values  $\mathbf{X}^C$  that correspond to the variance value  $\sigma_p^2$  with smallest final absolute error as new initial transmissivities. That is set  $\mathbf{X} = \mathbf{X}^C$ .

4 - If absolute error is below a given tolerance then stop. Otherwise, set  $i = i + 1$  and go to 2.

It should be noted that Algorithm A is not a normal Bayesian method. The prior remains constant throughout the whole process in a Bayesian method. As can be seen in the above algorithm, the prior is updated after every step used in Algorithm A. The reason for developing Algorithm A is that although the Bayesian conditioning method improved on results from the basis vector conditioning method it still did not give a close match to measured pressures. We define two separate sets of initial fracture transmissivities. Set A1 is the unconditioned fracture transmissivities that are homogeneous in each fracture set (shown in chapter 3) and set A2 is defined as the conditioned fracture transmissivities obtained from the basis vector conditioning method. By using set A2 with Algorithm A we are simply starting with different initial fracture transmissivities.

Figure 63 shows the relative error against the variance  $\sigma_p^2$  in the measured pressure values for each step in Algorithm A using set A1 as initial fracture transmissivities. Figure 64 shows the Bayesian conditioned pressure at each measurement point for each step of Algorithm A using set A1 as initial fracture transmissivities; it can be seen that with each step the conditioned pressure approaches the measured pressure value at every measurement point. Figure 65 shows the final conditioned pressures from Algorithm A using set A1 as initial

fracture transmissivities compared to the measured and unconditioned pressures at each measurement point.

Figure 66 shows a plot of the variance  $\sigma_p^2$  in the measured pressure values against the relative error for each step in Algorithm A using set A2 as initial fracture transmissivities. Figure 67 shows the Bayesian conditioned pressure at each measurement point for each step of Algorithm A using set A2 as initial fracture transmissivities; these pressures are compared to the measured and unconditioned pressures. Figure 68 shows the final conditioned pressures from Algorithm A using set A2 as initial fracture transmissivities compared to the measured and unconditioned pressures at each measurement point. Table 9 shows the absolute error and relative error in the conditioned pressures at each step of Algorithm A using set A1 as initial fracture transmissivities and Table 10 displays the same information for Algorithm A using set A2 as initial fracture transmissivities. Table 11 compares the final absolute error and relative error output by the basis vector conditioning method to Algorithm A using set A1 and Algorithm A using set A2. These results show Algorithm A produces a good fit to the measured pressures for both sets of initial fracture transmissivities used. Algorithm A yields a similar final absolute and relative error for both initial fracture transmissivity sets. The final relative errors from Algorithm A corresponding to the two different initial fracture transmissivity set A1 and A2 were both more than 26 times smaller than the basis vector conditioning method and 51 times smaller than the unconditioned fracture transmissivity values.

Algorithm A produces a far superior match to the measured pressures than the basis vector conditioning method for the Olkiluoto test case 1. This is true when using either set A1 or A2 as initial fracture transmissivities. Algorithm A takes 7

steps to produce a relative error of approximately 0.01, using the unconditioned set A1 as initial fracture transmissivities. When using the pre-conditioned set A2 as initial fracture transmissivities Algorithm A reaches a similar relative error in 5 steps. Thus, the time taken by Algorithm A to produce a given relative error will be dependent on the initial fracture transmissivities selected.

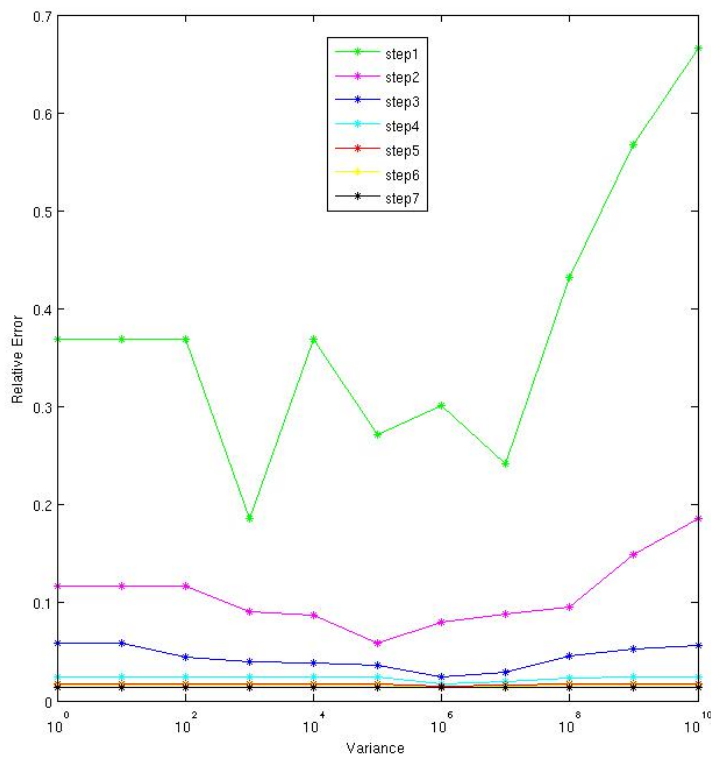


**Figure 63.** The relative error against the variance  $\sigma_p^2$  of the pressure measurements, shown for each step of Algorithm A using set A1 as initial fracture transmissivities for Olkiluoto test case 1.

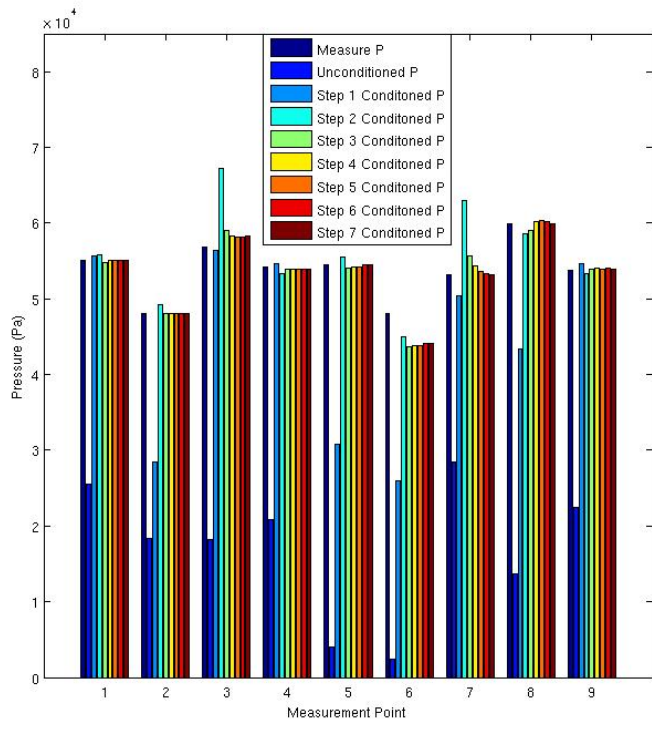


**Figure 64.** Pressure at each measurement point for each step of Algorithm A using set A1 as initial fracture transmissivities compared to the measured and unconditioned pressures for Olkiluoto test case 1.

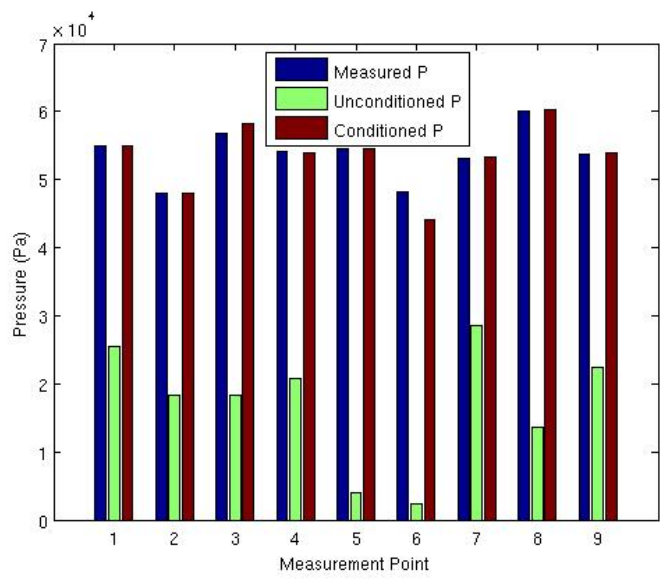


**Figure 65.** Final conditioned pressure at each measurement point from Algorithm A using set A1 as initial fracture transmissivities compared to the measured and unconditioned pressures for Olkiluoto test case 1.

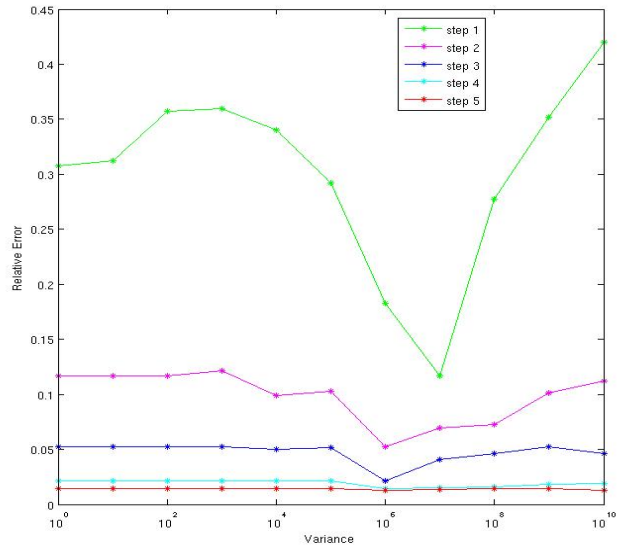


**Figure 66.** The relative error against the variance  $\sigma_p^2$  of the pressure measurements, shown for each step of Algorithm A using set A2 as initial fracture transmissivities for Olkiluoto test case 1.

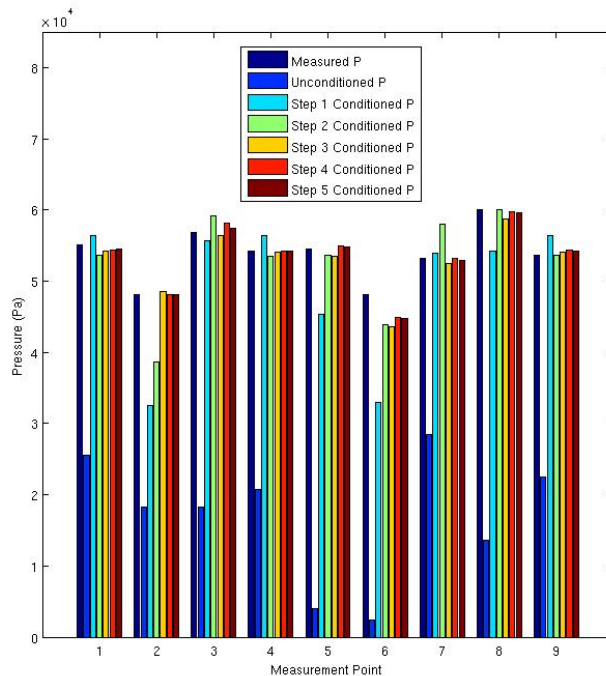


**Figure 67.** Pressure at each measurement point for each step of Algorithm A using set A2 as initial fracture transmissivities compared to the measured and unconditioned pressures for Olkiluoto test case 1.

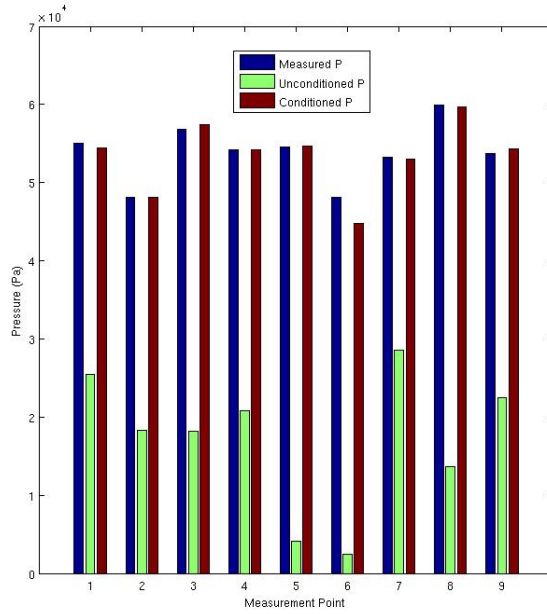


**Figure 68.** Final conditioned pressure at each measurement point from Algorithm A using set A2 as initial fracture transmissivities compared to the measured and unconditioned pressures for Olkiluoto test case 1.

Step	Absolute Error	Relative Error
Unconditioned	1.1128E+5	0.6828
1	4.1522E+4	0.1866
2	1.4791E+4	0.0587
3	5.6679E+3	0.0243
4	4.7318E+3	0.0175
5	4.5264E+3	0.0158
6	4.3127E+3	0.0141
7	4.2446E+3	0.0133

**Table 9.** Absolute error and relative error at each step of Algorithm A using set A1 as initial fracture transmissivities for Olkiluoto test case1.

Step	Absolute Error	Relative Error
Unconditioned	6.2327E+4	0.3574
1	2.4569E+4	0.1830
2	1.1798E+4	0.0525
3	5.0186E+3	0.0213
4	3.6417E+3	0.0142
5	3.5309E+3	0.0130

**Table 10.** Absolute error and relative error at each step of Algorithm A using set A2 as initial fracture transmissivities for Olkiluoto test case1.

Method	Final Absolute Error	Final Relative Error
Unconditioned	1.1128E+5	0.6828
Basis Vector	6.2327E+4	0.3574
Conditioning Method		
Algorithm A (set A1)	4.2446E+3	0.0133
Algorithm A (set A2)	3.5309E+3	0.0130

**Table 11.** Comparison of the conditioning methods used for Olkiluoto test case 1.

## 5.2.2 - CONDITIONED FRACTURE SETS

After applying Algorithm A using set A2 as initial fracture transmissivities, many of the conditioned fracture transmissivities differed from the unconditioned fracture transmissivities by several orders of magnitude, whereas some fracture transmissivities did not change by a considerable amount. There were two fractures whose conditioned transmissivities were far greater than any other fracture transmissivities in the model and it appears that these fractures provide an easy route for groundwater flow. As seen in chapter 4, there are thirteen different fracture sets in this model.

Fracture sets 1, 2, 3 and 7 are all in close proximity to the measurement points and contain fractures of short length. Conditioned fracture transmissivities in fracture sets 1 to 3 ( Figure 69 to Figure 71) showed practically no change from the unconditioned fracture transmissivities but fracture set 7 (Figure 75) contains a significant number of fracture transmissivities that are increased by approximately two orders of magnitude. The remaining fracture sets contain fractures of greater length which are spread across the domain and extend further away from the measurement points than the first four fracture sets introduced. Some of the conditioned fracture transmissivities in fracture set 4 (Figure 72) were increased by up to two orders of magnitude while the remaining fractures did not change by more than one order of magnitude. Conditioned fracture transmissivities did not differ from the unconditioned fracture transmissivities by much in fracture sets 8 to 11 (Figure 76 to Figure 79). The conditioned fracture transmissivities in fracture set 5 (Figure 73) contain a significant number of fracture transmissivities

that are increased by approximately two orders of magnitude. Fracture set 6 (Figure 74) has five conditioned fracture transmissivities that vary by approximately two orders of magnitude from the unconditioned fracture transmissivities. It also contains one very small conditioned fracture transmissivity. A similar pattern of conditioned fracture transmissivities to set 6 can be seen in fracture set 12 (Figure 80). Fracture set 13 (Figure 81) has the most noticeable change over many orders of magnitude in the conditioned fracture transmissivities compared to the unconditioned fracture transmissivities. There are two very large fracture transmissivities of order  $1.0E+0 \text{ m}^2/\text{s}$  (an aperture of approximately 2.5cm assuming the cubic law holds) and  $1.0E+1 \text{ m}^2/\text{s}$  (an aperture of approximately 1cm). However, it was found that these large transmissivity values have low sensitivities. As such, both the fracture transmissivities can be reduced to values equivalent to an aperture of 0.1cm (which is more physically reasonable) without greatly changing the fit to measured pressures. Indeed this change resulted in the absolute error increasing by only 17 and the relative error increasing by only  $2.9E-5$ . Alternatively, if these two fractures kept their large transmissivity values it may well indicate that instead of a single fracture there exists a cluster of fractures in the area with high transmissivities.

Fracture sets 4, 5, 8, 10, 12 and 13 all show a noticeable difference between the conditioned fracture transmissivities obtained using the basis vector conditioning method to those using the Bayesian conditioning method.

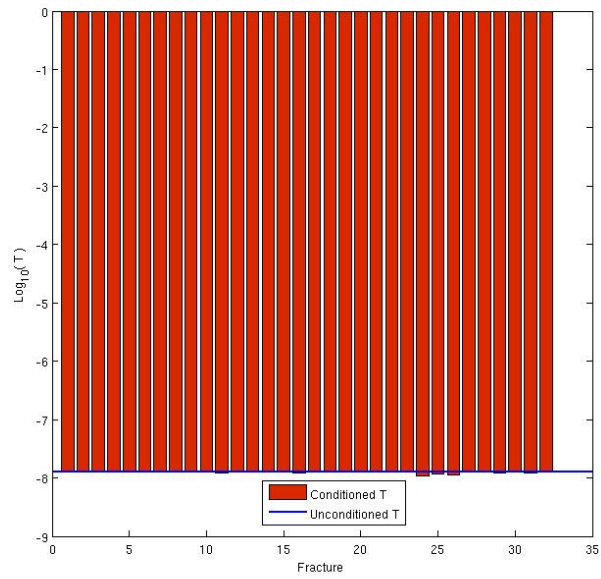


**Figure 69.** Conditioned fracture log transmissivities for fracture set 1. The unconditioned fracture log transmissivities have the value of -7.90 for all the fractures and are shown as a black line.

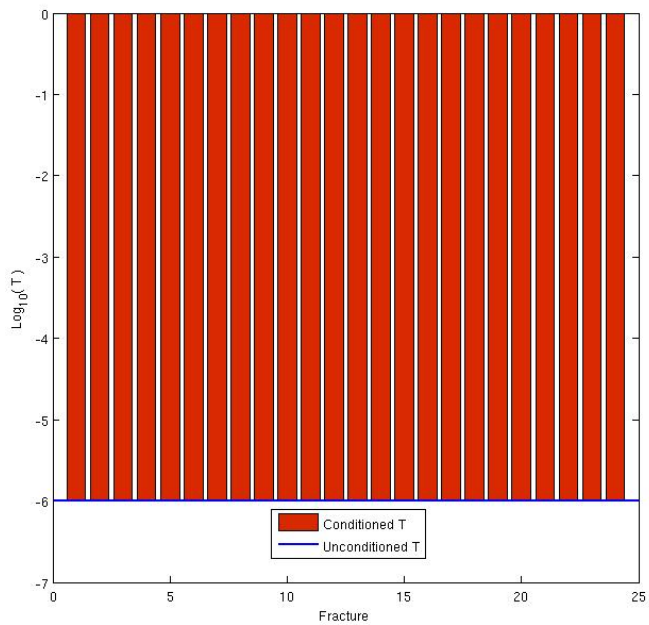


**Figure 70.** Conditioned fracture log transmissivities for fracture set 2. The unconditioned fracture log transmissivities have the value of -6.0006 for all the fractures and are shown as a black line.

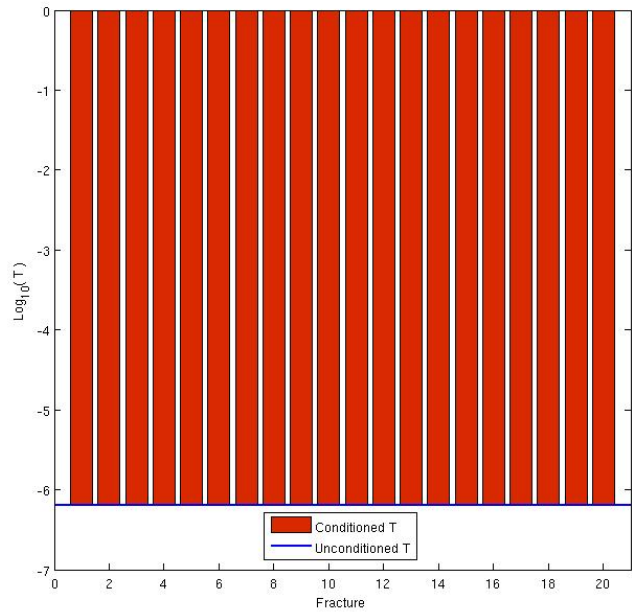


**Figure 71.** Conditioned fracture log transmissivities for fracture set 3. The unconditioned fracture log transmissivities have the value of -6.20 for all the fractures and are shown as a black line.

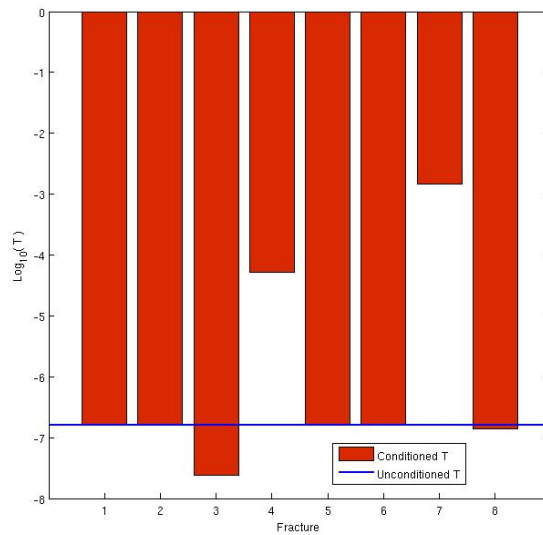


**Figure 72.** Conditioned fracture log transmissivities for fracture set 4. The unconditioned fracture log transmissivities have the value of -6.7999 for all the fractures and are shown as a black line.

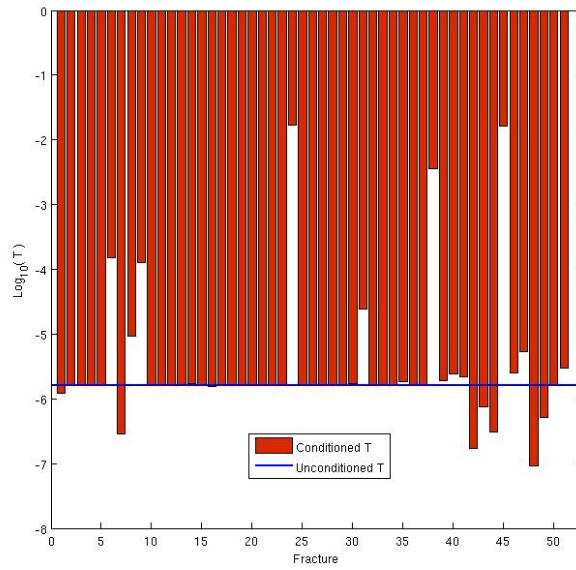


**Figure 73.** Conditioned fracture log transmissivities for fracture set 5. The unconditioned fracture log transmissivities have the value of -5.7999 for all the fractures and are shown as a black line.

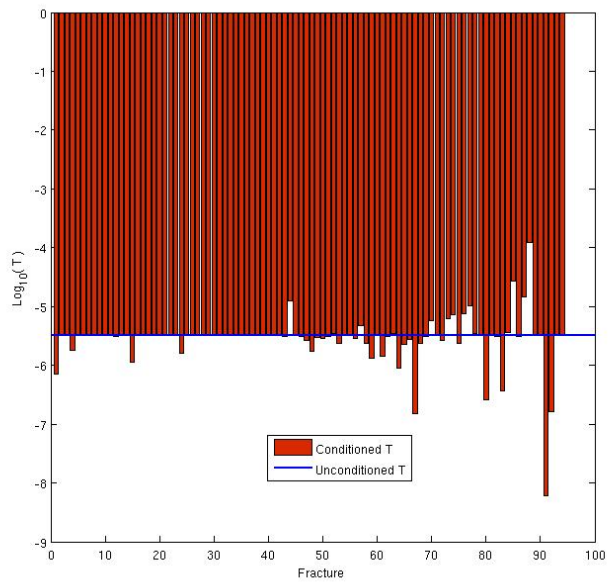


**Figure 74.** Conditioned fracture log transmissivities for fracture set 6. The unconditioned fracture log transmissivities have the value of -5.4998 for all the fractures and are shown as a black line.

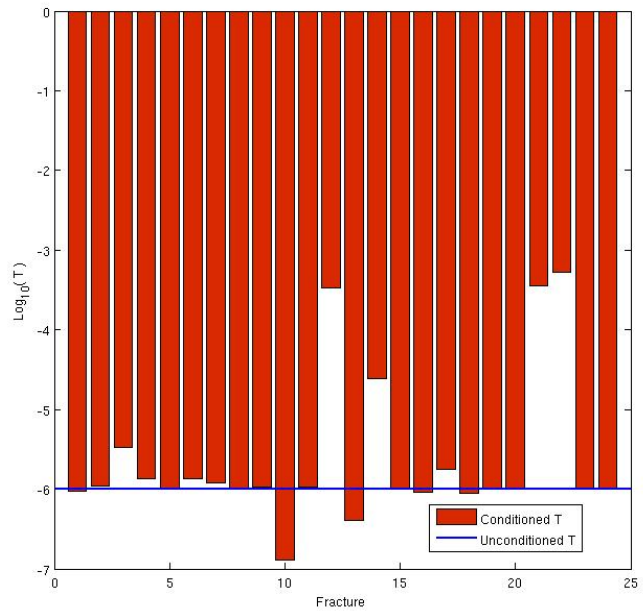


**Figure 75.** Conditioned log fracture transmissivities for fracture set 7. The unconditioned fracture log transmissivities have the value of -6.0006 for all the fractures and are shown as a black line.

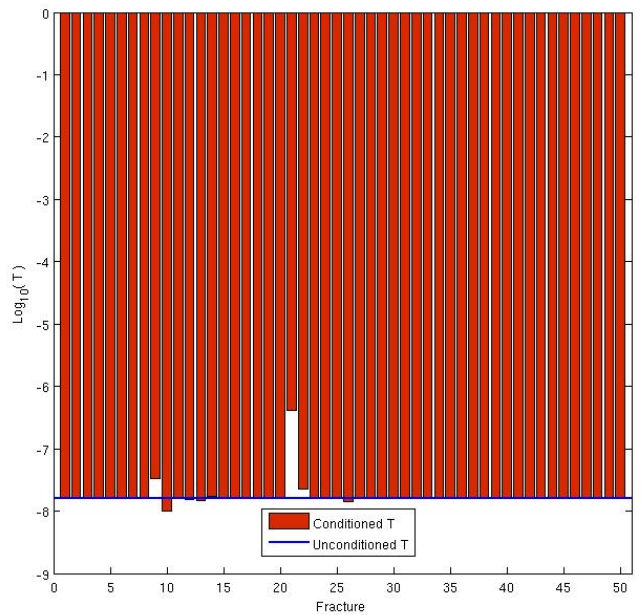


**Figure 76.** Conditioned fracture log transmissivities for fracture set 8. The unconditioned fracture log transmissivities have the value of -7.8002 for all the fractures and are shown as a black line.

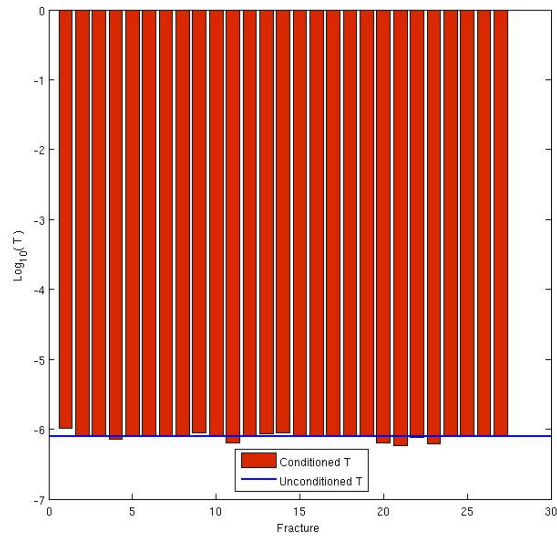
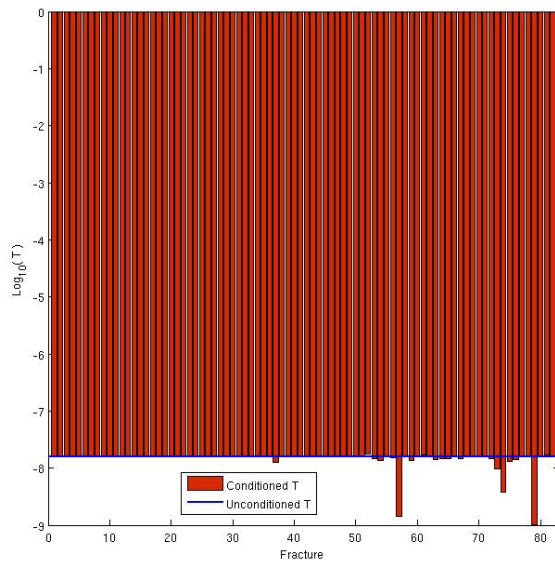
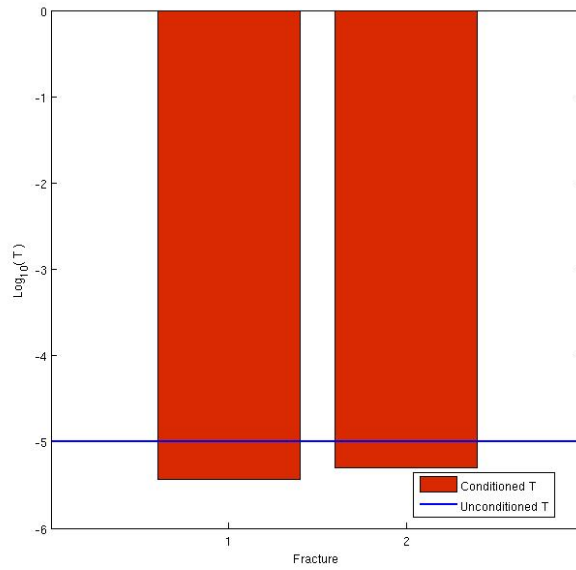


Figure 77. Conditioned fracture log transmissivities for fracture set 9. The unconditioned fracture log transmissivities have the value of -6.0999 for all the fractures and are shown as a black line.



**Figure 78.** Conditioned fracture log transmissivities for fracture set 10. The unconditioned fracture log transmissivities have the value of -7.8002 for all the fractures and are shown as a black line.



**Figure 79.** Conditioned fracture log transmissivities for fracture set 11. The unconditioned fracture log transmissivities have the value of -5.0 for all the fractures and are shown as a black line.

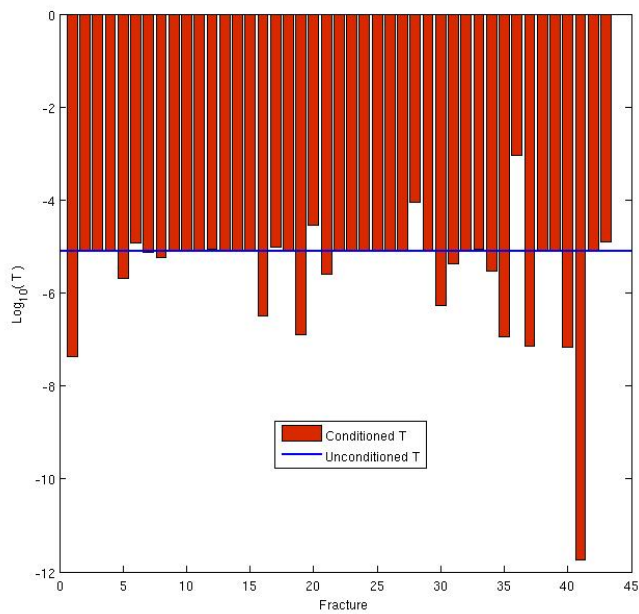


**Figure 80.** Conditioned fracture log transmissivities for fracture set 12. The unconditioned fracture log transmissivities have the value of -5.1110 for all the fractures and are shown as a black line.

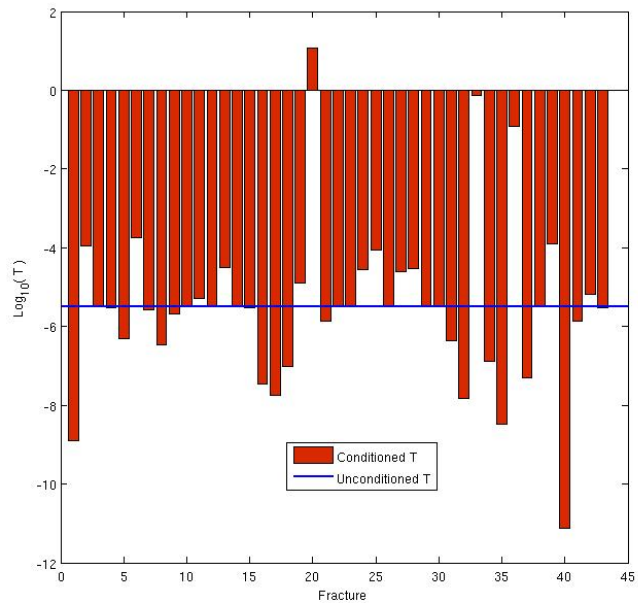


**Figure 81.** Conditioned fracture log transmissivities for fracture set 13. The unconditioned fracture log transmissivities have the value of -5.4998 for all the fractures and are shown as a black line.

### 5.3 – OLKILUOTO TEST CASE 2

This test case focuses on a smaller region of the Olkiluoto site to that modelled by Olkiluoto test case 1. The problem domain is a 300m by 300m by 500m cube approximately centred around nine boreholes located in the middle of the Olkiluoto island. This scenario was designed to analyse a series of cross-hole pump tests using the nine boreholes, where one borehole is pumped with a given flow rate and the responses of the remaining boreholes are recorded as measured pressures.

The geometry of the fracture network is semi-deterministic, containing two large scale macro fractures which are known to provide flow paths through the domain.

Additionally, there is a background fracture population consisting of many smaller fractures throughout the domain. The assertion that the macro fractures provide the main flow paths can be backed up by Figure 82; it shows that the inclusion of a background fracture population does not greatly change the match to measured pressures. It should be noted that Figure 82 shows unconditioned results. Conditioning was performed for two cases; first with only the two macro fractures and secondly with a background fracture population added to the two macro fractures.

As seen by the results of conditioning Olkiluoto test case 1, Algorithm A yielded a far smaller absolute error than the basis vector conditioning method. Algorithm A was used without pre-conditioning the initial fracture transmissivities to perform all the conditioning for Olkiluoto test case 2. Thus, there was no use of the basis vector conditioning method.

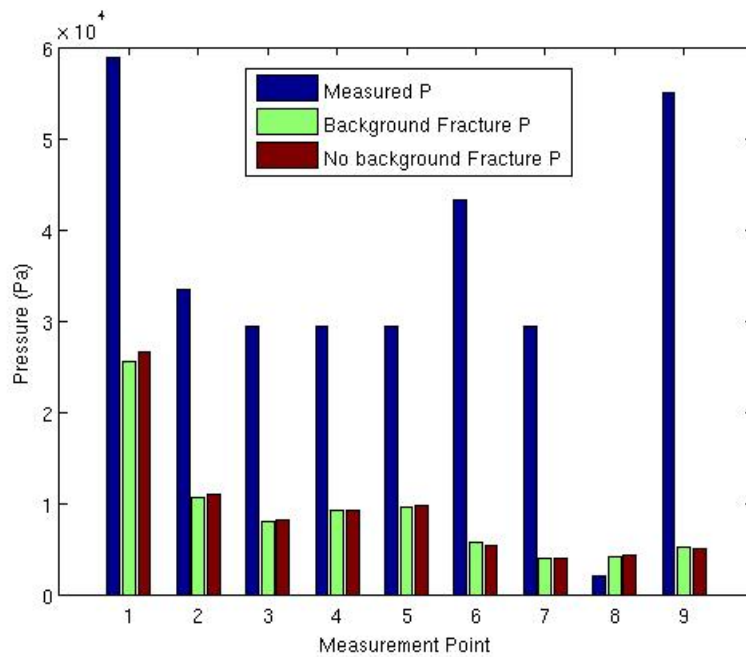


**Figure 82.** Measured pressure compared to the pressure calculated with two macro fractures including a background fracture population and the pressure calculated with only the two macro fractures in the domain at each measurement point.

### 5.3.1 OLKILUOTO TEST CASE 2a

The domain contains two large tessellated macro fractures which we call macro fracture 1 and macro fracture 2. Tessellation is the process of dividing a fracture into smaller sub-fractures and generating the transmissivity on each sub fracture independently. Both macro fractures have an area of 300m by 300m and have each been tessellated into 900 sub-fractures of area 10m by 10m. Macro fracture 1 and macro fracture 2 have mean transmissivities estimated from field experiments of  $2.2E-4 \text{ m}^2/\text{s}$  and  $1.0E-5 \text{ m}^2/\text{s}$ , respectively. The initial fracture apertures were generated from a normal distribution using corresponding aperture means to the transmissivity means. The initial transmissivities of the sub-fractures on each macro fracture were then assigned by converting the fracture apertures to fracture transmissivities using the cubic law.

The sub-fractures are assumed to be exponentially correlated. The correlation of sub-fractures on a macro fracture  $k$  is defined by the covariance matrix  $\mathbf{C}_k$ .

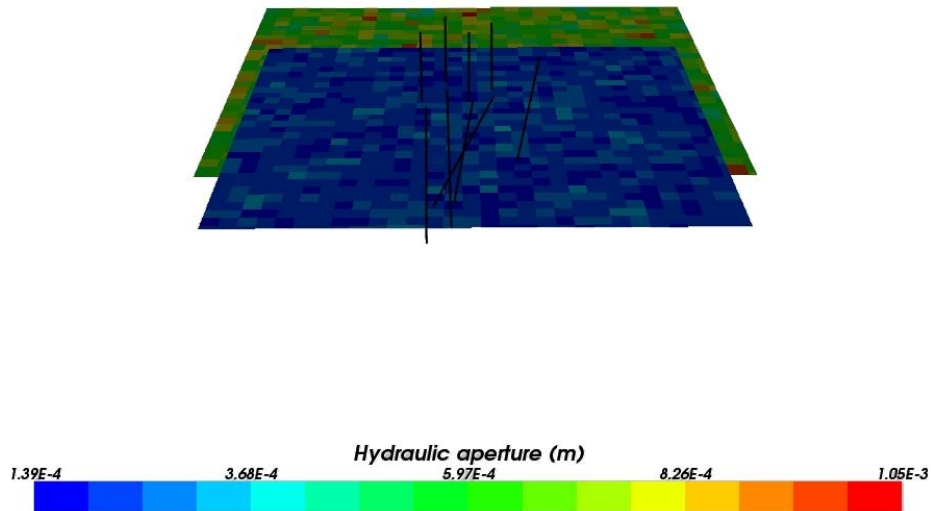
Thus, it is assumed that  $\mathbf{C}_k$  has an exponential structure. Defining the separation  $S_{ij}$  of two sub-fractures  $i$  and  $j$  as the distance between the centre of sub-fracture  $i$  and sub-fracture  $j$ , the standard deviation of sub fracture log transmissivities as  $\sigma_x$  (assumed to be constant for all sub fractures on the same macro fractures) and the correlation scale as  $\mu$ , then the covariance matrix of the sub-fracture transmissivities  $\mathbf{C}_k$  on macro fracture  $k$  is defined as

$$\mathbf{C}_k(i, j) = \begin{cases} \sigma_x^2, & \text{for } i = j, \\ \sigma_x^2 e^{-s_{ij}/\mu}, & \text{for } i \neq j. \end{cases} \quad (5.20)$$

Thus, a sub-fracture is highly correlated with sub-fractures close to its location; this correlation decays exponentially with the separation of the fractures and the rate of decay is dependent on the correlation scale.

There are zero pressure boundary conditions on all sides of the domain. One borehole is pumping, creating a borehole flow rate of  $4.1667\text{E-}4 \text{ m}^3/\text{s}$  while the remaining eight boreholes are non pumping. The domain is shown in Figure 83 with the initial values of fracture hydraulic apertures. The aperture values are used in the plot because they show the tessellation more clearly than transmissivity values.

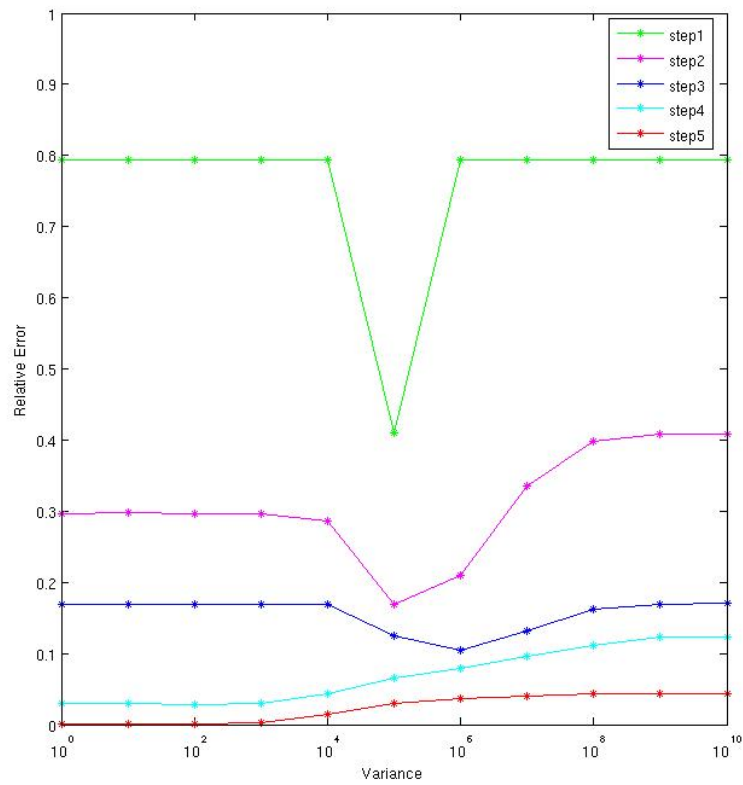
Algorithm A was used with  $\mathbf{C}$  given by (5.20) with a correlation scale  $\mu$  of 5.0 and a standard deviation of  $\sigma_x = 1/6$ . The initial values of the sub fracture log transmissivities on macro fracture 1 are shown in Figure 86 and the initial sub fracture log transmissivities on macro fracture 2 are shown in Figure 88.



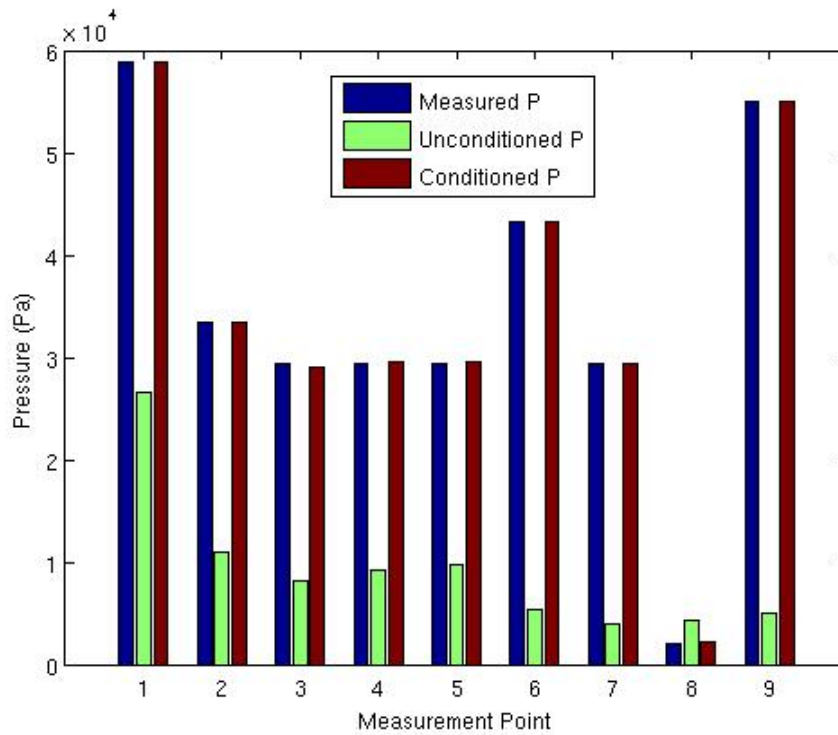
**Figure 83.** Domain of Olkiluoto test case 2a, where nine boreholes intersect two macro fractures, each of which is tessellated into 900 sub-fractures. Macro fracture 1 is mainly green coloured with macro fracture 2 mainly blue coloured.

Figure 84 plots the relative error against the variance in the pressure measurements at each of the five steps used in Algorithm A. The conditioned pressures after step 5 of Algorithm A at each of the measurement points are shown in Figure 85 and compared to the measured and unconditioned pressures. Table 12 compares the initial absolute error and relative error to their final values. The conditioned values of the sub fracture log transmissivities in macro fracture 1 are shown in Figure 87 and the conditioned values of the sub fracture log transmissivities in macro fracture 2 are shown in Figure 89. The conditioned pressures give an excellent match to the measured values. The vast majority of conditioned sub fracture transmissivities on macro fracture 1 are lower than the mean value of the unconditioned macro fracture 1 transmissivity.

However, there are some large values of conditioned fracture transmissivities located near the centre of macro fracture 1. There is less variation in the values of conditioned fracture transmissivities on macro fracture 2 and they are mostly smaller than the mean value of the unconditioned macro fracture 2.



**Figure 84.** Plot of the relative error against variance in the pressure measurements for each step of Algorithm A for Olkiluoto test case 2a.



**Figure 85.** Conditioned pressures after step 5 of Algorithm A at each measurement point compared to the measured and unconditioned pressure values for Olkiluoto test case 2a.

Initial Absolute Error	Final Absolute Error	Initial Relative Error	Final Relative Error
8.5860E+4	8.1150E+1	0.7929	0.0007

**Table 12.** Comparison of the initial absolute error and relative error to the final absolute error and relative error for Olkiluoto test case 2a.

Step	Absolute Error	Relative Error
Unconditioned	8.5860E+4	0.7929
1	3.8363E+4	0.4094
2	1.3904E+4	0.1695
3	7.9760E+3	0.1242
4	1.9890E+3	0.0429
5	8.1150E+1	0.0007

**Table 13.** Minimum absolute error and corresponding relative error at each step of Algorithm A for Olkiluoto test case 2a.

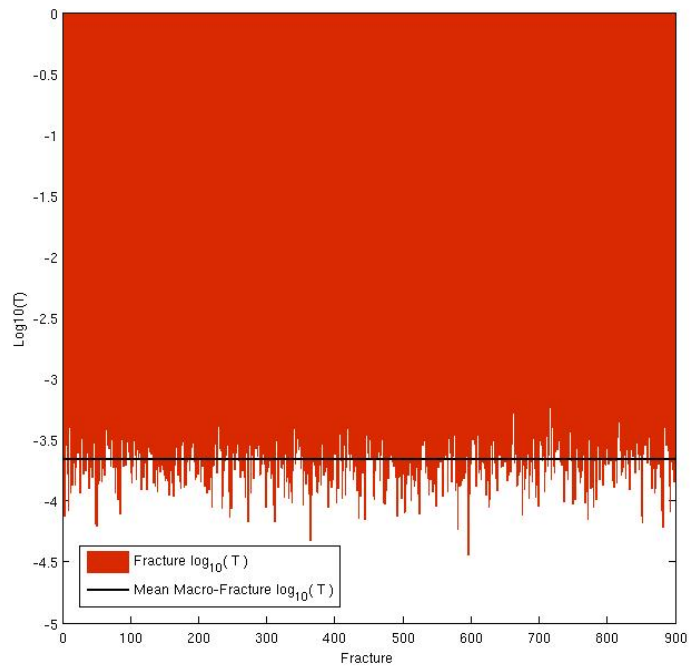


**Figure 86.** Initial sub fracture log transmissivities on macro fracture 1 compared to the mean log transmissivity of macro fracture 1 for Olkiluoto test case 2a.

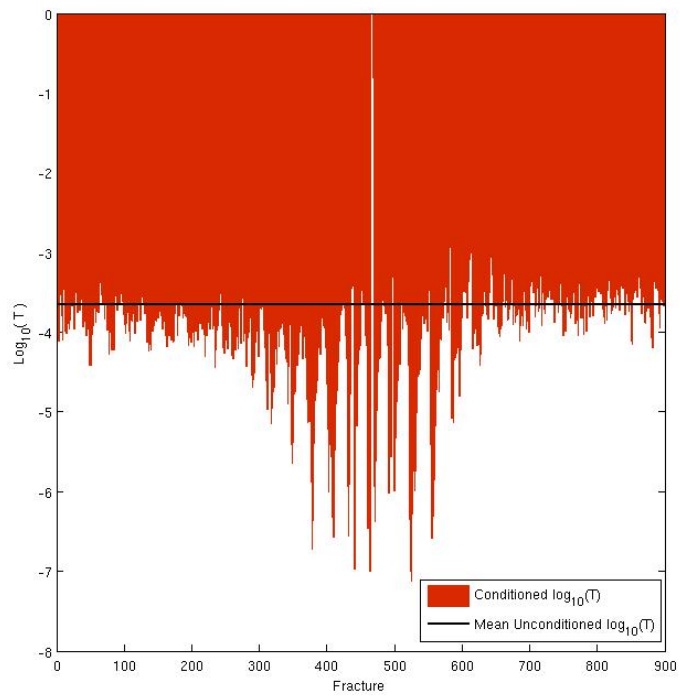


**Figure 87.** Conditioned sub fracture log transmissivities on macro fracture 1 compared to the initial mean log transmissivity of macro fracture 1 for Olkiluoto test case 2a.

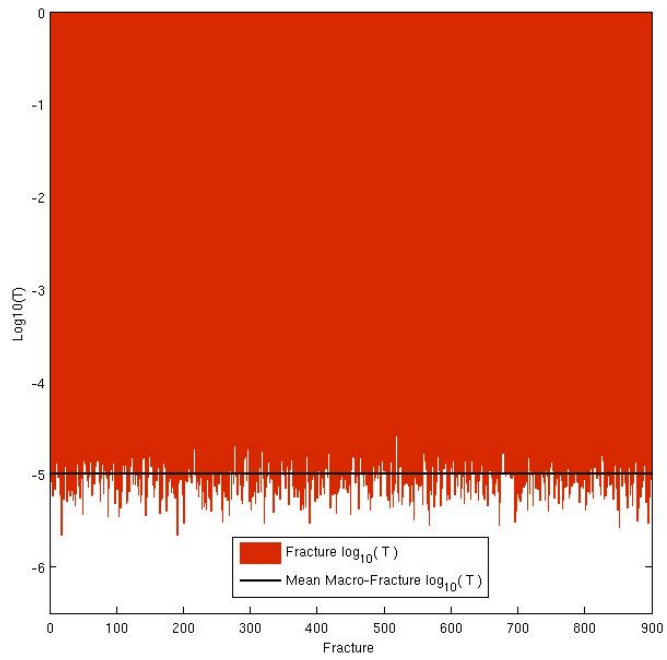


**Figure 88.** Initial sub fracture log transmissivities on macro fracture 2 compared to the mean log transmissivity of macro fracture 2 for Olkiluoto test case 2a.

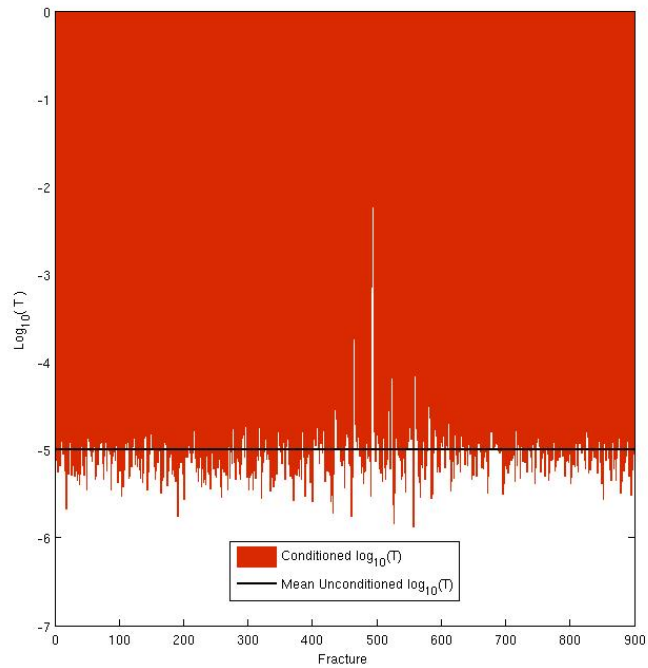


**Figure 89.** Conditioned sub fracture log transmissivities on macro fracture 2 compared to the initial mean log transmissivity of macro fracture 2 for Olkiluoto test case 2a.

### 5.3.2 – OLKILUOTO TEST CASE 2b

In addition to the two tessellated macro fractures a background fracture population was added into the model domain. The background fracture population provides additional flow paths between the two macro fractures and the boreholes contained in the model. Here, 24926 background fractures were included and defined from borehole orientation and location data. The main unknown of the background fracture population was the fracture size which was chosen so that the background fractures were large enough to make a well connected system between the macro fractures and domain boundaries. The model domain is shown in Figure 90.

A total of 26726 fractures to be conditioned meant that it was computationally too expensive to run the Bayesian conditioning algorithm fully. Instead fractures to be conditioned were selected depending on their initial sensitivity values. Fractures that had a sensitivity value of 1.0 or greater with respect to any of the measured pressures were selected for conditioning. A total of 2205 fracture transmissivities (with the greatest sensitivity values) were conditioned while leaving the remaining fracture transmissivities constant at their initial value throughout the conditioning procedure. In other words, only selected fracture transmissivities were conditioned, but pressure values were re-calculated using all of the fracture transmissivities in the network (including those held constant). Furthermore, due to the computational time taken to perform the conditioning of the fracture transmissivities the values of  $\sigma_p^2$  in each step of Algorithm A were

limited to 1.0E+3, 1.0E+4, 1.0E+5 and 1.0E+6. This selection was based on results from the previous test cases where no value of  $\sigma_p^2$  greater than 1.0E+6 minimised the absolute error at any step of Algorithm A.

Additionally, values of  $\sigma_p^2$  less than 1.0E+3 did not minimise the absolute error for the first few steps in previous test cases.

Figure 91 plots the relative error against the variance in the pressure measurements for each step of Algorithm A. In the first two steps the majority of relative error values are greater than the initial relative error. This is due to the small measured pressure value at measurement point 8. In the first two steps the conditioned pressure at this measurement point was greater than the measured value by two or three times. This naturally leads to a large relative error value. The absolute error is plotted against the variance in the pressure measurement for each step of Algorithm A in Figure 92. The measured pressure at measurement point 8 does not affect the absolute error to the same extent as the relative error and it can be seen that the absolute error is reduced with every step of algorithm A. The final conditioned pressures are compared at each measurement point to the measured and unconditioned pressures in Figure 93. It can be seen that the conditioned pressures give an excellent match to the measured pressures at all measurement points. Table 14 compares the initial absolute error and relative error to their final values and Table 15 shows the minimum absolute error and relative error at each step of Algorithm A.

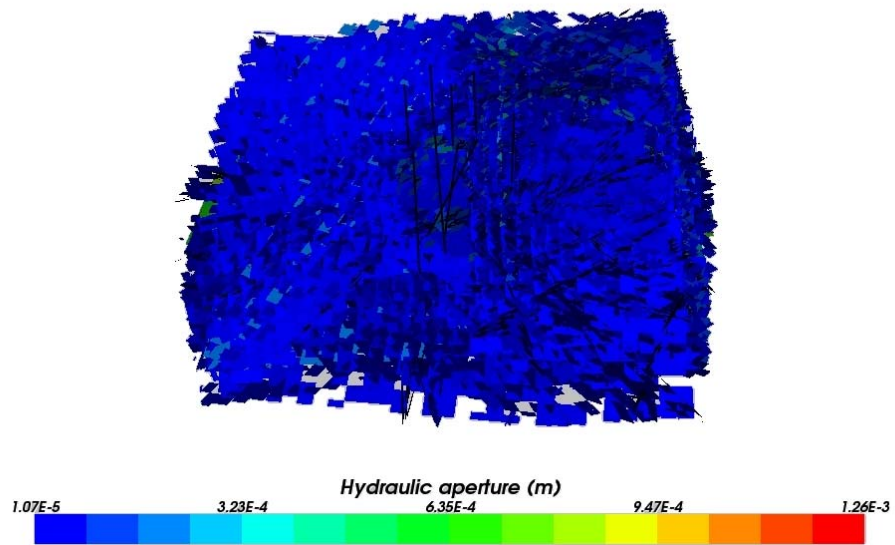


**Figure 90.** Domain of Olkiluoto test case 2b with two macro fractures with a background fracture population.

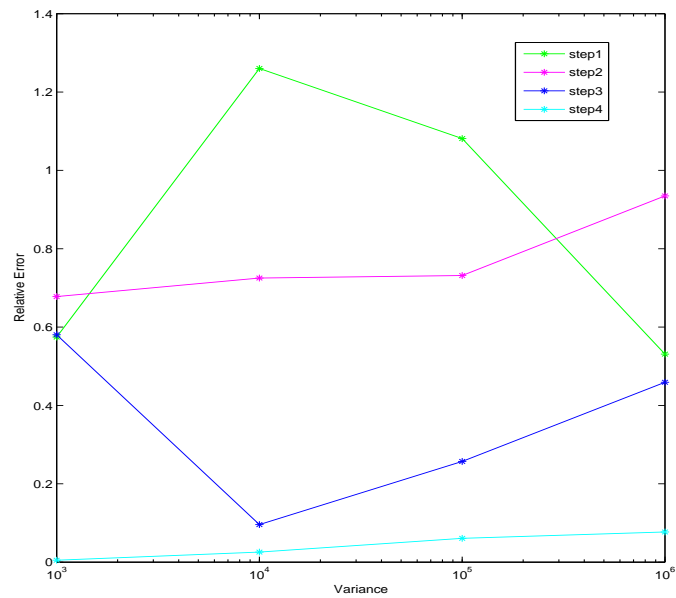


**Figure 91.** Plot of the relative error against variance in the pressure measurements for each step of Algorithm A for Olkiluoto test case 2b.

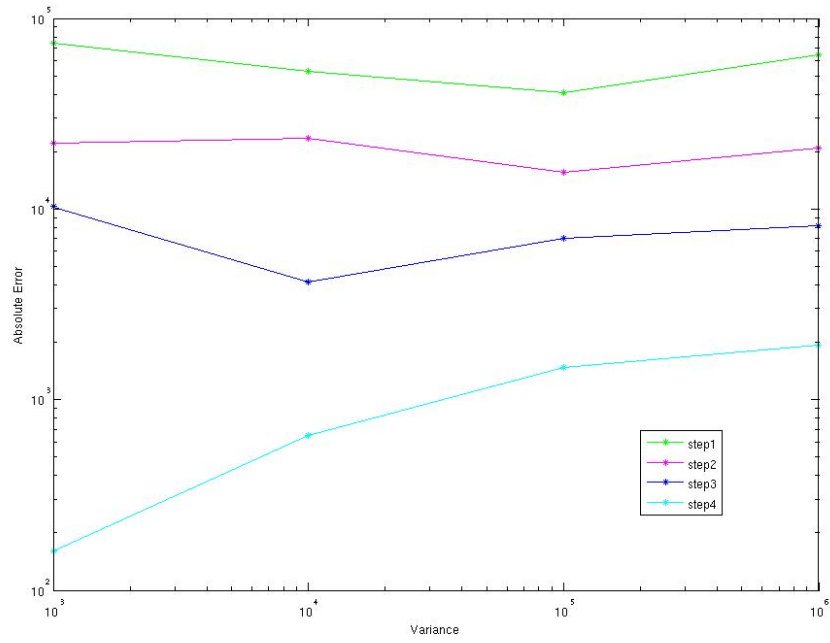


**Figure 92.** Plot of the absolute error against variance in the pressure measurements for each step of Algorithm A for Olkiluoto test case 2b.

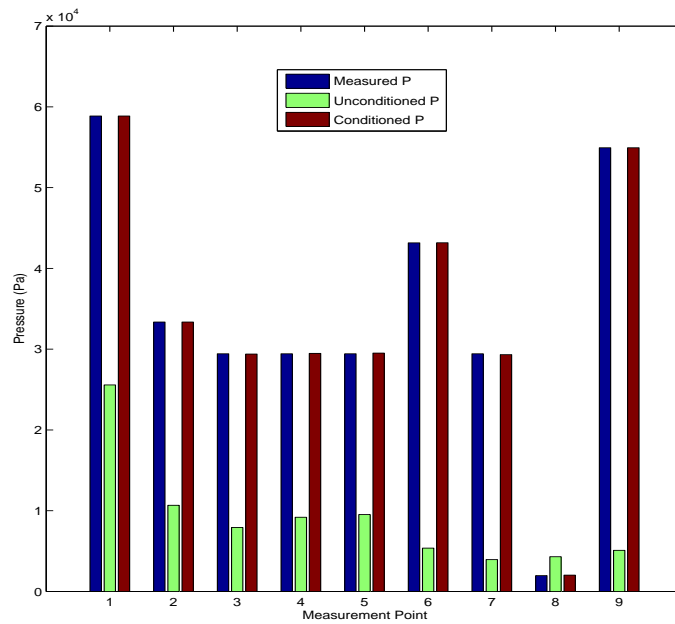


**Figure 93.** Conditioned pressures after step 4 of Algorithm A at each measurement point compared to the measured and unconditioned pressure values for Olkiluoto test case 2b.

Initial Absolute Error	Final Absolute Error	Initial Relative Error	Final Relative Error
8.9737E+4	1.6182E+2	0.7984	0.0048

**Table 14.** Comparison of the initial absolute error and relative error to the final absolute error and relative error for Olkiluoto test case 2b.

Step	Absolute Error	Relative Error
Unconditioned	8.9737E+4	0.7984
1	4.0773E+4	1.0812
2	1.5625E+4	0.7318
3	4.1325E+3	0.0960
4	1.6182E+2	0.0048

**Table 15.** Minimum absolute error and corresponding relative error at each step of Algorithm A for Olkiluoto test case 2b.

## 5.4 - CHAPTER SUMMARY AND CONCLUSIONS

A Bayesian method for conditioning fracture transmissivities on measured pressures was developed. This algorithm was used to condition 501 fracture transmissivities on 9 pressure measurements for the Olkiluoto test case 1; here it was assumed that the fracture transmissivities were uncorrelated. When using the Bayesian conditioning method it was found that the final absolute error obtained after conditioning was dependent on the variance  $\sigma_p^2$  of the error in the measured pressures. The absolute error was at a minimum for a value of  $\sigma_p^2 = 1.0E+3$  with a value of 4.1522E+4 while the final relative error was 0.1866. In comparison, the

basis vector conditioning method gave a final absolute error of 6.2327E+4 and a final relative error of 0.3574.

A numerical algorithm (Algorithm A) was developed in an effort to further reduce the final absolute error obtained by the Bayesian conditioning method. Algorithm A is not a Bayesian method as the prior values of fracture transmissivities are changed with each step. A set of initial fracture transmissivities were selected and conditioned using the Bayesian conditioning method with different  $\sigma_p^2$  values; each  $\sigma_p^2$  value used produced a different final absolute error. The transmissivity set that yielded the smallest final absolute error was further conditioned in the next step of Algorithm A. Two different initial fracture transmissivity sets were used. Firstly, an unconditioned set was used (set A1) and secondly a set pre-conditioned using the basis vector conditioning method was used (set A2). Algorithm A was run separately using both initial fracture transmissivity sets. Algorithm A gave a good match to the measured pressures using both initial fracture transmissivity sets, giving final relative errors of 0.0133 and 0.0130, for set A1 and set A2, respectively. These final relative errors are more than 26 times smaller than the final relative error obtained from the basis vector conditioning method and 51 times smaller than the relative error corresponding to the unconditioned fracture transmissivity values.

When Algorithm A was employed the conditioned fracture transmissivities varied over many orders of magnitude. Some of the fracture sets showed hardly any change in the conditioned fracture transmissivities compared to the unconditioned fracture transmissivities, while some of the conditioned fracture transmissivities were changed by up to six orders of magnitude compared to the unconditioned values.

A new test case called Olkiluoto test case 2 was introduced and is a DFN model containing two large tessellated macro fractures intersected by nine boreholes (one of which was pumping) with a background fracture population. This was separated into two test cases; Olkiluoto test case 2a and Olkiluoto test case 2b. Olkiluoto test case 2a contained two macro fractures tessellated into 1800 sub-fractures which were conditioned on 9 pressure measurements. Olkiluoto test case 2b had the same set up as Olkiluoto test case 2a but with the addition of 24926 background fractures. Algorithm A was chosen to condition these test cases using unconditioned initial fracture transmissivities because it produced good results when used with Olkiluoto test case 1 and moreover does not require the application of the basis vector conditioning method.

The conditioned pressures for Olkiluoto test case 2a gave excellent agreement to the measured pressures with a final relative error of 0.0007. The majority of the conditioned sub fracture transmissivities were smaller than the mean transmissivities of the macro fractures but there were still a group of sub fractures with large values of conditioned fracture transmissivities.

Adding a background fracture population to the two macro fractures greatly increased the computational time needed for conditioning Olkiluoto test case 2b. As such, the fractures to be conditioned were filtered by their initial sensitivity values. Fracture transmissivities with sensitivity greater than 1.0 with respect to any pressure measurement were conditioned and the remaining fracture transmissivities were held constant at their initial value throughout the conditioning algorithm. The conditioned pressures gave an excellent agreement to the measured pressures at all measurement points with a final relative error of 0.0048 after 4 steps of Algorithm A.

## 6 – SUMMARY AND CONCLUSIONS

The aim of this thesis was to develop numerical methods that condition fracture transmissivities on measured pressure values in a DFN. The first method developed, referred to as the basis vector conditioning method, conditioned fracture transmissivities on measured pressure values by adopting a linear approximation when fracture transmissivities were mildly heterogeneous; the generalisation of this approach to the minimisation of an objective function when fracture transmissivities were highly heterogeneous was also considered. This method represents an extension of the ideas employed for the conditioning of transmissivities or hydraulic conductivities in a CPM.

The linear approximation exploited certain basis vectors; each basis vector represents the change to the log transmissivity of the fractures in the network that results in a unit increase in the pressure at one measurement point, whilst keeping the pressure at the remaining measurement points constant. These basis vectors were calculated using sensitivity values of each of the measured pressures with respect to each of the fracture transmissivities in the model. To this end, an adjoint method was developed to calculate the desired sensitivities.

In the case of a highly heterogeneous system the same linear approximation was exploited whilst minimising an objective function using the Levenberg-Marquardt method. Thus, fracture transmissivities were updated and the objective function minimised in an iterative manner.

The basis vector method was first used to condition some small scale test cases with few fractures and simple geometry. The conclusions taken from testing on these simple test cases were that the sensitivities should be updated with each iteration of the minimisation procedure in order to improve the robustness of the basis vector conditioning method. It was apparent that the convergence of the method was dependent on the geometry of the fractures and the boundary conditions employed. Furthermore, the basis vector conditioning method was used on a test case based on data from a potential site for radioactive waste disposal at Olkiluoto, Finland; this fracture network model consisted of 501 fractures with 9 measured pressure values (Olkiluoto test case 1). The fractures were divided into 13 separate fracture sets; each set had its own mean value of fracture transmissivity which all fractures in that set were assigned.

The fracture transmissivities were conditioned on nine measured pressures from field data. The conditioning gave a considerable improvement to the calculated pressure at every measurement point but failed to agree exactly with the measured pressure values. The initial relative error between measured and conditioned pressures was 0.6828 and the final relative error after conditioning was 0.3574.

The sensitivity values computed showed that certain fracture sets had more influence on the pressures computed at measurement points. Indeed, the fracture transmissivities varied over many orders of magnitude in these fracture sets and differed greatly from the unconditioned values.

To test the robustness of the method, “artificial” pressure values, obtained from generated sets of fracture transmissivities, were used to condition the

initial fracture transmissivities; the geometry of the fractures was not changed. Four different cases were studied, each with different target fracture transmissivities. The resulting pressures for the four cases were used as “artificial” measured pressures that were conditioned on. The conditioning method gave an exact agreement with the “artificial” measured pressures for three of the cases where the variance of the fracture transmissivities was small. It gave a close but not exact agreement in the fourth case, where the fracture transmissivity distribution had a larger variance.

Based on results from chapter 4, the basis vector conditioning method showed good convergence properties when the measured pressures were close to the unconditioned pressures. However, when the measured pressures differ greatly from the unconditioned pressures the method struggles to match the measured pressures.

There were many potential reasons why the conditioned pressures in the Olkiluoto test case 1 did not exactly match the measured pressures. The lack of a match to measured pressure was either as a result of an inaccurate conceptual model or due to convergence problems with the basis vector conditioning method. Some assumptions in the conceptual model that could give rise to inaccurate calculated pressures were discussed in chapter 4. However, it was decided to concentrate on the numerical side of the problem in an attempt to get a better match to measured pressures. A homotopy method was used with the basis vector conditioning method but failed to improve the match to measured pressures. This lack of agreement motivated the development of a new Bayesian conditioning method.

The Bayesian conditioning method exploited Bayes' theorem to give an expression of proportionality for the posterior distribution of fracture log transmissivities in terms of the prior distribution of fracture log transmissivities and the data available through pressure measurements. The fracture transmissivities were assumed to be normally distributed with a given covariance and the measured pressures were assumed to be normally distributed values each with a given error.

From the expression of proportionality for the posterior distribution of fracture transmissivities, it was possible to find a mode of the posterior distribution; that is the most likely set of fracture transmissivities that would produce the measured pressure values. A mode of the posterior distribution can be found numerically using Newton's method. The Bayesian method allowed the input of a fracture transmissivity covariance matrix and a covariance matrix for the errors in the pressure measurements. It was assumed that the fracture transmissivities were uncorrelated and errors in the measured pressures were independent. With this assumption, it was found that the absolute error (describing the match between measured and conditioned pressures) was dependent on the variance in the pressure measurements.

The variance of the pressure measurements was changed for separate runs to investigate its effect. It was found that certain values gave a better match to the measured pressures than the basis vector conditioning method; these variance values were always less than the order of magnitude of the measured pressures. In order to improve this match further a numerical algorithm (Algorithm A) was devised. A set of initial fracture

transmissivities were selected and conditioned using the Bayesian conditioning method with different variance values in the pressure measurements. The variance which yielded the best match to the measured pressure gave an output set of fracture transmissivities and these were used as the input in the next step where again different variance values of the pressure measurements were employed. Algorithm A was run separately using two different sets of initial fracture transmissivities for Olkiluoto test case 1. Set A1 contained unconditioned fracture transmissivities while set A2 contained fracture transmissivities that were pre-conditioned using the basis vector conditioning method.

Algorithm A gave an excellent match to the measured pressure values using both set A1 and A2 for Olkiluoto test case 1. The relative error between measured and conditioned pressures was 0.3574 for the basis vector conditioning method while the relative errors from Algorithm A was 0.0133 and 0.0130, for set A1 and set A2, respectively.

The conditioned fracture log transmissivities output from Algorithm A using initial fracture transmissivity set A2 were studied. Some of the conditioned fracture transmissivities were increased by many orders of magnitude. Indeed it was found that the fracture sets that exhibited the greatest change in conditioned and unconditioned fracture transmissivities were the same sets that exhibited the greatest change in the basis vector conditioning method. Some of the fracture transmissivities that were significantly changed in these sets had the same conditioned value regardless of the conditioning method used. However, a lot of fracture transmissivities that were not considerably changed in the basis vector conditioning method had

their values changed by several orders of magnitude using the Bayesian method.

Algorithm B was used to condition fracture transmissivities in a further test case called Olkiluoto test case 2. Algorithm B was chosen because it gave good results when tested on Olkiluoto test case 1 and it has no reliance on the basis vector conditioning method. Olkiluoto test case 2 comprised of two large macro fractures intersected by nine boreholes (one of which was pumping) with a background fracture population. This was split into Olkiluoto test case 2a and Olkiluoto test case 2b. Olkiluoto test case 2a contained the two macro fractures each tessellated into 900 sub fractures. Thus, there were 1800 sub fractures to condition on the 9 pressure measurements. Olkiluoto test case 2b had the same setup as Olkiluoto test case 2a but with the addition of 24926 background fractures.

The conditioned pressures for Olkiluoto test case 2a gave excellent agreement to the measured pressures reducing the initial relative error from 0.7929 to a final value of 0.0005. A similarly excellent match to measured pressures was obtained for Olkiluoto test case 2b. The initial relative error of 0.7984 was reduced to 0.0048 after 4 steps of Algorithm A.

Despite giving an improvement in the match to measured pressures, the basis vector method was not as successful as Algorithm A in conditioning fracture transmissivities on measured pressures in a physically relevant case. However, it did provide a useful insight to the Olkiluoto test case 1. The sensitivity analysis and plots of conditioned fracture transmissivities showed the fracture sets and individual fractures that were influential to the

measured pressures. As well as this, the adjoint method was used to calculate sensitivities in the Bayesian method.

The use of Algorithm A with the Bayesian method proved to work well when an estimate of the fracture transmissivities was given and the variance in the pressure measurements was assumed unknown.

The lack of available conditioning methods applied to DFNs means that there is opportunity for future work in this subject area. Based on results shown in this thesis a Bayesian conditioning approach would be recommended. The Bayesian method could be modified to condition on fracture flow measurements and possibly a combination of flow and pressure measurements. This would increase the number of test sites that the method is applicable to. Currently, the Bayesian method does not allow known fracture transmissivities to be included in the conditioning process. Thus, the Bayesian method could be modified so that selected fracture transmissivities are held constant throughout the conditioning process. Furthermore, in the Bayesian algorithms used, each value for the variance in the pressure measurements represents a separate run of the Bayesian conditioning method. It would be useful for each of these separate runs to be combined so that each Bayesian conditioning algorithm represents a single run.

Both conditioning methods take a fracture network with a fixed geometry as input. The fracture network could be a deterministic model or it could be a single realisation from a stochastic model where the geometry is fixed for each realisation. A natural extension to this work is to modify the conditioning methods so they can be used in a stochastic approach with multiple realisations. Each individual realisation would be conditioned and

an acceptance criterion would decide whether to keep or discard a given realisation based on the match to measured pressures after conditioning. It is common during well tests to monitor the change of pressure with time. A useful extension to the conditioning methods would be to modify them so that they can condition on the transient case, where measurements are pressure variations with time at measurement wells. The approach of the conditioning methods would not be changed but sensitivities would have to be calculated based on the transient groundwater flow equation. Additionally, a new objective function would have to be selected that takes into account the difference between measured and calculated pressures over time at measurement wells. Furthermore, when conditioning transient pumping tests it is necessary to model groundwater as a compressible fluid. Thus, a constitutive equation between the groundwater pressure and density would need to be selected and incorporated into the transient groundwater flow equation.

# APPENDIX A: MODIFICATION OF THE SENSITIVITIES TO HANDLE MULTIPLE BOREHOLE INTERSECTIONS

In order to deal with multiple borehole intersections it is necessary to add borehole flow equations to the original FE equations (2.59). These borehole equations model groundwater flow in the boreholes contained in the DFN. Fractures are represented by nodes from a FE approximation, as explained in chapter 2. When considering the effect of multiple borehole intersections the global nodes are divided into three groups as opposed to two groups as in chapter 2. The groups are:

*D* - global nodes at which there is a Dirichlet boundary condition for the pressure.

*A* - global nodes corresponding to intersections with a borehole.

*E* - the remaining nodes.

Corresponding to each global node in *A* is a borehole node, and we define the set of borehole nodes as *B*. The borehole nodes are ordered down the borehole with water being abstracted at or above the uppermost borehole node. The flow equations originally defined in (2.59) can be written as

$$\begin{pmatrix} \mathbf{A}_{EE} & \mathbf{A}_{ED} & \mathbf{A}_{EA} \\ \mathbf{A}_{DE} & \mathbf{A}_{DD} & \mathbf{A}_{DA} \\ \mathbf{A}_{AE} & \mathbf{A}_{AD} & \mathbf{A}_{AA} \end{pmatrix} \begin{pmatrix} \mathbf{P}_E \\ \mathbf{P}_D \\ \mathbf{P}_A \end{pmatrix} = \begin{pmatrix} \mathbf{Q}_E \\ \mathbf{Q}_D \\ \mathbf{Q}_A \end{pmatrix}, \quad (\text{A.1})$$

with Dirichlet boundary conditions

$$\mathbf{P}_D = \mathbf{P}_{D0}, \quad (\text{A.2})$$

Using the notation introduced in chapter 2.

The borehole equation defined in (2.58) can be written as

$$\mathbf{Q}_A = \mathbf{S}(\mathbf{P}_B - \mathbf{P}_A), \quad (\text{A.3})$$

where  $\mathbf{S}$  is a diagonal matrix with entries equal to  $-\gamma T_f$  of the fracture  $f$  corresponding to the node. On a given borehole, the borehole flow equations are expressed as

$$\begin{aligned} Q_{A1} + (P_{B2} - P_{B1})K_{21} &= Q, \\ Q_{A2} + (P_{B2} - P_{B1})K_{21} + (P_{B3} - P_{B2})K_{32} &= 0, \\ \dots\dots\dots \\ Q_{A(n-1)} + (P_{Bn} - P_{B(n-1)})K_{n(n-1)} &= 0, \end{aligned} \quad (\text{A.4})$$

where  $n$  denotes the number of borehole intersections,  $Q$  is the pumping rate of the borehole,  $Q_i$  is the flow into borehole intersection node  $i$ ,  $K_{i(i-1)}$  is the borehole hydraulic conductivity between nodes  $i$  and  $i-1$ . The borehole flow equations (A.4) apply Darcy's law to the different sections of the borehole that are intersected by fractures. Figure 94 shows an example of a borehole intersected by 3 fractures. In this case, Darcys law is applied to

the two sections of the borehole with hydraulic conductivity  $K_{21}$  and  $K_{23}$ .

The borehole flow equations (A.4) can alternatively be written in matrix form as

$$\begin{pmatrix} Q_{A1} \\ Q_{A2} \\ \dots \\ \dots \\ Q_{An} \end{pmatrix} + \begin{pmatrix} -K_{21} & K_{21} & 0 & \dots & \dots & 0 \\ -K_{21} & K_{21} - K_{32} & K_{32} & & & \\ 0 & \dots & \dots & \dots & & \\ \dots & & & \dots & \dots & \\ \dots & & & & & 0 \\ 0 & \dots & \dots & 0 & -K_{n(n-1)} & K_{n(n-1)} \end{pmatrix} \begin{pmatrix} P_{B1} \\ P_{B2} \\ \dots \\ \dots \\ P_{Bn} \end{pmatrix} = \begin{pmatrix} Q \\ 0 \\ 0 \\ \dots \\ \dots \\ 0 \end{pmatrix}, \quad (\text{A.5})$$

or say

$$\mathbf{Q}_A + \mathbf{K}\mathbf{P}_B = \mathbf{Q}e_1, \quad (\text{A.6})$$

where  $\mathbf{K}$  is a tridiagonal matrix taking the form shown in (A.5) and  $e_1$  is a  $n$  vector with 1 in the first entry and zeros elsewhere.

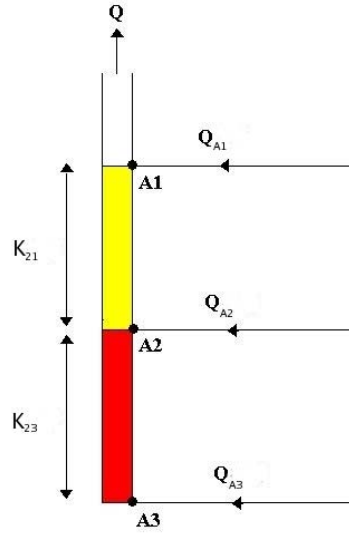


**Figure 94.** Example of the borehole model for 3 fractures intersecting a borehole.

The borehole flow equations (A.6) can be used to eliminate  $Q_A$  from the fracture flow equations (A.1) to give

$$\begin{aligned} \mathbf{A}_{AE}\mathbf{P}_E + \mathbf{A}_{AD}\mathbf{P}_D + \mathbf{A}_{AA}\mathbf{P}_A &= \mathbf{Q}_A = -\mathbf{K}\mathbf{P}_B + \mathbf{Q}e_1, \\ \Rightarrow \mathbf{A}_{AE}\mathbf{P}_E + \mathbf{A}_{AD}\mathbf{P}_D + \mathbf{A}_{AA}\mathbf{P}_A + \mathbf{K}\mathbf{P}_B &= \mathbf{Q}e_1. \end{aligned} \quad (\text{A.7})$$

The borehole equation (A.3) is also used to eliminate  $Q_A$  from the fracture flow equations (A.1)

$$\begin{aligned} \mathbf{A}_{AE}\mathbf{P}_E + \mathbf{A}_{AD}\mathbf{P}_D + \mathbf{A}_{AA}\mathbf{P}_A &= \mathbf{Q}_A = \mathbf{S}(\mathbf{P}_B - \mathbf{P}_A), \\ \mathbf{A}_{AE}\mathbf{P}_E + \mathbf{A}_{AD}\mathbf{P}_D + (\mathbf{A}_{AA} - \mathbf{S})\mathbf{P}_A + \mathbf{S}\mathbf{P}_B &= \mathbf{0}. \end{aligned} \quad (\text{A.8})$$

Equations (A.7) and (A.8) lead to equations in the form

$$\begin{pmatrix} \mathbf{A}_{EE} & \mathbf{A}_{ED} & \mathbf{A}_{EA} & \mathbf{0} & \mathbf{0} \\ \mathbf{A}_{DE} & \mathbf{A}_{DD} & \mathbf{A}_{DA} & -\mathbf{I} & \mathbf{0} \\ \mathbf{A}_{AE} & \mathbf{A}_{AD} & \mathbf{A}_{AA} + \mathbf{S} & \mathbf{0} & -\mathbf{S} \\ \mathbf{0} & \mathbf{I} & \mathbf{0} & \mathbf{0} & \mathbf{0} \\ \mathbf{A}_{AE} & \mathbf{A}_{AD} & \mathbf{A}_{AA} & \mathbf{0} & \mathbf{K} \end{pmatrix} \begin{pmatrix} \mathbf{P}_E \\ \mathbf{P}_D \\ \mathbf{P}_A \\ \mathbf{Q}_D \\ \mathbf{P}_B \end{pmatrix} = \begin{pmatrix} \mathbf{Q}_E \\ \mathbf{0} \\ \mathbf{0} \\ \mathbf{P}_{D0} \\ \mathbf{Qe}_1 \end{pmatrix}. \quad (\text{A.9})$$

The matrix system (A.9) can be written in the form

$$\mathbf{F} = \mathbf{MP} - \mathbf{R} = \mathbf{0}. \quad (\text{A.10})$$

Using the adjoint method, the sensitivity can be expressed as

$$\frac{\partial \mathbf{G}}{\partial \mathbf{X}_f} = (\boldsymbol{\theta}^T) \frac{\partial \mathbf{F}}{\partial \mathbf{X}_f} + \frac{\partial \mathbf{G}}{\partial \mathbf{X}_f}, \quad (\text{A.11})$$

where the adjoint satisfies

$$\boldsymbol{\theta}^T \frac{\partial \mathbf{F}}{\partial \mathbf{P}} = -\mathbf{e}_{B1}, \quad (\text{A.12})$$

where  $\mathbf{e}_{B1}$  is a vector with 1 in the entry corresponding to  $P_{B1}$  and 0

elsewhere.

The matrix  $\mathbf{M}$  is the only matrix in (A.10) that is dependent on  $\mathbf{X}$ . The  $\mathbf{A}$  matrices and the matrix  $\mathbf{S}$  shown in (A.9) are linearly dependent on the transmissivity of a fracture; the transmissivity is given by

$$\mathbf{T}_f = 10^{\mathbf{X}_f}. \quad (\text{A.13})$$

Thus, we can write

$$\frac{\partial \mathbf{M}}{\partial \mathbf{X}_f} = \ln(10) \begin{pmatrix} \mathbf{A}_{EE} & \mathbf{A}_{ED} & \mathbf{A}_{EA} & \mathbf{0} & \mathbf{0} \\ \mathbf{A}_{DE} & \mathbf{A}_{DD} & \mathbf{A}_{DA} & \mathbf{0} & \mathbf{0} \\ \mathbf{A}_{AE} & \mathbf{A}_{AD} & \mathbf{A}_{AA} + \mathbf{S} & \mathbf{0} & -\mathbf{S} \\ \mathbf{0} & \mathbf{0} & \mathbf{0} & \mathbf{0} & \mathbf{0} \\ \mathbf{A}_{AE} & \mathbf{A}_{AD} & \mathbf{A}_{AA} & \mathbf{0} & \mathbf{0} \end{pmatrix}, \quad (\text{A.14})$$

for a fracture  $f$ , and from (A.10)

$$\frac{\partial \mathbf{F}}{\partial \mathbf{X}_f} = \ln(10) \begin{pmatrix} \mathbf{A}_{EE} & \mathbf{A}_{ED} & \mathbf{A}_{EA} & \mathbf{0} & \mathbf{0} \\ \mathbf{A}_{DE} & \mathbf{A}_{DD} & \mathbf{A}_{DA} & \mathbf{0} & \mathbf{0} \\ \mathbf{A}_{AE} & \mathbf{A}_{AD} & \mathbf{A}_{AA} + \mathbf{S} & \mathbf{0} & -\mathbf{S} \\ \mathbf{0} & \mathbf{0} & \mathbf{0} & \mathbf{0} & \mathbf{0} \\ \mathbf{A}_{AE} & \mathbf{A}_{AD} & \mathbf{A}_{AA} & \mathbf{0} & \mathbf{0} \end{pmatrix} \begin{pmatrix} \mathbf{P}_E \\ \mathbf{P}_D \\ \mathbf{P}_A \\ \mathbf{Q}_D \\ \mathbf{P}_B \end{pmatrix}. \quad (\text{A.15})$$

Thus, the sensitivity is given by

$$\frac{d\mathbf{G}}{d\mathbf{X}_f} = \ln(10) \boldsymbol{\theta}^T \begin{pmatrix} \mathbf{A}_{EE} & \mathbf{A}_{ED} & \mathbf{A}_{EA} & \mathbf{0} & \mathbf{0} \\ \mathbf{A}_{DE} & \mathbf{A}_{DD} & \mathbf{A}_{DA} & \mathbf{0} & \mathbf{0} \\ \mathbf{A}_{AE} & \mathbf{A}_{AD} & \mathbf{A}_{AA} + \mathbf{S} & \mathbf{0} & -\mathbf{S} \\ \mathbf{0} & \mathbf{0} & \mathbf{0} & \mathbf{0} & \mathbf{0} \\ \mathbf{A}_{AE} & \mathbf{A}_{AD} & \mathbf{A}_{AA} & \mathbf{0} & \mathbf{0} \end{pmatrix} \begin{pmatrix} \mathbf{P}_E \\ \mathbf{P}_D \\ \mathbf{P}_A \\ \mathbf{Q}_D \\ \mathbf{P}_B \end{pmatrix} + \frac{\partial \mathbf{G}}{\partial \mathbf{X}_f}. \quad (\text{A.16})$$

The partial derivative of the consequence  $\frac{\partial \mathbf{G}}{\partial \mathbf{X}_f}$  is the same as that calculated

in (3.56). There are three contributions to the evaluation of the sensitivity

(A.16). The first arises from the  $\mathbf{A}$  entries in the upper left 3x3 sub-matrix,

the second arises from the terms in  $\mathbf{S}$  and the third arises from the lower 1x3

sub-matrix. The first contribution is equivalent to (3.55) that was used in the calculation of the sensitivities in section 3.6. The second contribution is given by

$$\ln 10 \boldsymbol{\theta}_A^T \mathbf{T}_f \boldsymbol{\gamma} (\mathbf{P}_B - \mathbf{P}_A), \quad (\text{A.17})$$

for a fracture  $f$ , where  $\boldsymbol{\theta}_A^T$  denotes the transpose of the adjoint on nodes contained in group  $A$ . The third term can be expressed as

$$\ln 10 \boldsymbol{\theta}_B^T (\mathbf{A}_{AD} \mathbf{P}_D + \mathbf{A}_{AE} \mathbf{P}_E + \mathbf{A}_{AA} \mathbf{P}_A). \quad (\text{A.18})$$

where  $\boldsymbol{\theta}_B^T$  denotes the transpose of the adjoint on nodes contained in group  $A$ . Equation (A.18) can be manipulated using the flow equations (A.1) and the borehole equation (A.3) to become

$$\ln 10 \boldsymbol{\theta}_B^T \mathbf{S} (\mathbf{P}_B - \mathbf{P}_A). \quad (\text{A.19})$$

Thus, (A.17) and (A.19) are added to the calculated sensitivities (3.60) to represent multiple borehole intersections.

## REFERENCES

- Adler, P. M. and J.-F. Thovert (1999). Fractures and Fracture Networks. Dordrecht, Kluwer Academic Publishers.
- Ahokas, H. and L. Koskinen (April 2005). Task 7: Modelling the KR24 long-term pumping test at Olkiluoto.
- Archie, G. E. (1942). "The electrical resistivity log as an aid in determining some reservoir characteristics." Petroleum Technology **5**: 8.
- Bakhmeteff, B. A. and N. V. Feodoroff (1937). "Flow through granular beds." Journal of Applied Mechanics **4**: 7.
- Bear, J. (1972). Dynamics of Fluids in Porous Medium. New York, American Elsevier Publishing Company.
- Bear, J. (1993). Modeling flow and contaminant transport in fractured rocks, Flow and Contaminant Transport in Fractured Rocks. San Diego, Academic Press.
- Bear, J. and A. Verruijt (1987). Modeling Groundwater Flow and Pollution, D. Reidel Publishing Company.
- Berkowitz, B. and R. P. Ewing (1998). "Percolation Theory and Network Modeling Applications in Soil Physics." Surveys in Geophysics **19**(1): 49.
- Bogdanov, I. I., V. V. Mourzenko, J.-F. Thovert and P. M. Adler (2003). "Effective permeability of fractured porous media with power-law distribution of fracture sizes." Water Resources Research **39**(1): 1023.
- Bonnans, J. F., J. C. Gilbert, C. Lemarechal and C. A. Sagastizabal (2006). Numerical Optimization: Theoretical and Practical Aspects. Berlin Heidelberg, Springer-Verlag.
- Bonnet, E., O. Bour, N. E. Odling, P. Davy, I. Main, P. Cowie and B. Berkowitz (2001). "Scaling of fracture systems in geological media " Reviews of Geophysics **39**(3): 36.
- Cacas, M. C., E. Ledoux, G. d. Marsily, A. Barbreau, P. Calmels, B. Gaillard and R. Margritta (1990). "Modeling Fracture Flow With a Stochastic Discrete Fracture Network: Calibration and Validation 2. The Transport Model." Water Resources Research **26**(3): 9.

- Cacas, M. C., E. Ledoux, G. d. Marsily, B. Tillie, A. Barbreau, E. Durand, B. Feuga and P. Peaudecerf (1990). "Modeling Fracture Flow With a Stochastic Discrete Fracture Network: Calibration and Validation 1. The Flow Model." Water Resources Research **26**(3): 10.
- Carrera, J., A. Alcolea, A. Medina, J. Hidalgo and L. J. Slooten (2005). "Inverse problem in hydrogeology." Journal of Hydrogeology **13**: 16.
- Carrera, J. and S. P. Neuman (1986). "Estimation of Aquifer Parameters Under Transient and Steady State Conditions: 1. Maximum likelihood Method Incorporating Prior Information." Water Resources Research **13**: 206-222.
- Cauffman, T. L. and A. M. LaVenue (1990). Groundwater Flow Modelling of the Culebra Dolomite. Volume II: Data Base, Sandia National Laboratories. **Technical Report SAND89-7068/2**.
- Cauffman, T. L., A. M. LaVenue and J. F. Pickens (1990). Groundwater Flow Modelling of the Culebra Dolomite. Volume I: Model Calibration Sandia National Laboratories. **Report SAND89-7068/1**.
- Chavent, G. (1974). Identification of Functional Parameters in Partial Differential Equations. Identification of Parameters in Distributed Systems, University of Texas.
- Chavent, G. (2009). Nonlinear Least Squares for Inverse Problems, Springer.
- Cliffe, K. A. and C. P. Jackson (1993). Stochastic Modelling of Groundwater Flow at the WIPP Site. International High Level Radioactive Waste Management Conference, Las Vegas, USA.
- Cliffe, K. A. and C. P. Jackson (1995). "Conditioning stochastic groundwater flow models on head data." Materials Research Society Symposium Proceedings **353**: 7.
- Cliffe, K. A. and C. P. Jackson (2000). A New Method for Conditioning Stochastic Groundwater flow Models on Head Data. Harwell, AEA Technology.
- Cooley, R. L. (1985). "A comparison of several methods of solving nonlinear-regression groundwater flow equations." Water Resources Research **21**(10): 1525-1538.
- Darcy, H. (1856). Les Fontaines Publiques de la Ville de Dijon. Dalmont, Paris.
- Delhomme, J. P. (1978). "Kriging in the Hydrosciences." Advances in Water Resources **1**(5).

Delleur, J. W. (1999). The Handbook of Groundwater Engineering, CRC Press LLC.

Domenico, P. A. and F. W. Schwartz (1990). Physical and Chemical Hydrogeology. New York, John Wiley & Sons.

Dreuzy, J. R., P. Davy and O. Bour (2001). "Hydraulic properties of two-dimensional random fracture networks following a power law length distribution: 1 Effective connectivity." Water Resources Research **37**(8): 2065-2078.

Fine, T. (1973). Theories of Probability, Academic Press.

Frampton, A. and V. Cvetkovic (2010). "Inference of field-scale fracture transmissivities in crystalline rock using flow log measurements." Water Resources Research **46**.

Frampton, A., V. Cvetkovic and D. Holton (February 2008). Aspo task Force on modelling of groundwater flow and transport of solutes - Task 7A Task 7A1 and 7A2: Reduction of performance assessment uncertainty through modelling of hydraulic tests at Olkiluoto, Finland.

Freeze, R. A. and J. A. Cherry (1979). Groundwater. Englewood Cliffs, NJ, Prentice-Hall Inc.

Ge, S. (1997). "A Governing Equation For Fluid Flow in Rough Fractures." Water Resources Research **33**(1): 8.

Giles, M. B. and N. A. Pierce (2000). "An Introduction to the Adjoint Approach to Design." Flow, Turbulence and Combustion **65**: 22.

Grisak, G. E. and J. F. Pickens (1980). "Solute Transport Through Fractured Media, 1, The Effect of Matrix Diffusion." Water Resources Research **16**(4): 719-730.

Hadamard, J. (1902). "Sur les problèmes aux dérivées partielles et leur signification physique." Princeton University Bulletin **49--52**.

Hajek, A. (2010). "Interpretations of Probability." from <http://plato.stanford.edu/archives/spr2010/probability-interpret/>.

Hartley, L., D. Holton and A. R. Hoch (2008). NAPSAC release 9.5 technical summary document, Serco Assurance, Oxfordshire, UK.

Hill, M. C. and C. R. Tiedeman (2007). Effective Groundwater Model Calibration. New Jersey, John Wiley & Sons Inc.

Hoeksema, R. J. and P. K. Kitanidis (1984). "An Application of the Geostatistical Approach to the Inverse Problem in Two-Dimensional Groundwater Modeling." Water Resources Research **20**(7): 17.

Huyakorn, P. S., B. H. Lester and C. R. Faust (1983). "Finite Element Techniques for Modeling Groundwater Flow in Fractured aquifers." Water Resources Research **19**(4): 1019-1035.

Isaaks, E. H. and R. M. Srivastava (1989). An Introduction to Applied Geostatistics. New York, Oxford University Press Inc.

Jing, L. (2003). "A Review of Techniques, Advances and Outstanding Issues in Numerical Modelling for Rock Mechanics and Rock Engineering." International Journal of Rock Mechanics & Mining Sciences **40**: 70.

Journel, A. G. and C. J. Huijbregts (1978). Mining Geostatistics. London, Academic Press Limited.

Kitanidis, P. K. (1996). "On the Geostatistical Approach to the Inverse Problem." Water Resources Research **19**(6): 9.

Krumbein, W. C. and G. D. Monk (1943). "Permeability as a function of the size parameters of unconsolidated sands " Transaction of the American Institute of Mineral, Metallurgical and Petroleum Engineers. **151**: 10.

Kurtzman, D., R. Nativ and E. M. Adar (2007). "Flow and transport predictions during multi-borehole tests in fractured chalk using discrete fracture network models." Hydrogeology Journal **15**: 23.

Lee, P. M. (1997). Bayesian Statistics: An Introduction, John Wiley & Sons Inc.

Lindquist, Q. (1933). On the Flow of water through porous soil. Premier Congres des grands barrages. Stockholm. **5**: 20.

Marrett, R. (1996). "Aggregate properties of fracture populations." Journal of Structural Geology **18**(2/3): 9.

Marsily, G. d. (1997). "Calculating Equivalent Permeability: A Review." Advances in Water Resources **20**(5-6): 25.

Mays, L. W. (2005). Water Resources Engineering, John Wiley & Sons, Inc.

McDonald, M. G. and A. W. Harbaugh (1988). A modular three-dimensional finite-difference ground-water flow model. Techniques of Water-Resources Investigations, Book 6 U.S. Geological Survey.

Mood, A. M., A. G. Franklin and C. B. Duane (1974). Introduction to the Theory of Statistics, McGraw-Hill International

Moreno, L., Y. W. Tsang, C. F. Tsang, F. V. Hale and I. Neretnieks (1988). "Flow and Tracer Transport in a Single Fracture: A Stochastic Model and Its

Relation to Some Field Observations." Water Resources Research **24**(12): 15.

Neuman, S. P. (1973). "Calibration of Distributed Parameter Groundwater Flow Models Viewed as a Multiple-Objective Decision Process under Uncertainty " Water Resources Research **9**(4): 1006-1021.

Neuman, S. P. (1977). "Theoretical derivation of Darcy's law." Acta Mechanica **25**: 17.

Neuman, S. P. (1987). Stochastic continuum representation of fractured rock permeability as an alternative to the REV and fracture network concepts. Rock Mechanics: proceedings of the 28th US Symposium, Tuscon, Arizona.

Neuman, S. P. and I. Neretnieks, Eds. (1990). Hydrogeology of low permeability environments. Selected papers on hydrogeology. Verlag Heinz Heise, Hannover, Germany.

Neuman, S. P. and E. S. Simpson (1985). Hydrogeology of rocks of low permeability Memoirs of Int Assoc Hydrogeol, Parts 1 and 2, . Proc 17th Int IAH Congress. Tuscon, Arizona. **XVII**.

Neuman, S. P. and S. Yakowitz (1979). "A Statistical Approach to the Inverse Problem of Aquifer Hydrology 1. Theory." Water Resources Research **15**(4).

Nordqvist, A. W., Y. W. Tsang, C. F. Tsang, B. Dverstorp and J. Andersson (1992). "A Variable Aperture Fracture Network Model for Flow and Transport in Fracture Rocks." Water Resources Research **28**: 10.

Pinder, G. F. and W. G. Gray (1977). Finite Element Simulation in Surface and Subsurface Hydrology, Academic Press, Inc.

Posiva OY (1999). The final disposal facility for spent nuclear fuel. Environmental Impact Report. General Summary., Posiva.

Press, W. H., B. P. Flannery, S. A. Teukolsky and W. T. Vetterling (1986). Numerical Recipes, Cambridge.

Quarteroni, A. and A. Valli (1999). Domain Decomposition Methods for Partial Differential Equations, Oxford University Press.

Ramsey, F. P. (1926). Truth and Probability. The Foundations of Mathematics and other Logical Essays. R. B. Braithwaite. London, Kegan, Paul, Trench, Trubner & Co.: p156-198.

Schneebeli, G. (1955). "Experiences sur la limite de validite de la loi de darcy et l'appartition de la turbulence dans une ecoulement de filtration." La Houille Blanche **10**: 8.

- Selroos, J., D. D. Walker, A. Strom, B. Gylling and S. Follin (2001). "Comparison of alternative modelling approaches for groundwater flow in fractured rock." Journal of Hydrogeology **257**: 14.
- Snow, D. T. (1970). "The frequency and apertures of fractures in rock." Rock Mechanics and Mineral Sciences **7**: 23-40.
- Stuart, A. M. (2010). "Inverse Problems: A Bayesian Perspective." Acta Mechanica.
- Sun, N. Z. (1999). Inverse Problem in Groundwater Modeling, Kluwer Academic Publishers.
- Sun, N. Z. and W. W.-G. Yeh (1985). "Identification of Parameter Structure in Groundwater Inverse Problem." Water Resources Research **21**(6): 14.
- The U.S. Department of Energy. (2010). "Waste Isolation Pilot Plant." from <http://www.wipp.energy.gov>.
- Tiedeman, C. R., D. J. Goode and P. A. Hsieh (1998). "Characterizing a Ground Water Basin in a New England Mountain and Valley Terrain." Groundwater **36**(4).
- Tikhonov, A. N. (1963). "Methods for solving ill-posed problems." Doklady AN SSSR.
- Tikhonov, A. N. and V. I. A. Arsenin (1977). Solutions of ill-posed problems, Winston (Washington and New York).
- Tolikas, P. K., E. G. Sidiropoulos and C. D. Tzimopoulos (1984). "A Simple Analytic Solution for the Boussinesq One-Dimensional Groundwater Flow Equation " Water Resources Research **20**(1): 4.
- Tsang, Y. W. and C. F. Tsang (1987). "Channel Model of Flow Through Fractured Media." Water Resources Research **23**(3): 12.
- Witherspoon, P. A. (1991). Geological Problems in Radioactive Waste Isolation: A World Wide Review.
- Witherspoon, P. A. (1996). Geological Problems in Radioactive Waste Isolation: Second Worldwide Review.
- Witherspoon, P. A. and G. S. Bodvarsson (2001). Geological Challenges in Radioactive Waste Isolation: Third Worldwide Review.
- Witherspoon, P. A. and G. S. Bodvarsson (2006). Geological Challenges in Radioactive Waste Isolation: Fourth Worldwide Review.

Yager, R. M. (1997). Simulated Three-Dimensional Ground-Water Flow in the Lockport Group, a Fractured-Dolomite Aquifer near Niagara Falls, New York, U.S. Geological Survey Water Supply Paper 2487.

Yeh, W. W.-G. (1986). "Review of Parameter Identification Procedures in Groundwater Hydrology." Water Resources Research **22**(2): 13.

Zimmerman, R. W. and G. S. Bodvarsson (1996). "Hydraulic Conductivity of Rock Fractures." Transport Porous Media **23**(1): 30.